NASA Technical Memorandum 78480 AVRADCOM Technical Report 78-33(AM)

Computational Wing Optimization and Comparisons With Experiment for a Semi-Span Wing Model

E.G. Waggoner, H.P. Haney, and W.F. Ballhaus

June 1978

National Aeronautics and Space Administration

United States Army Aviation Research and Development Command

NASA Technical Memorandum 78480 AVRADCOM Technical Report 78-33(AM)

Computational Wing Optimization and Comparisons With Experiment for a Semi-Span Wing Model

E.G. Waggoner and H.P. Haney, Vought Corporation, Dallas, Texas
W.F. Ballhaus, Aeromechanics Laboratory
AVRADCOM Research and Technology Laboratories
Ames Research Center, Moffett Field, California

National Aeronautics and Space Administration
Ames Research Center
Moffett Field, California 94035

United States Army
Aviation Research and Development Command
St. Louis, Missouri 63166

TABLE OF CONTENTS

LIST OF FIGURES

LIST OF TABLES

COMPUTATIONAL WING OPTIMIZATION AND COMPARISONS WITH EXPERIMENT FOR A SEMI-SPAN WING MODEL

E. G. Waggoner*, H. P. Haney†, and W. F. Ballhaus‡

Ames Research Center

1.0 SUMMARY

A computational wing optimization procedure has been developed and verified by an experimental investigation of a semi-span variable camber wing model in the NASA Ames Research Center 14 foot transonic wind tunnel. The Bailey-Ballhaus transonic potential flow analysis and Woodward-Carmichael linear theory codes were linked to Vanderplaats constrained minimization routine to optimize model configurations at several subsonic and transonic design points. The 35° swept wing is characterized by multi-segmented leading and trailing edge flaps whose hinge lines are swept relative to the leading and trailing edges of the wing. By varying deflection angles of the flap segments, camber and twist distribution can be optimized for different design conditions.

The tested configurations had been optimized at lift coefficients of 0.2, 0.4, and 0.6 for Mach numbers of 0.6 and 0.9. Several configurations which had proven to be the most efficient designs from an earlier parametric study were also tested. This offered a baseline for comparison of the computationally optimized configurations.

Following the test an improved version of the Bailey-Ballhaus code was used to analyze test configurations. Computationally predicted wing pressure distributions were compared with experimental data at selected conditions.

Study results indicate that numerical optimization can be both an effective and efficient design tool. The optimized configurations had as good or better lift to drag ratios at the design points as the best designs previously tested during an extensive parametric study. In addition, the predicted pressure distributions agreed well with the experiment when the improved Bailey-Ballhaus code was used.

---

*Lead Engineer, Vought Corporation, Dallas, Texas.

†Engineering Specialist, Vought Corporation, Dallas, Texas.

‡Ames Research Center, NASA and Aeromechanics Laboratory, U.S. Army AVRADCOM, Moffett Field, California.

2.0 INTRODUCTION

Tremendous strides have been taken in the field of computational fluid mechanics during the past decade. In general, these have paralleled the developments in computer hardware and software. These developments have broadened the scope of fluid flow problems that can be addressed, thus providing the designer with new and powerful tools. To date numerical solutions have advanced to the point where many 3-D inviscid and 2-D viscous transonic flow problems may be practically solved.

One of the major advantages of numerical solutions compared to experimental testing is the relative ease of modifying a configuration. This capability enables a designer to investigate many configurations or pertubations to a given configuration in a relatively short time. With this added flexibility a design problem may be thought of in different terms. As shown in the simplified design problem representation in Figure 1, preliminary analysis may encompass a much larger design space, thereby increasing the possibility of the target design being in the design space. The space is then reduced computationally to a size that is commensurate with the accuracy and validity of the computational tool. Experimental refinement and verification are then performed in a much smaller design space reducing both the cost and time required.

The computational techniques must be applied in a systematic manner to ensure efficient, accurate reduction of the design space. One method of solving a wing design problem computationally is to couple the aerodynamic analysis techniques to a numerical optimization procedure. Basically, this involves systematic perturbation of certain design variables to arrive at an optimum configuration relative to some specific object parameter (e.g. minimum drag at a given lift, pressure gradient at a specific chordwise location, etc.). This approach was taken by Ray Hicks at NASA Ames for optimizing airfoil contours. Linking a 2-D compressible flow analysis routine to an optimization technique, he

sucessfully optimized airfoil geometries for both subsonic and transonic design conditions, Reference 1. The next logical step is to apply this approach to a three dimensional problem and to identify effective wing design procedures.

Vought's wing optimization studies evolved from efforts begun in the early 1970's centering around development of a wing designed for efficient transonic maneuverability without penalizing subsonic performance. A design approach was used in which the wing planform characteristics and maximum airfoil thickness were optimized for advanced fighter missions. An innovative concept for varying the camber distribution featuring multi-segmented leading and trailing edge flaps resulted from the study. This afforded the wing a large operating envelope of buffet free transonic performance. The uniqueness of the design was characterized by the flap hinge lines being skewed relative to the leading and trailing edges of the wing, Figure 2. This allowed camber to be concentrated where it was most effective; i.e. the leading edge of the wing tip and the trailing edge of the wing root. An extensive range of spanwise camber and twist variation is obtainable by varying the segmented flap deflections. A highly instrumented model employing the skewed hinge line concept had been constructed and tested in NASA Langley's eight-foot transonic wind tunnel, Reference 2. The experimental investigation bore out the preliminary assumptions of the performance improvements available. While generating a great amount of invaluable data, the studies proved to be both costly and time consuming.

The extensive data base available on the variable camber wing offered a unique opportunity to investigate the feasibility of three dimensional numerical optimization. A joint effort involving Vought Corporation and NASA Ames Research Center was undertaken to develop a computational wing optimization procedure, apply the procedure to several wing design problems and verify the resultant designs through experimental testing.

The purpose of this report is to describe the optimization procedures, to present results of the experiment, and to compare computational predictions of pressure distributions with the experimental data. The detailed description of the wind tunnel test (including model geometry) and the data from the test are included in Reference 3.

The authors wish to thank Ray Hicks (NASA-Ames) for many interesting discussions and to acknowledge the substantial computer programming efforts of Juanita Frick (Informatics, Inc., Palo Alto, California).

3.0 COMPUTATIONAL TECHNIQUES

Two theoretical analysis techniques and a constrained minimization procedure were used for defining the configurations to be tested. It is not necessary to understand the complicated inner workings of these techniques to understand the optimization procedure or to appreciate the comparisons of theory with experiment. However, a brief summary description is helpful in identifying the distinguishing characteristics of the two analysis codes. In addition, a simplified description of CONMIN, Reference 4, the optimization technique, is included and should be beneficial in understanding the basic wing optimization procedure.

3.1 Bailey-Ballhaus Transonic Analysis

The Bailey-Ballhaus transonic analysis code, Reference 5 and 6, provides a computerized method for calculation of three-dimensional transonic flows about wing-body combinations. A non-linear problem formulation is required to model the mixed subsonic and supersonic flow on the surface of a lifting configuration in transonic flight. This is accomplished by using the small disturbance transonic velocity potential equation to model the flow field. By using the Murman-Cole mixed finite difference approximation with successive line over-relaxation, the resulting system of non-linear algebraic equations are solved.

The numerical solution technique requires that certain restrictions be placed on the configurations for which the method is applicable. Included in these geometric constraints are:

(1) The wing leading edge must be a single valued function of span.
(2) The wing must be relatively thin, and the leading edge cannot be too blunt.
(3) The wing sweep must not be excessively large.
(4) The wing tip chord must be finite.

(5) The wing cannot have dihedral.

(6) The wing angle-of-attack must not be too large.

Additional constraints are placed on the flow field:

(1) The freestream Mach number is less than one.

(2) The embedded shock waves are weak.

(3) The boundary layer is negligibly thin and attached.

(4) The flow at the wing trailing edge is subsonic.

A precise definition of "too blunt", "too large", etc. cannot be given. The user must rely on judgement to determine the degree of validity for a solution.

The method yields small disturbance surface pressure coefficients, spanwise loading parameters, total wing force and moment coefficients, local flow Mach number, and the location of the sonic line.

3.2 Woodward-Carmichael Linear Analysis

The Woodward-Carmichael linear theory code, Reference 7 provides a method for calculating pressure distributions on wing-body combinations of arbitrary planform in subsonic, supersonic, or hypersonic flow using the small perturbation assumption. Subsonic and supersonic analyses are based on linearized aerodynamic influence coefficients using trapezoidal panels to conform to the actual configuration geometry. The wing-body combination is replaced by a distribution of singularities satisfying the linearized potential flow equation. Strengths of these singularities are adjusted such that the resultant flow is tangent to the surface at the panel centroid. Wing thickness is represented by sources and sinks located on the wing reference plane. Wing camber, twist and incidence are represented by planar vortex distributions. Once the singularity strengths which satisfy boundary conditions are computed, the surface

pressure distributions, lift, drag, and pitching moment on the wing and body may be obtained. The forces and moments are computed by integration of the surface pressures.

3.3 Constrained Minimization Code

CONMIN is a subroutine, developed by Garret Vanderplaats at NASA Ames, which affords the user the solution of linear or non-linear constrained minimization problems. Being particularly well suited for wing design, the routine has been linked at Vought to several aerodynamic analysis routines, including the Bailey-Ballhaus and Woodward-Carmichael codes, using the geometry of the variable camber wing as the interface.

An example of a simple wing optimization problem is to find the camber distribution yielding minimum drag at a given lift and Mach number for the variable camber wing. Constraints might be to allow only hinge lines 4 and 5 to be deflected. Schematically the solution to this simple case is presented in Figure 3. The deflection angles of the two hinge lines, δ_4 and δ_5 define the design space which is represented by lines of constant drag. Superimposed on the design space is the lift constraint, $C_L = C_{L_{MIN}}$, which acts as a boundary for the solution. Assume that an initial condition, point A, is given such that no constraints are violated. CONMIN would alternately command the analysis routine to evaluate small changes in each of the deflection angles. Once all deflections have been perturbed, gradients are computed to determine the direction and step size to vary each hinge line to achieve the largest drag reduction. CONMIN commands the solution to step in the desired direction changing all variables simultaneously until either the drag increases (point B) or a constraint is encountered (point C). Then new gradients, along with a new move direction, are computed. If a constraint has indeed been reached (point C), directions will be determined which not only reduce drag but also avoid violating the constraint. When drag cannot be reduced further without violating a constraint (point D), the optimum camber distribution, defined by the hinge line deflections,

has been found. It should be noted that a local minimum may have been determined instead of a global minimum, and several optimizations with different starting conditions may be required by some problems to determine the optimum configuration.

4.0 WING OPTIMIZATION PROCEDURE

A computational wing design procedure was formulated by utilizing potential flow wing analysis techniques and numerical optimization within the geometric constraints of the variable camber wing. The Bailey-Ballhaus transonic potential flow analysis and Woodward-Carmichael linear potential flow analysis codes were linked to Vanderplaat's constrained minimization code (CONMIN) through a geometry module. The procedure consisted of using the flap hinge line deflections and angle of attack as decision variables to define a camber and twist distribution to minimize drag for the wing at a given lift coefficient and Mach number. As discussed in Section 3.3, the controlling module of CONMIN systematically determined the directions and magnitudes to deflect the flap segments to minimize drag at the design condition. Through iteratively applying this technique within the constraints of the design space, the optimization technique predicted an optimum camber and twist distribution. The constraints imposed on the designs were the physical limits of the flap deflections and a maximum and minimum pitching moment limit. The pitching moment constraint was imposed on the design space to restrict the trim drag penalty incurred with anticipated aft wing loading.

Six primary design points were targeted for wing optimization. These consisted of .2, .4 and .6 lift coefficients at a subsonic (M=0.6) and a transonic (M=0.9) Mach number. The Woodward-Carmichael linear theory code was used for the subsonic optimizations. All eight hinge line deflection angles and angle of attack were optimized simultaneously.

The Woodward-Carmichael code was also used to provide a set of starting cambers to be used for the transonic optimizations. The original plan for the transonic optimizations was to fix the leading edge camber at the starting value and allow the trailing edge to be optimized. This would be accomplished using only the four trailing edge flap deflection angles and angle of attack as the decision variables. Then after the trailing edge was optimized, the leading edge deflections were to be

optimized holding the optimized trailing edge fixed. In practice, however, the leading edge cambers proved to be ineffective at reducing drag. This was probably due to a combination of two computational compromises made in formulating the design procedure. Constraints on central processor time due to the number of flow field solutions necessary for each optimization iteration required the solution mesh to be coarser and the convergence to be less stringent than would be desirable for accurate configuration analysis. These conditions in conjunction with the small perturbation assumption of the Bailey-Ballhaus code caused inaccuracies in the leading edge region of the wing. Hence, the design approach may not have allowed the leading edge to be effective since the first step (trailing edge optimization) possibly drove the solution near enough to a local minimum that improvements in the design were the same order of magnitude as the force prediction capability of the analysis code. These factors prompted a decision to hold the leading edge constant at the cambers defined by linear theory and to optimize the configuration using only the four trailing edge flap segments.

One exercise was performed which used the leading edge flaps to predict an optimum design which could be verified experimentally. Hinge line four deflection angle and angle of attack were used as decision variables to predict an optimum configuration at C_L=.3 and M=0.9. The four leading edge flap segments then acted together as a full span flap. This configuration was tested along with configurations derived by varying hinge line four over a range of deflection angles which encompassed the experimental optimum at the design lift coefficient. It was then possible to compare the computationally predicted and experimentally defined optimum flap deflection angles to assess the accuracy of the procedure. It should be noted that the design was initialized away from the design point and the complete leading edge flap system acted in unison. Hence, the results are not inconsistent with the leading edge ineffectiveness described in the preceding paragraph.

5.0 EXPERIMENT

A test was conducted in the NASA Ames 14 foot transonic wind tunnel to experimentally verify both the subsonic and transonic optimizations. Testing the semi-span model in this tunnel posed unique installation problems primarily related to the boundary layer on the wind tunnel floor. Several solutions were considered with the final decision being to mount the semi-span wing root flush with the wind tunnel floor turntable to submerge the large integral wing mounting block, Figure 4. The porous tunnel floor was covered with steel plates which acted as the configuration plane of symmetry. Provisions were included in the test schedule to investigate the boundary layer on the tunnel floor at the location of the model. These data are presented for the range of design Mach numbers in Figure 5. Although the boundary layer rake used did not encompass the entire boundary layer, enough data were obtained to estimate a displacement thickness of 1.25 inches.

The total schedule included seven optimized configurations, the best two configurations which had previously been tested at NASA Langley and a series of configurations used to experimentally verify an optimization. Data were obtained at angles of attack of -2^{o} to 10^{o} in 1^{o} increments over the Mach range from .6 to .9. The majority of configurations were tested at Mach numbers of .6, .7, .8, .85 and .9 for Reynolds numbers based on the mean geometric chord of 6.5×10^{6} to 8.0×10^{6}. For the configurations which had been designed to a specific lift coefficient and Mach number, data were obtained at this design point. Both force and pressure data were obtained at each test point. The wing pressures were measured at 269 points distributed over the wing's upper and lower surfaces along seven spanwise stations. These data are presented in Reference 3.

Although this report is primarily concerned with the comparisons of theory and experiment, a summary discussion of the more pertinent experimental results is appropriate. At each of the design points the computa-

tionally defined configurations proved to be as efficient, as indicated by the ratio of lift to drag, as the most efficient configurations from the Langley test. This was significant and bore out the optimization procedure as a valid design approach. Perhaps as meaningful were the unexpected characteristics of the optimized configurations at points away from the design points. When compared with a Langley configuration designed for the same point, the computationally defined configuration had significantly better characteristics at the off-design points. This observation is limited in scope and inferences should be made with care. However, it should be pointed out that it is possible and highly desirable in many cases to use the off-design points as constraints in defining the design space. Presented in Figure 6 are data for the two best configurations from the parametric study compared with data for one of the optimized configurations from the present study. The data from the optimized configuration encompasses the range of lift to drag ratios available from the parametric study. It should be noted that these results would have been more dramatic had either the pitching moment constraint been removed or an effective leading edge optimization been performed. As was discussed in Section 4.0, the pitching moment constraints were imposed on the design space to limit the trim drag penalty. The same end could be accomplished by optimizing a trimmed lift to drag ratio. By specifying a corresponding tail effectiveness and moment arm, the pitching moment at each point of calculation could be trimmed instead of restricting the pitching moment to be within certain bounds. This would have the effect of altering the design space instead of bounding the feasible (design) region with constraint lines.

In order to validate the computationally optimized configurations, a simple study was conducted during the testing to determine an experimental optimum. An optimum had been predicted at 0.3 C_L and 0.9 Mach number using only one of the wing's hinge lines and angle of attack as decision variables. Starting from a configuration optimized at 0.2 C_L, hinge line 4 and angle of attack were allowed to vary to predict an optimum at 0.3 C_L. This configuration was tested along with three variations of the

configuration. The variations were derived by varying the subject hinge line over a range of deflection angles which encompassed the experimental optimum at the design condition while holding the other hinge line deflections constant. The variation of lift to drag ratio at constant lift levels as a function of hinge line deflection is presented in Figure 7. Superimposed on the experimental data is an indication of the computationally predicted optimum hinge line deflection at the design point. The results of the experimental and computation optimization agree quite well lending a great deal of confidence to the computational optimization procedure.

6.0 WING OPTIMIZATION COMPARISONS

The initial optimization procedure did not allow for potential flow solutions to be obtained on a fine mesh or to be carried to a high degree of convergence. Each run, which consisted of three optimization iterations using a relatively crude grid and liberal convergence criterion, required approximately one hour of CDC 7600 Central Processor time. Economics forced the optimizations to be performed in this manner, although it was recognized relaxation solutions to classical three dimensional small-disturbance (CSD) theory are compromised under these conditions. In this instance, the crude mesh degraded the solution accuracy near the wing leading edge and the lack of convergence affected the repeatability and introduced noise into the design space. In order to verify the analytical predictions by comparison with the experimental data, it was desirable to analyze the configurations on a much finer grid network and allow the solutions to be relaxed to a smaller residual (an indication of solution convergence). An improved version of the Bailey-Ballhaus transonic analysis code had also been developed following the test. The improvements made the refined code attractive to use during this phase of the study. A modified small-disturbance (MSD) equation, derived by retaining two previously neglected terms, enhanced the solution in regions along the span where the flow is essentially two dimensional in a plane normal to the sweep direction. Although the improved equation is a consistent approximation to the full potential equation over a wider range of sweep angles; use of it, in itself, does not guarantee that shock waves will be properly captured by the computational method. A complementary finite differencing scheme was also incorporated into the coding, Reference 8. This was necessary to enforce shock conditions consistent with the governing equation, to insure suitable solution stability, and to avoid excessive dispersive or dissipative distortion of the shock profile.

The Bailey-Ballhaus analysis code is a very flexible analytical tool. Users are allowed interactions which can influence the accuracy and

convergence rate through variations in grid spacing, convergence criteria, relaxation parameters, etc. Enough interaction is allowed such that it is possible to "fine-tune" a solution. An example of this would be concentrating grid points near an expected shock to improve the prediction of the flow field in the vicinity of the shock wave. This is certainly advantageous in many cases, however, these comparisons would be more meaningful if the computational solutions differed by only the geometric differences in the various configurations. Therefore, a set of computational groundrules were established to insure that equal computational attention would be given to each of the configurations chosen for additional analysis. Essentially, these entailed holding all the program variables constant which were not geometry dependent. The study groundrules are summarized below.

- o The solutions would be obtained on the same coarse, medium and fine meshes.
- o Each solution would be relaxed to the same level of convergence.
- o Optional program variables were held constant for all runs. These included subsonic and supersonic relaxation parameters, Riegel's rule factor, Mach number scaling for the similarity parameter, and the non-conservative differencing scheme.
- o Comparisons with experimental data were to be made at the same lift coefficient (except as noted). All of the optimized configurations had been designed to a specific lift coefficient. Viscous effects cause experimental wing loadings to be lower than predicted by potential flow theory when compared at the same angle of attack. This anomaly coupled with the fact that the wind tunnel flow angularities and wall interference were not well defined, made it desirable not to tie the comparisons to a specific angle of attack but rather to use wing lift coefficient as the common denominator.

The design configurations included in the additional analyses are presented in Table 1 along with a listing of the flap hinge line deflections defining the camber distributions for each of the configurations.

The Appendix includes the comparisons of theory and experiment for each of these designs. The salient features of the comparisons are summarized below and illustrated through the presentation of selected examples.

In previous analysis attempts using the original Bailey-Ballhaus code at Vought, the prediction of the flow expansion over the wing leading edge had not been entirely satisfactory. The reasons associated with this problem were mainly grid spacing and the simplified version of the governing equation used in the code. The present analysis showed remarkedly good agreement near the wing leading edge, Figure 8a, b and c. This is particularly impressive due to the small disturbance properties of the governing equation. It is interesting to note the comparison in Figure 8b which presents comparisons for the theory and experiment at the same geometric angle of attack rather than the same lift coefficient. The excellent agreement at the section leading edge is due to the angles of attack being the same in the experiment and analysis. Off-setting the agreement at the leading edge, however, is the higher loading predicted over the remainder of the chord. The overall satisfactory agreement near the leading edge for all the configurations is attributed not only to the code improvements but to the fine mesh distribution in the forward 10% of the local chord and the relatively thin nature of the leading edge for the subject wing.

One of the configurations developed a double shock experimentally, Figure 8c. The leading edge shock was apparently not captured properly by the theory. This discrepancy is probably a viscous effect in the form of a leading edge vortex and should not be construed as a defect in the analysis. A pressure distribution is predicted, however, which would lead a keen observer to suspect this type of viscous interaction to develop.

A predicted expansion just forward of an aft located shock was fairly prevalent in the analysis but was observed experimentally in only one case. The trend was most noticeable inboard and dissipated progressing outboard along the span, Figure 9a and b. This apparent anomaly

is actually the result of a difference in shock location between the experiment and theory and is addressed in the next paragraph.

Where differences occurred, the analyses consistently indicated shocks positioned aft of the experimental shock location. Figure 10a shows an analytical prediction of a shock approximately 10% of the local chord further aft than the experiment at an inboard span location. A comparison for the same configuration at an outboard span station, Figure 10b, shows excellent agreement in the shock location prediction. These differences are attributed to several factors. (1) The shock/boundary layer interaction along the wind tunnel floor was not modelled in the computations, where the floor was the reflection plane for the isolated wing configuration. (2) Small differences in experimental Mach number at the wing can cause large shifts in the shock location. For a 2-D airfoil, these shifts can be as large as 10% chord per .01 difference in Mach number, as reported in Reference 9. During the experiment it was not possible to monitor the local Mach number at the wing location. (3) Viscous effects on the wing surface tend to move the experimental shock forward. (4) More important than the preceding factors is the manner in which the comparisons were made. Matching wing lift coefficient causes the theory to compensate for under prediction in one region by over prediction in another region. Hence, if the loading at the leading edge is low the theory will be pushed to a higher angle of attack, resulting in shifting the theoretical shock aft.

The plateau like upper surface pressure distributions shown in Figures 8a, 8b and 11 are predicted quiet accurately. This shape is characteristic of a pressure distribution on a supercritical airfoil in transonic flow. Results showing a pressure distribution which is inherent to an efficient transonic airfoil shape lend confidence to the optimization procedure.

Additional observations have been made and are discussed briefly below. The predicted loadings forward of an aft located shock show

excellent agreement with the experiment, Figures 8 through 11. The experimental shock wave is weaker at the inboard stations and agrees quite well with predictions further out along the span. Viscosity tends to affect the potential flow in this manner. At locations where the shock position is accurately predicted, the flow compression through the shock wave also shows good agreement. Pressure distributions on the wing lower surface are adequately predicted, with expected deviations occurring at the wing trailing edge.

7.0 CONCLUSIONS

Study results indicate that numerical optimization can be both an effective and efficient design tool. The effectiveness is a direct function of the analysis used for the design. Essentially this means the more accurate the physics of the problem are modeled, the more effective the optimization will be. In general, this involves a trade-off of cost (computer time) and solution accuracy. However, as efficient refinements are included in the analysis codes, improved resolution at reduced cost is possible. An example of this is Boppe's imbedded mesh technique, Reference 10, which has been incorporated into the latest Bailey-Ballhaus code since the comparisons presented here were completed.

Overall the comparisons of theoretical and experimental pressure distributions were very good when the improved Bailey-Ballhaus code was used for the analyses. In order to partially compensate for effects of viscosity on the pressure distributions the theory and experiment should be compared at the same wing lift coefficient. Reasonably good agreement occurred at the wing leading edge, particularly considering the limitations of the governing equation. This was attributed to the fine grid used in the solution and the relatively thin nature of the wing leading edge. The prediction of shock wave location and the flow compression through the shock wave were predicted quite well on the outboard 75% of the wing span. The differences observed on the inboard 25% were attributed to the shock/boundary layer interaction along the wind tunnel floor.

The computationally optimized configurations had as good or better lift to drag ratios at the design points as configurations which had been tested during an extensive parametric study. The characteristics of the optimized configurations at points away from the design points were generally much better than the parametrically defined configurations.

Work is currently being performed to extend the optimization procedure to include more arbitrary wing designs. This will include optimization of

wing sections for several different wing planforms and design conditions. The optimization code will also be linked to other analysis techniques such as the three dimensional Jameson full potential code, Reference 11 and 12, and the Hess wing-body code, Reference 13.

REFERENCES

1. Hicks, R. M.; and Vanderplaats, G. N.: Application of Numerical Optimization to the Design of Supercritical Airfoils without Drag Creep. SAE Paper 770440, Business Aircraft Meeting of the SAE, Wichita, Kansas, March 29-April 1, 1977.

2. Ferris, J. C.: Wind Tunnel Investigation of a Variable Camber and Twist Wing. NASA TN D-8475, August 1977.

3. Waggoner, E. G.; Haney, H. P.; and Ballhaus, W. F.: Wind Tunnel Investigation of Computationally Optimized Variable Camber Wing Configurations. NASA TM-78479, 1978.

4. Vanderplaats, G. N.: CONMIN-A Fortran Program for Constrained Function Minimization, Users Manual. NASA TM X-62282, August 1973.

5. Ballhaus, W. F.; and Bailey, F. R.: Numerical Calculation of Transonic Flow About Swept Wings. AIAA Paper 72-677, June 1972.

6. Ballhaus, W. F.; and Bailey, F. R.: Relaxation Methods for Transonic Flow About Wing-Cylinder Combinations and Lifting Swept Wings. Lecture Notes in Physics, vol. 19, Springer-Verlag, 1972, pp. 2-9.

7. Woodward, F. A.: A Unified Approach to the Analysis and Design of Wing-Body Combinations at Subsonic and Supersonic Speeds. AIAA Paper 68-55, 1968.

8. Ballhaus, W. F.; Bailey, F. R.; and Frick, J.: Improved Computational Treatment of Transonic Flow About Swept Wings. Advances in Engineering Sciences, vol. IV, NASA CP-2001, 1976, pp. 1213-1231.

9. Blackwell, J. A.; and Pounds, G. A.: Wind Tunnel Wall Interference on a Supercritical Airfoil at Transonic Speeds. Proceedings of AIAA 9th Aerodynamic Testing Conference, Arlington, Texas, 1976, pp. 1-11.

10. Boppe, C. W.: Calculation of Transonic Wing Flows by Grid Imbedding. AIAA Paper 77-207, January, 1977.

11. Jameson, A.; Caughey, D. A.; et al: A Brief Description of the Jameson-Caughey NYU Transonic Swept-Wing Computer Program - FLO 22. NASA TM X-73996, December, 1976.

12. Jameson, A.: Transonic Flow Calculations. VKI Lecture Series, Computational Fluid Dynamics, Von Karman Institute for Fluid Dynamics, Rhode - St. Genese, Belgium, March 15-19, 1976.

13. Hess, J. L.: Calculation of Potential Flow About Arbitrary Three-Dimensional Lifting Bodies. McDonnell Douglas Corporation, Report MDC J5679-01, 1972.

Table 1 Configurations for Comparison of Variable Camber Pressure Distributions with Theoretical Predictions

Configuration	Mach	C_L	Deflection Angle*							
			δ_1	δ_2	δ_3	δ_4	δ_5	δ_6	δ_7	δ_8
A92	.9	.2	.2	.6	1.3	2.0	1.6	1.2	.5	.8
A62	.9	.3	.3	.9	1.8	2.9	2.2	1.7	1.1	.5
A94	.9	.4	.3	.8	1.7	2.7	2.0	1.4	-1.4	6.2
A94	.9	†	.3	.8	1.7	2.7	2.0	1.4	-1.4	6.2
A94W	.9	.4	.3	1.0	1.8	2.8	2.7	2.2	1.5	.8
L5/TO	.9	.2	8.9	3.8	2.1	.8	0.	0.	0.	0.
L5/TO	.9	.3	8.9	3.8	2.1	.8	0.	0.	0.	0.

*For $\delta_1 - \delta_4$, leading edge down deflections are positive. For $\delta_5 - \delta_8$, trailing edge down deflections are positive.
†Comparisons between experiment and theory are at $\alpha = 3.15°$.

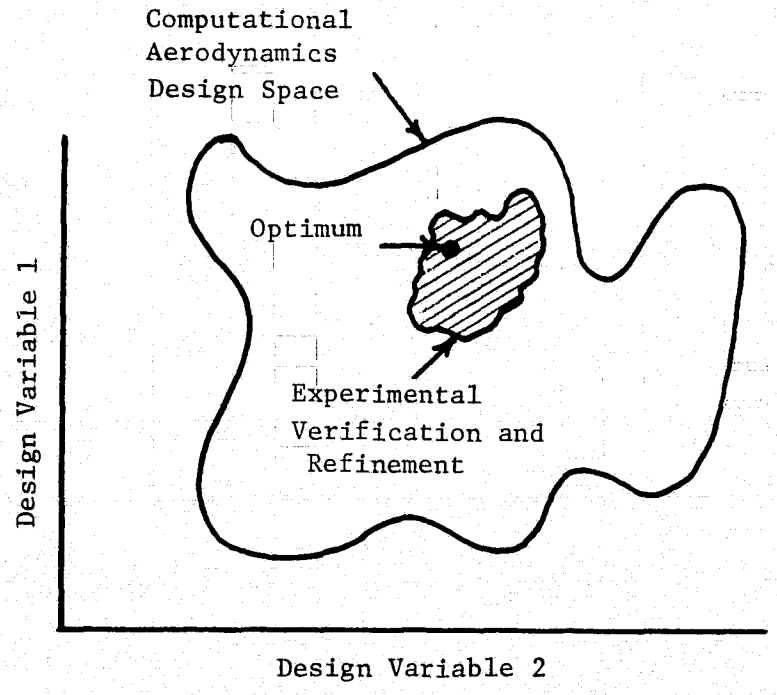

Figure 1 Computational Aerodynamics Design Approach

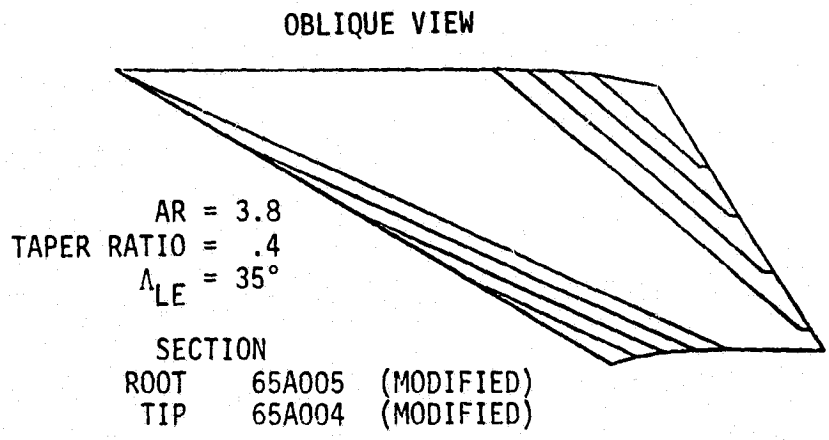

Figure 2 Vought Variable Camber Wing

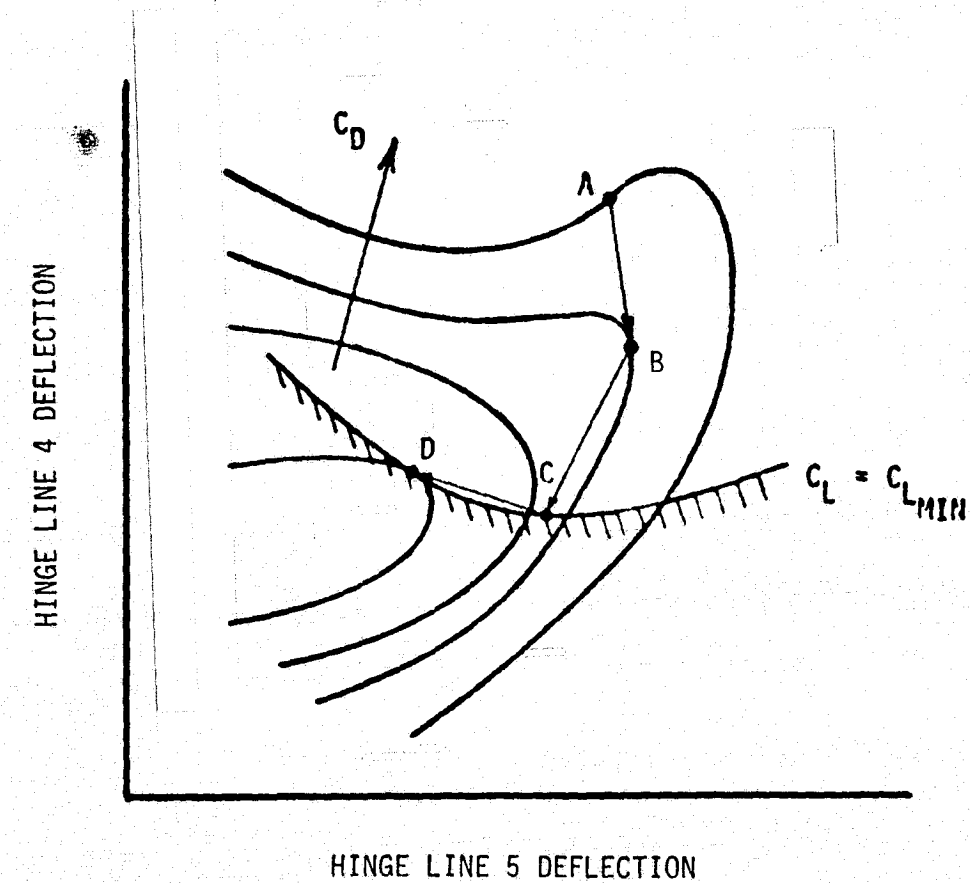

Figure 3 Wing Optimization Example

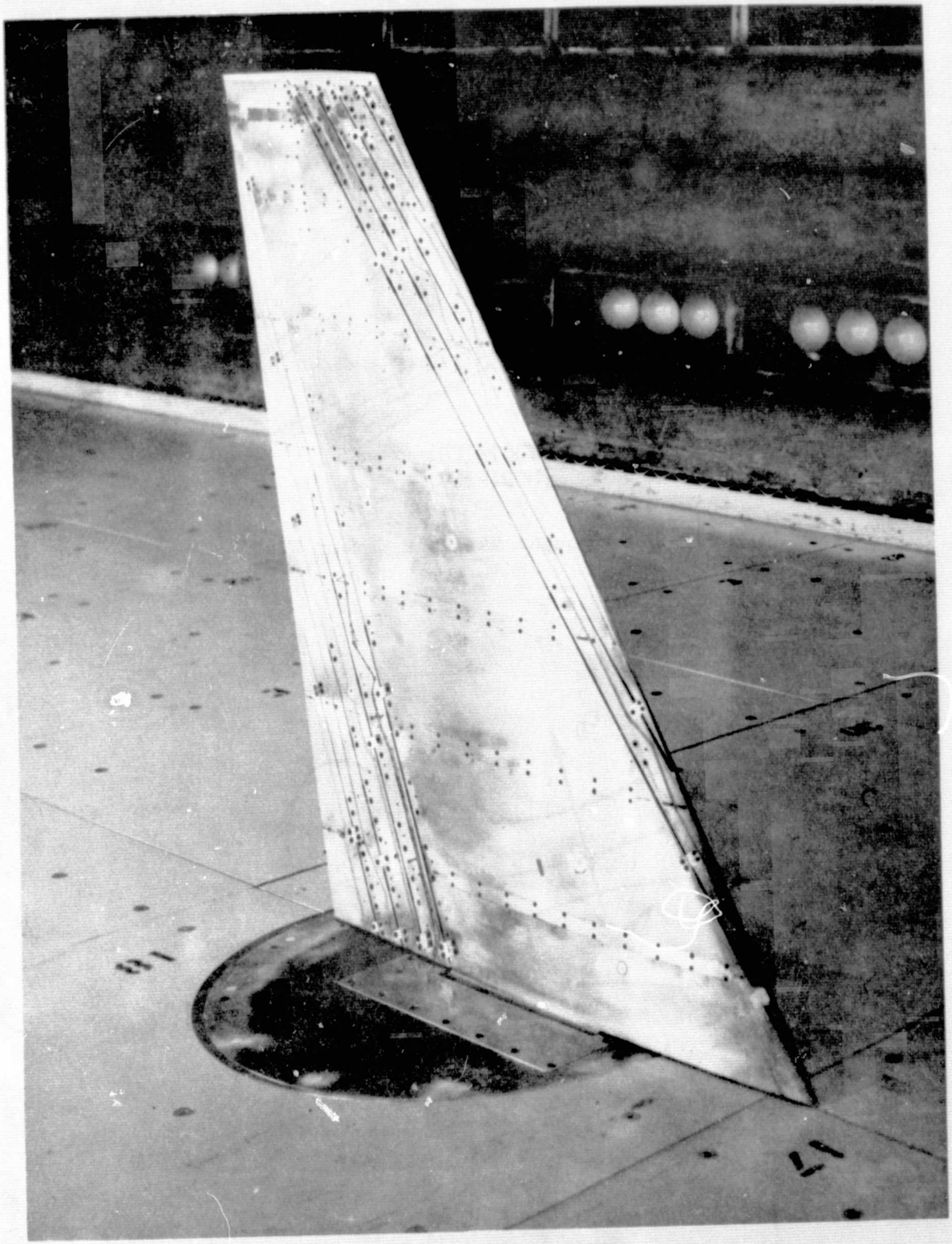

Figure 4 Wind Tunnel Installation

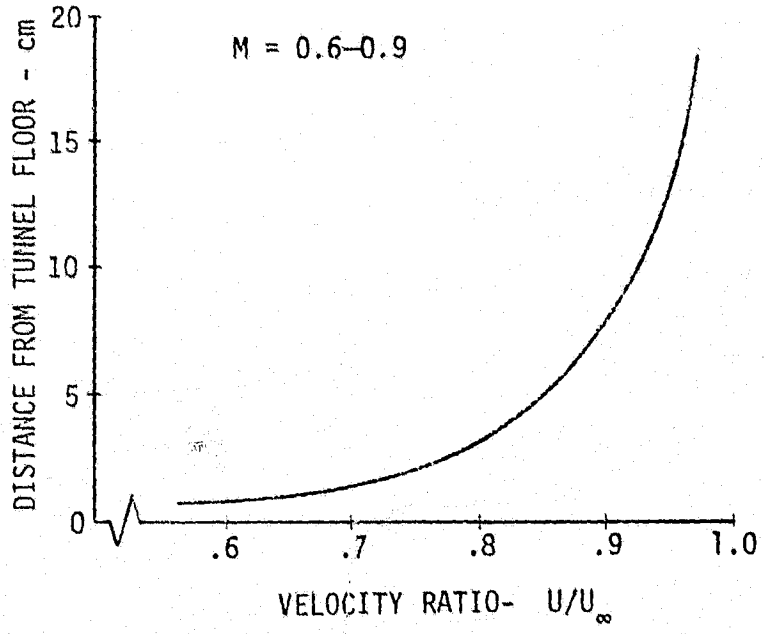

Figure 5 Velocity Distribution in the Vicinity of the Wind Tunnel Floor

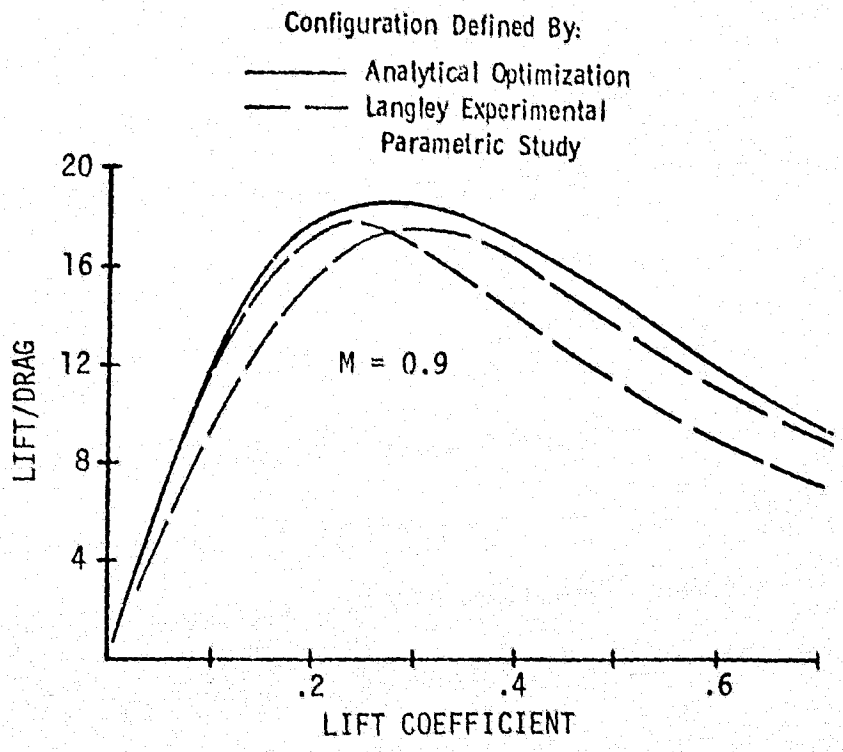

Figure 6 Experimental Lift to Drag Ratio Comparison of Ames Optimization Test Configuration

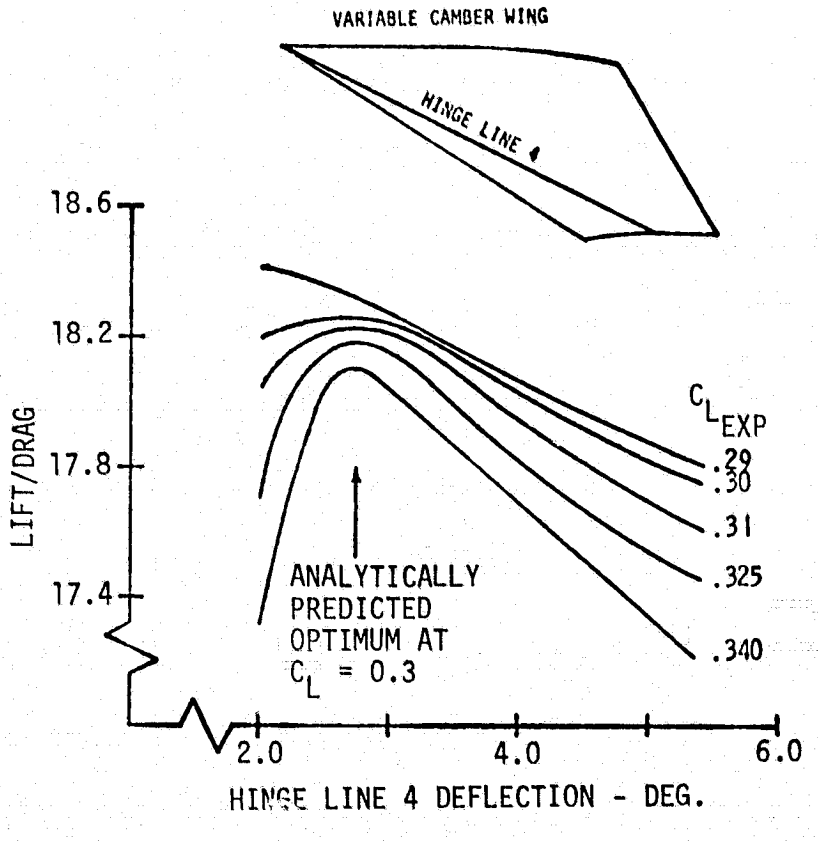

Figure 7 Comparison of Experimental and Computational One Hinge Line Optimization

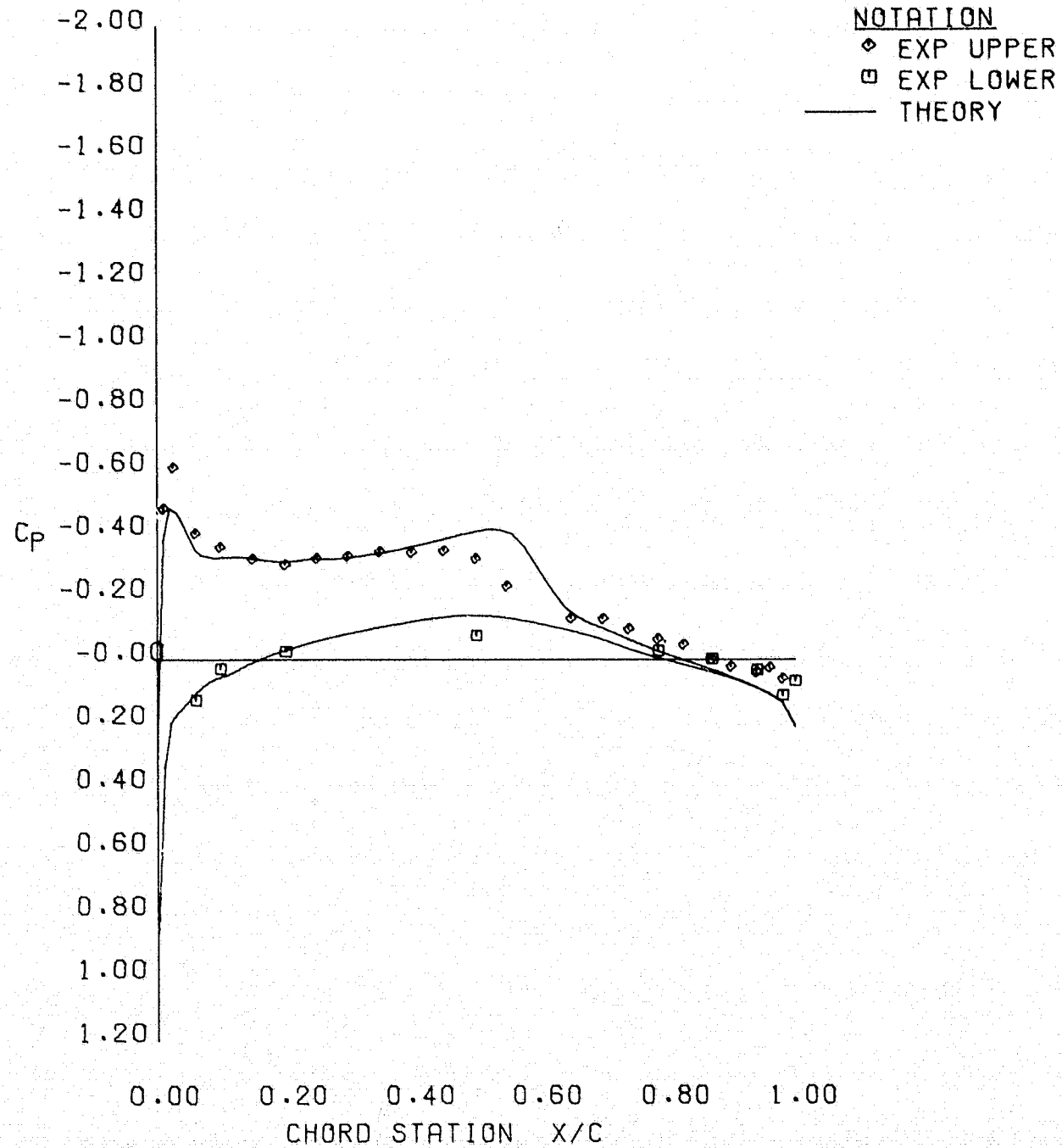

	ETA	MACH	ALPHA	CL	
EXPERIMENT	0.400	0.898	2.710	0.201	RUN = 53
THEORY	0.388	0.900	2.300	0.180	

(a) L5/T0, C_L = .44, η = .388

Figure 8 Comparison of Variable Camber Leading Edge Pressure Distributions with Bailey-Ballhaus Code Predictions

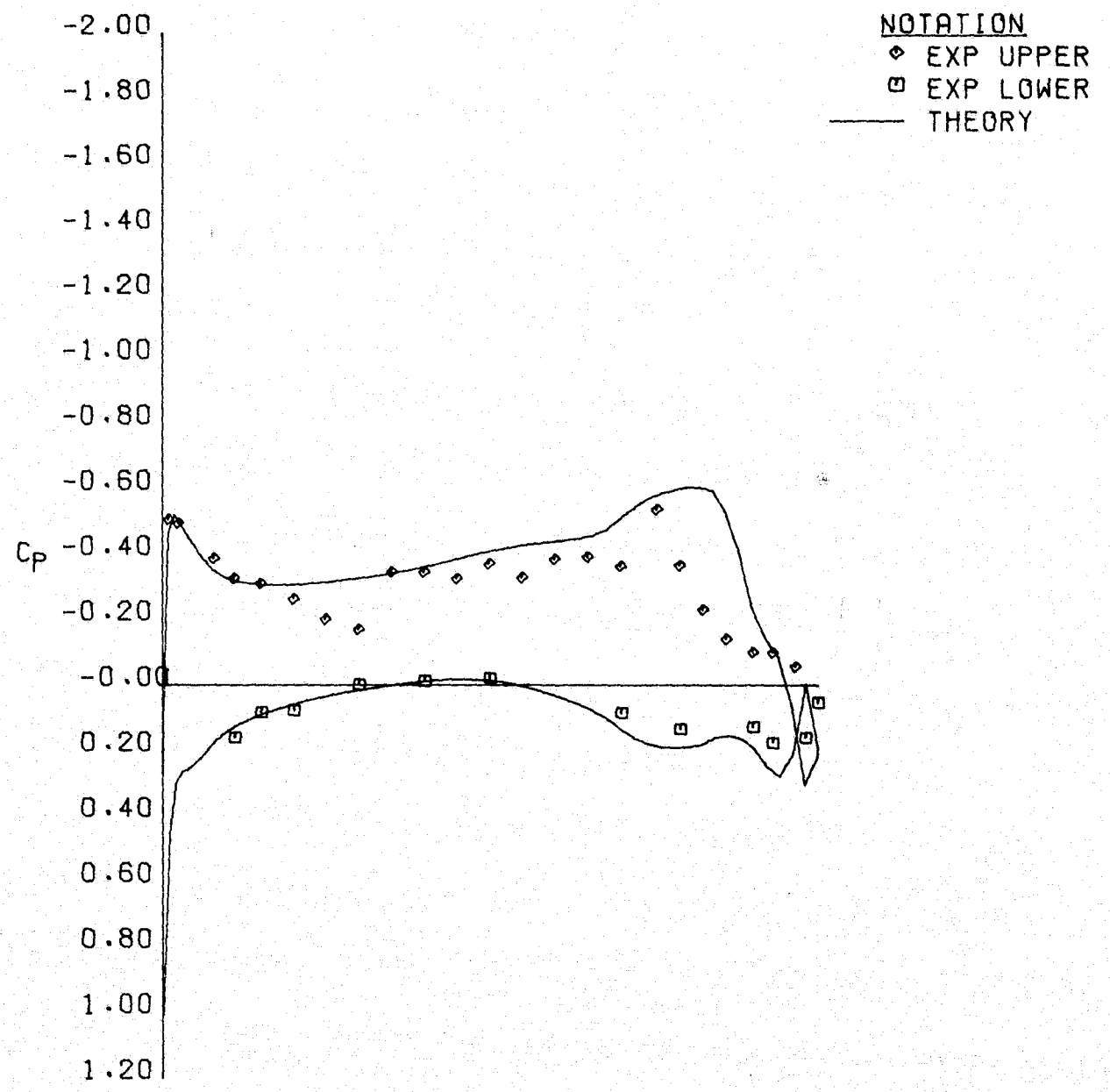

	ETA	MACH	ALPHA	CL	
EXPERIMENT	0.250	0.900	3.150	0.395	RUN = 16
THEORY	0.230	0.900	3.150	0.440	

(b) A94, C_L = .32, η = .23

Figure 8 Continued

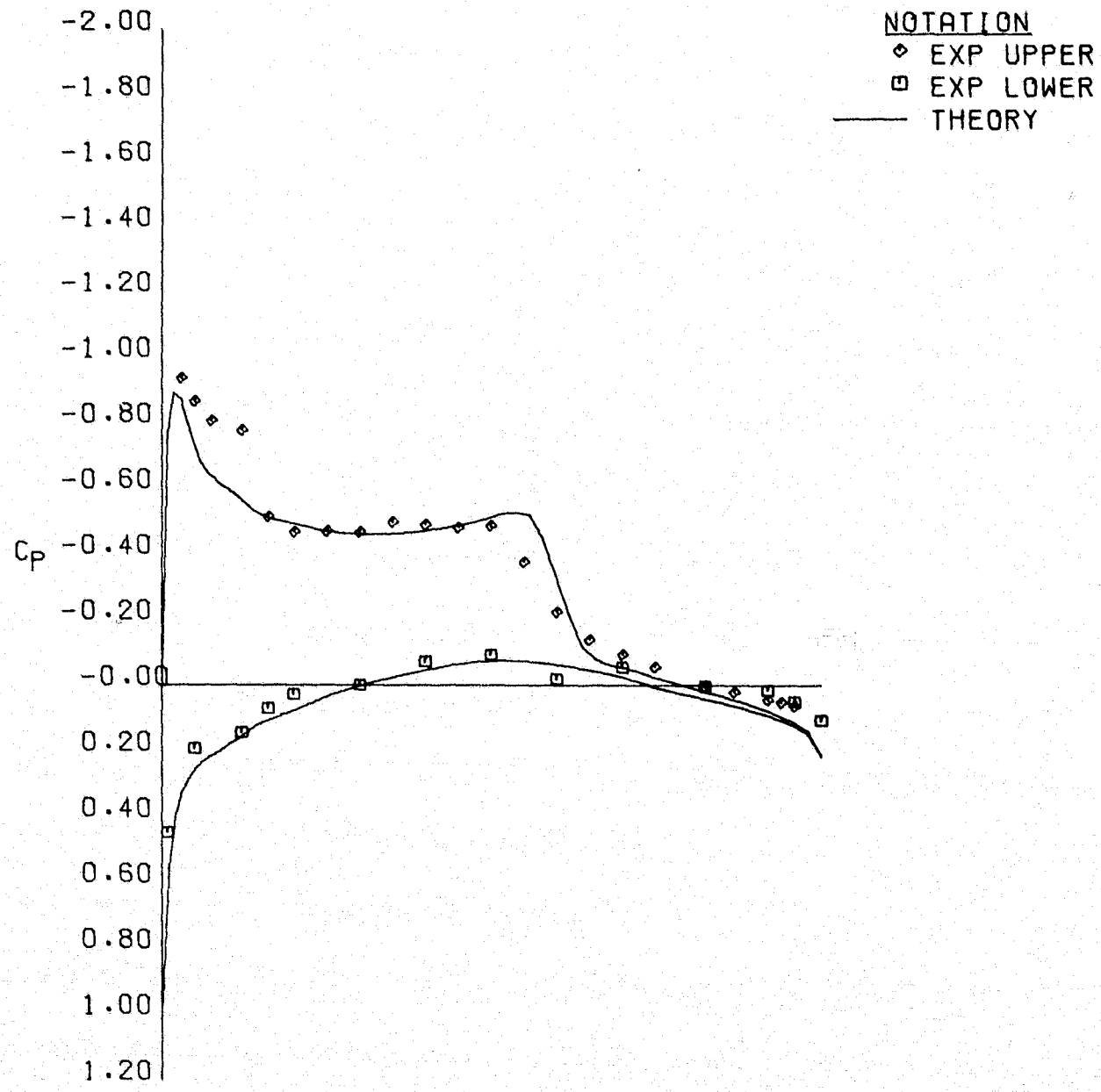

	ETA	MACH	ALPHA	CL	
EXPERIMENT	0.550	0.899	4.120	0.317	RUN = 53
THEORY	0.547	0.900	3.800	0.300	

(c) L5/T0, C_L = .20, η = .547

Figure 8 Concluded

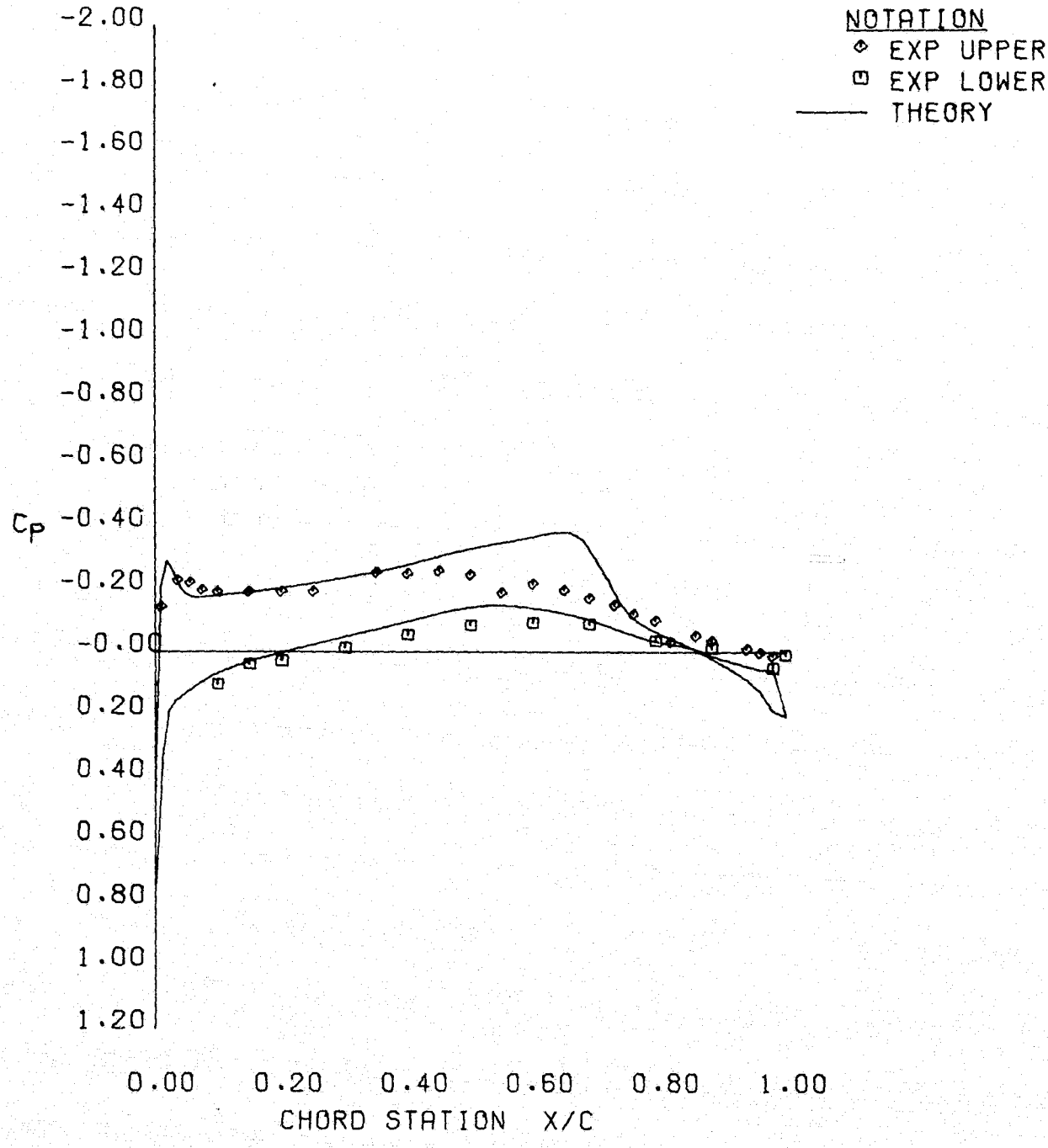

	ETA	MACH	ALPHA	CL	
EXPERIMENT	0.100	0.898	2.710	0.201	RUN = 53
THEORY	0.097	0.900	2.300	0.180	

(a) L5/T0, C_L = .20, η = .097

Figure 9 Prediction of Pressure Distributions on the Variable Camber Wing in the Vicinity of the Shock Wave by the Bailey-Ballhaus Code

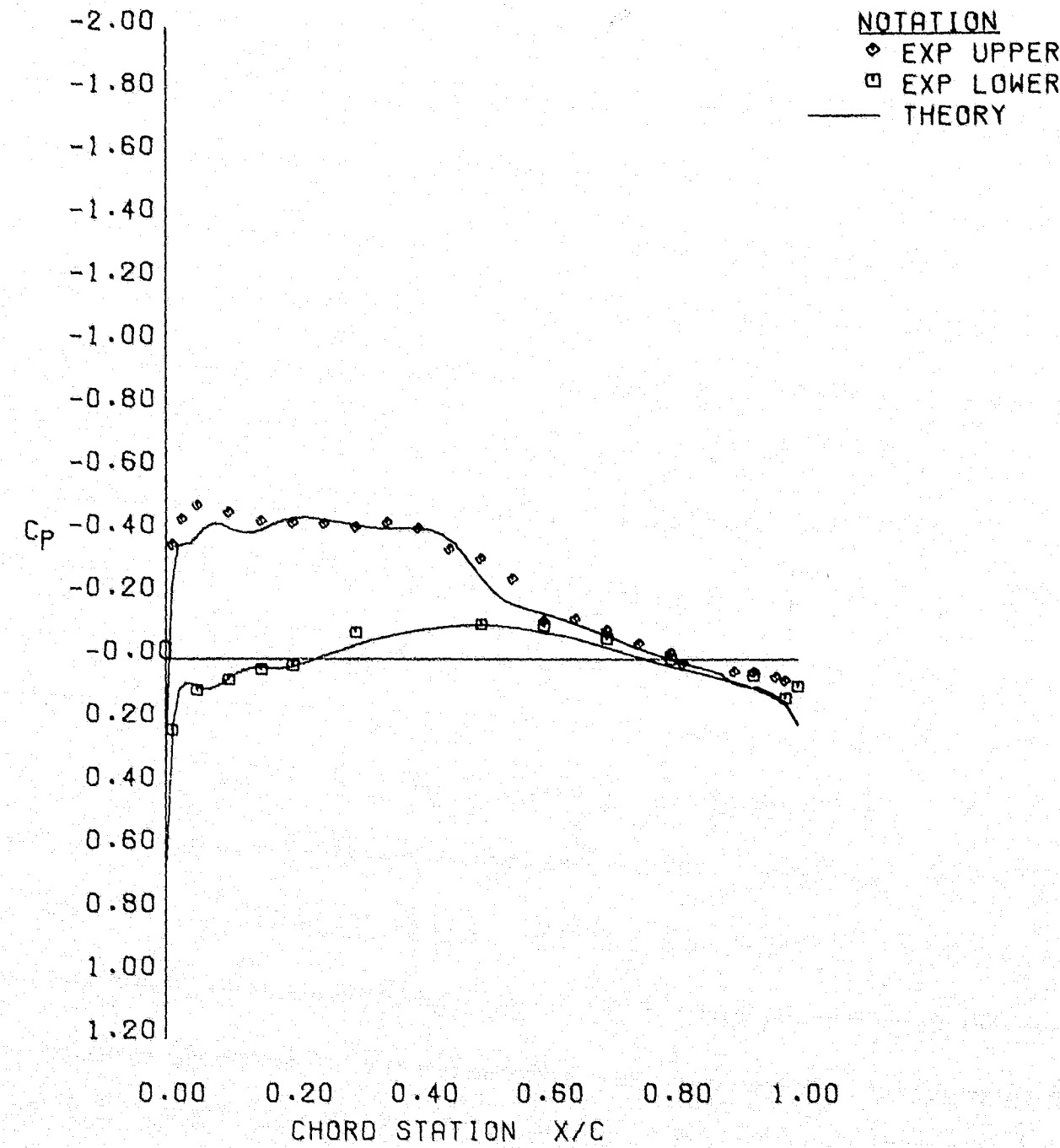

	ETA	MACH	ALPHA	CL	
EXPERIMENT	0.700	0.898	2.710	0.201	RUN = 53
THEORY	0.706	0.900	2.300	0.180	

(b) L5/TO, C_L = .20, η = .706

Figure 9 Concluded

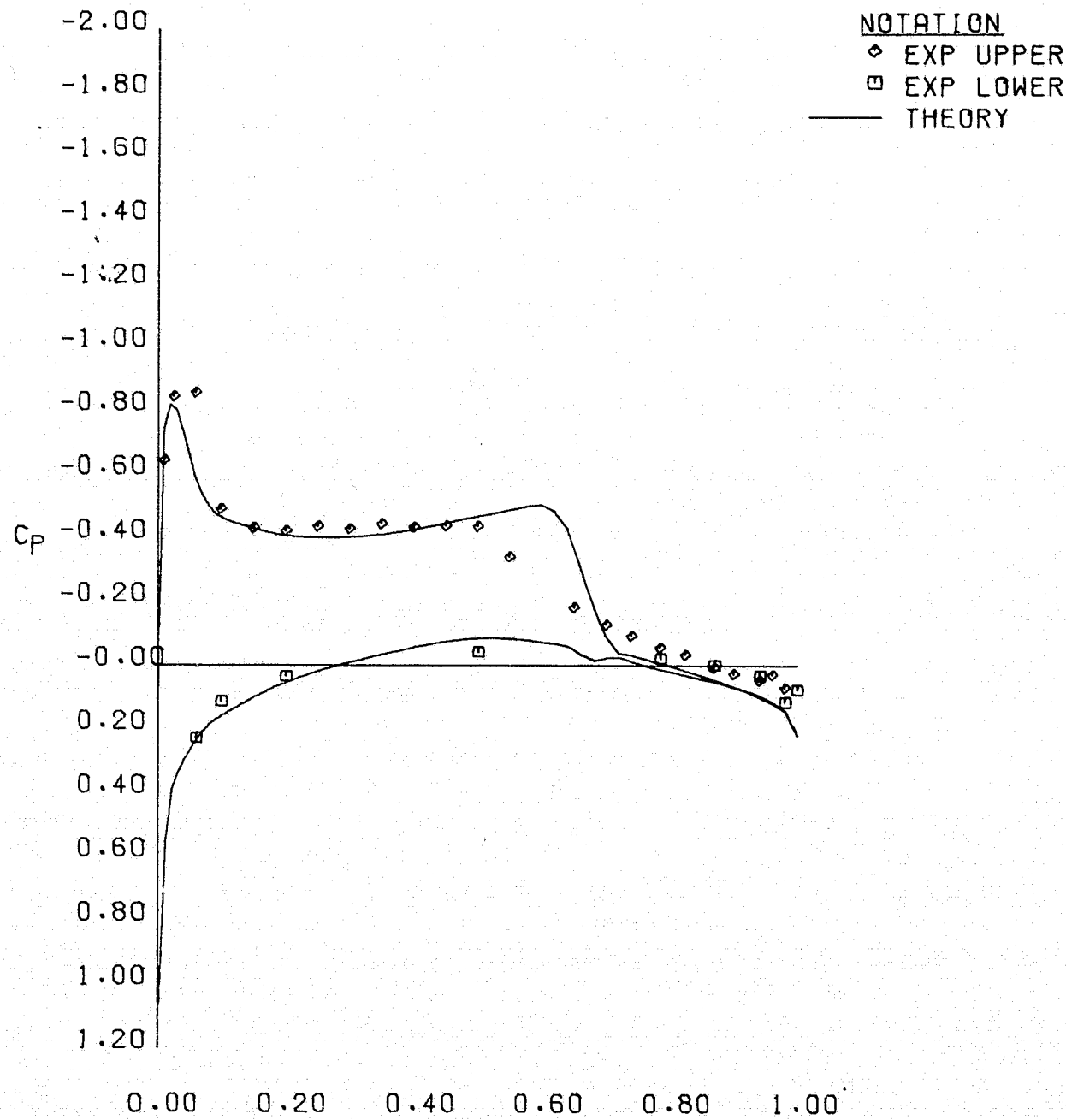

	ETA	MACH	ALPHA	CL	
EXPERIMENT	0.400	0.899	4.120	0.317	RUN = 53
THEORY	0.388	0.900	3.800	0.300	

(a) L5/TO, C_L = .32, η = .388

Figure 10 Prediction of Shock Location on the Variable Camber Wing by the Bailey-Ballhaus Code

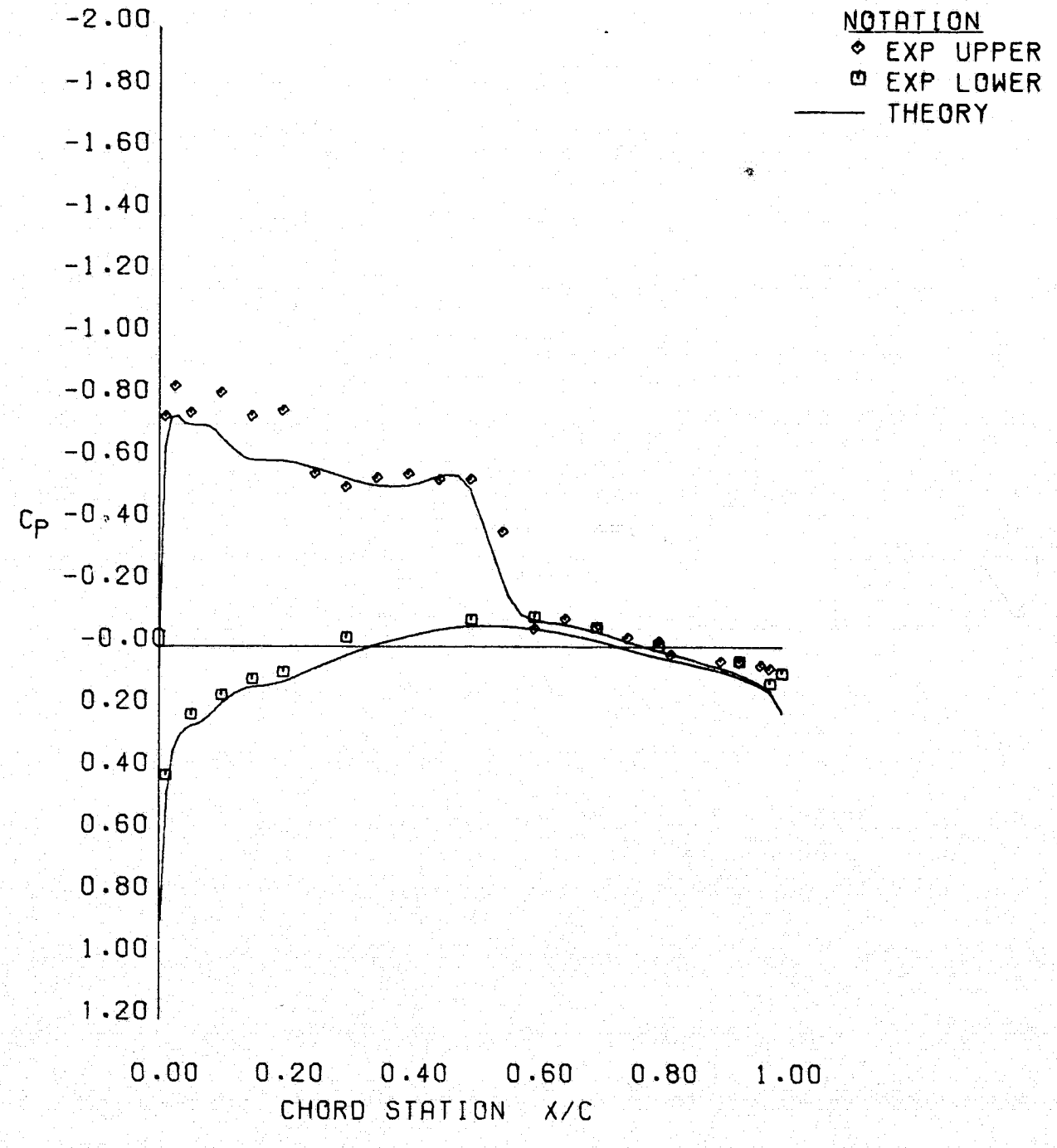

	ETA	MACH	ALPHA	CL	
EXPERIMENT	0.700	0.899	4.120	0.317	RUN = 53
THEORY	0.706	0.900	3.800	0.300	

(b) L5/T0, C_L = .32, η = .706

Figure 10 Concluded

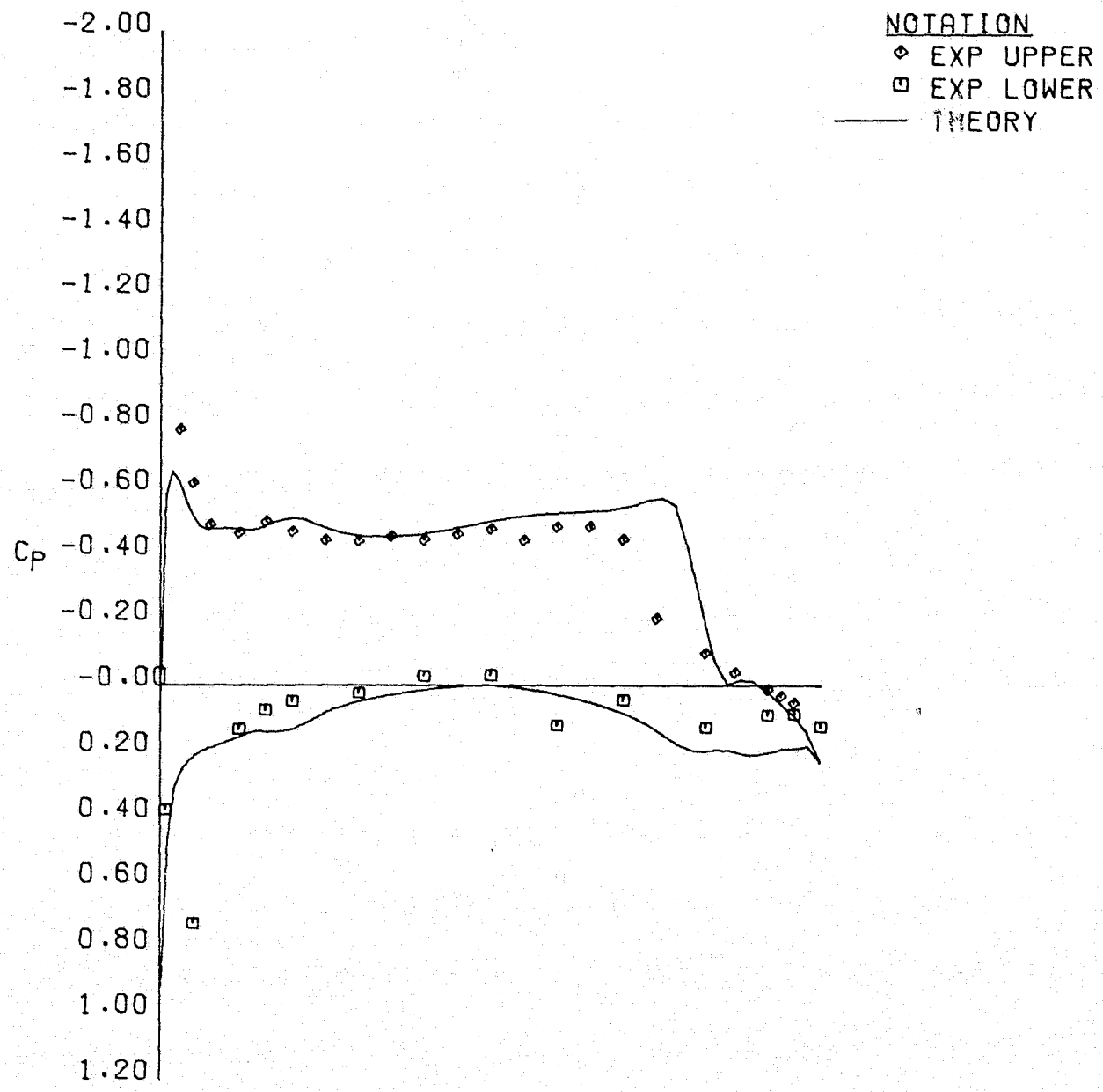

	ETA	MACH	ALPHA	CL	
EXPERIMENT	0.550	0.900	3.150	0.395	RUN = 16
THEORY	0.547	0.900	3.150	0.440	

Figure 11 Comparison of Upper Surface Pressure Distribution on the Variable Camber Wing with Bailey-Ballhaus Code Prediction

APPENDIX

COMPARISONS OF VARIABLE CAMBER WING PRESSURES WITH BAILEY-BALLHAUS TRANSONIC ANALYSIS ROUTINE

LIST OF FIGURES

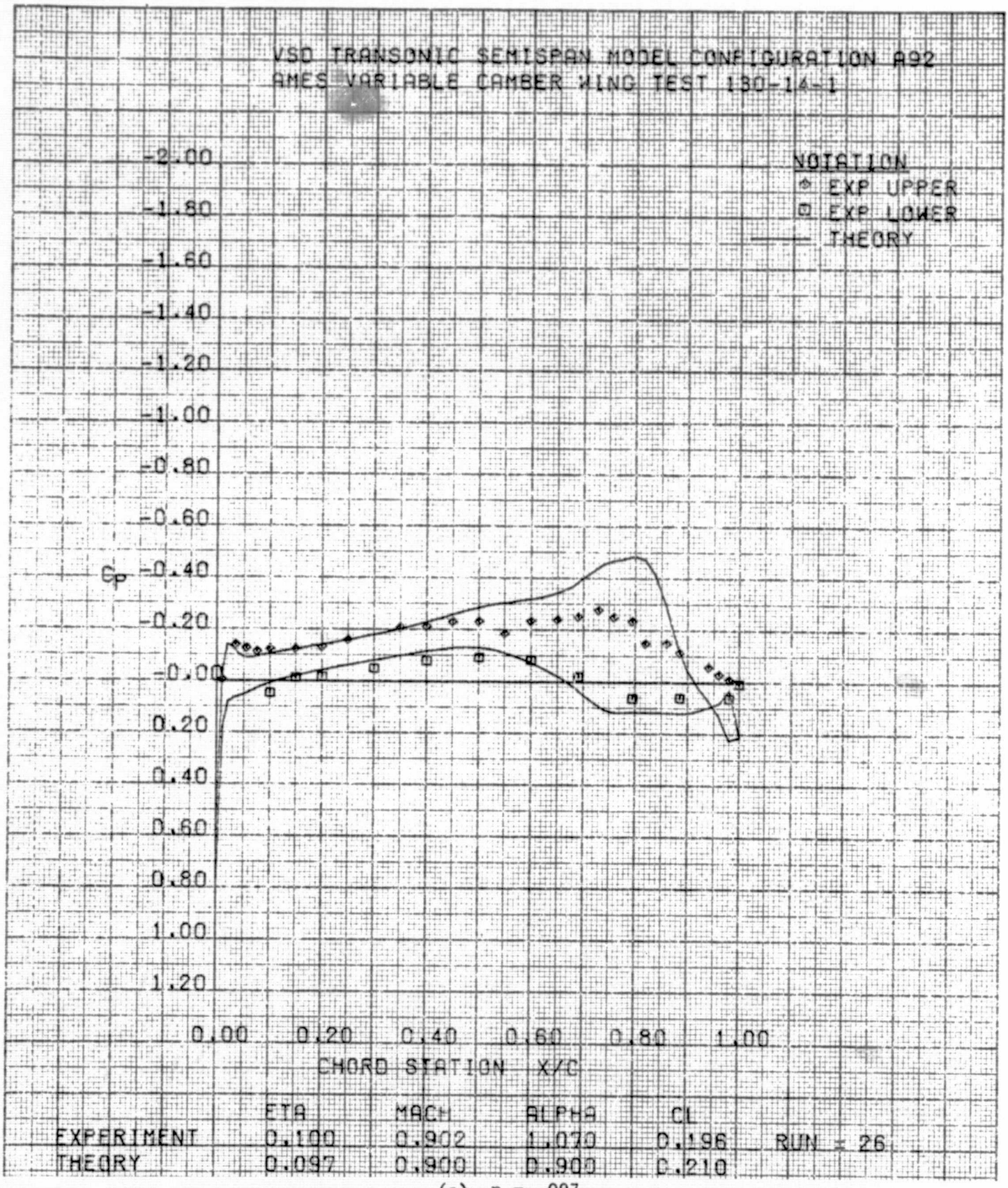

(a) η = .097

Figure 1 Comparison of Theoretical and Experimental Wing Pressures for Variable Camber Configuration A92 at C_L = .2

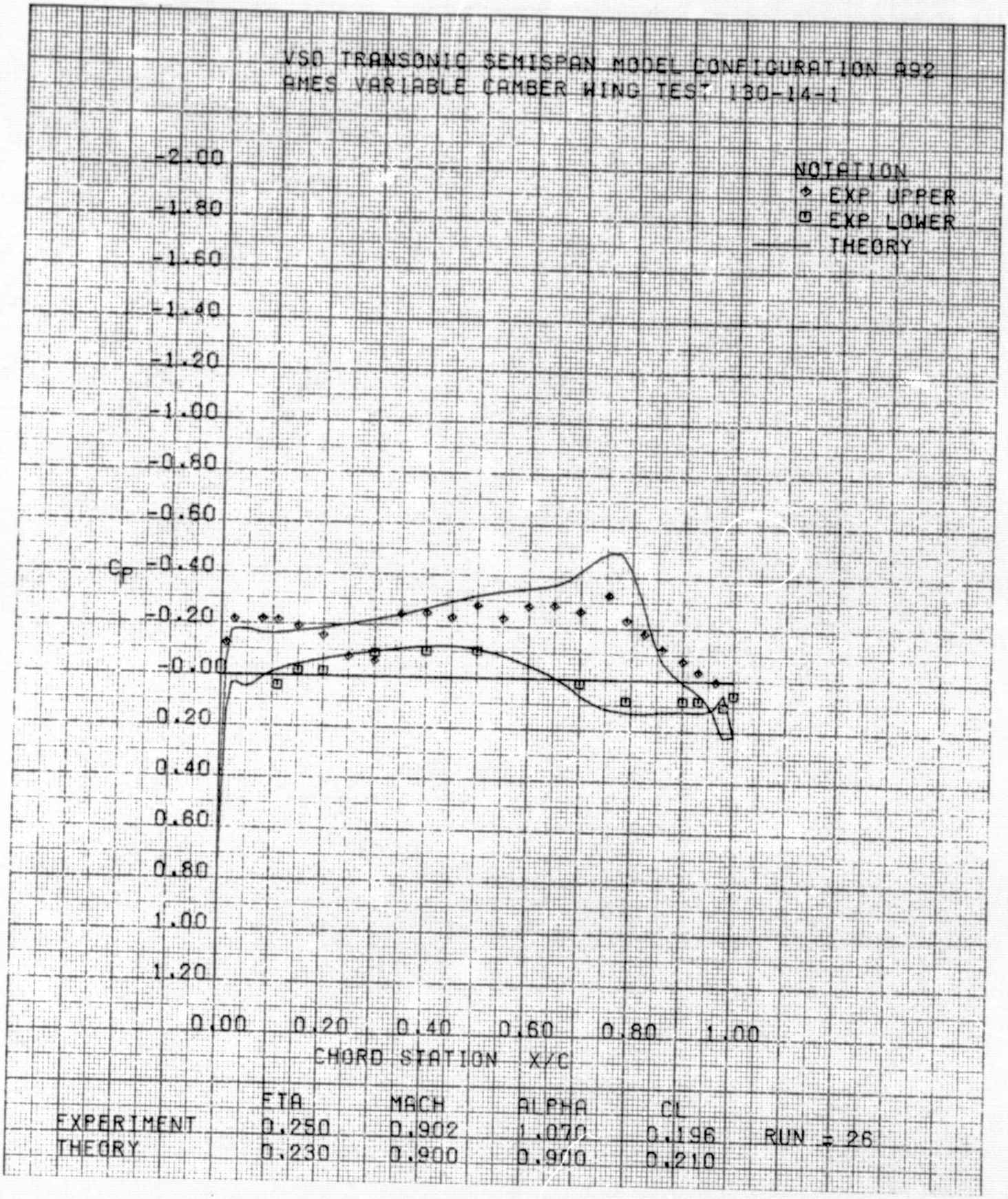

(b) η = .230

Figure 1 Continued

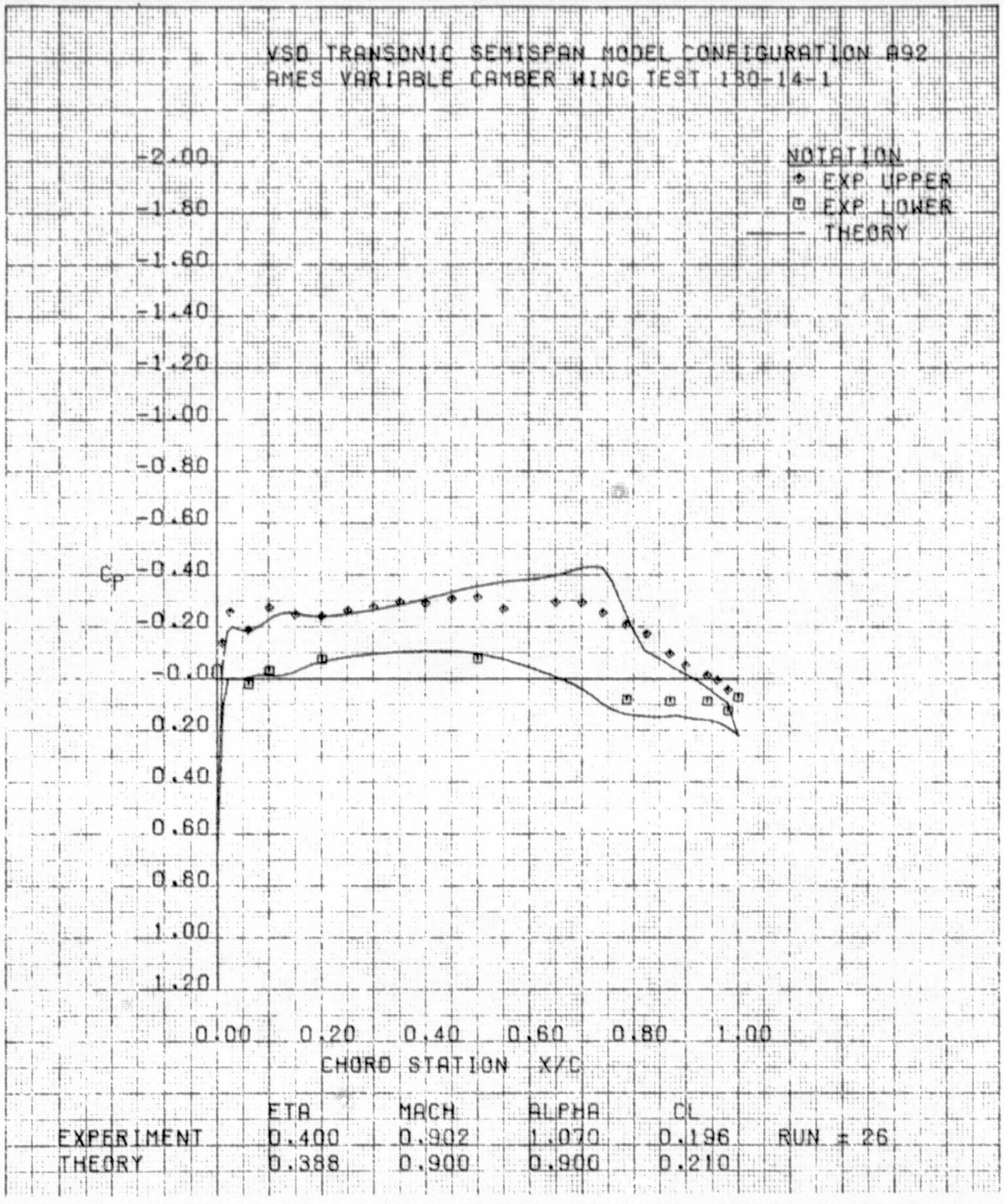

(c) η = .388

Figure 1 Continued

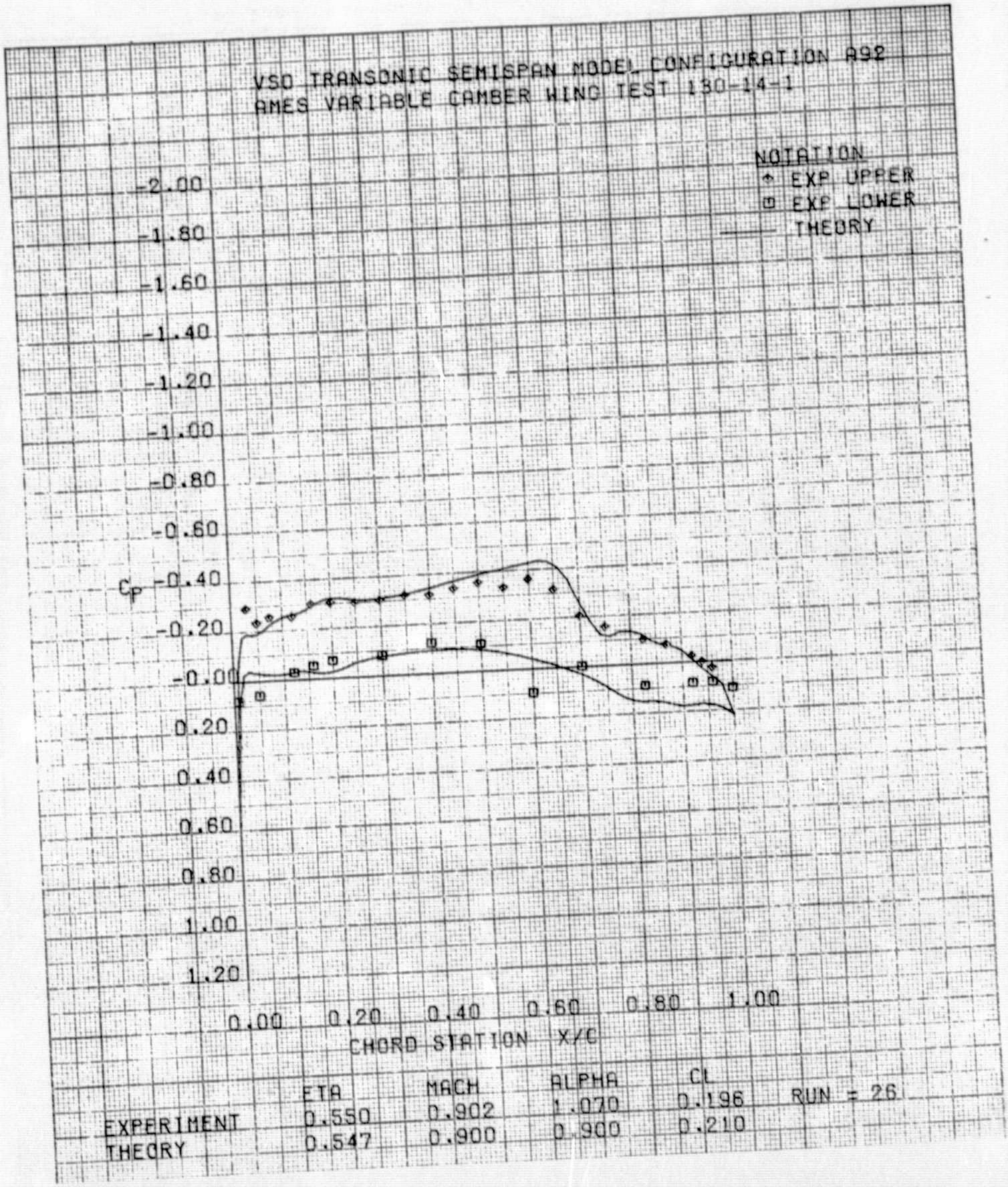

(d) $\eta = .547$

Figure 1 Continued

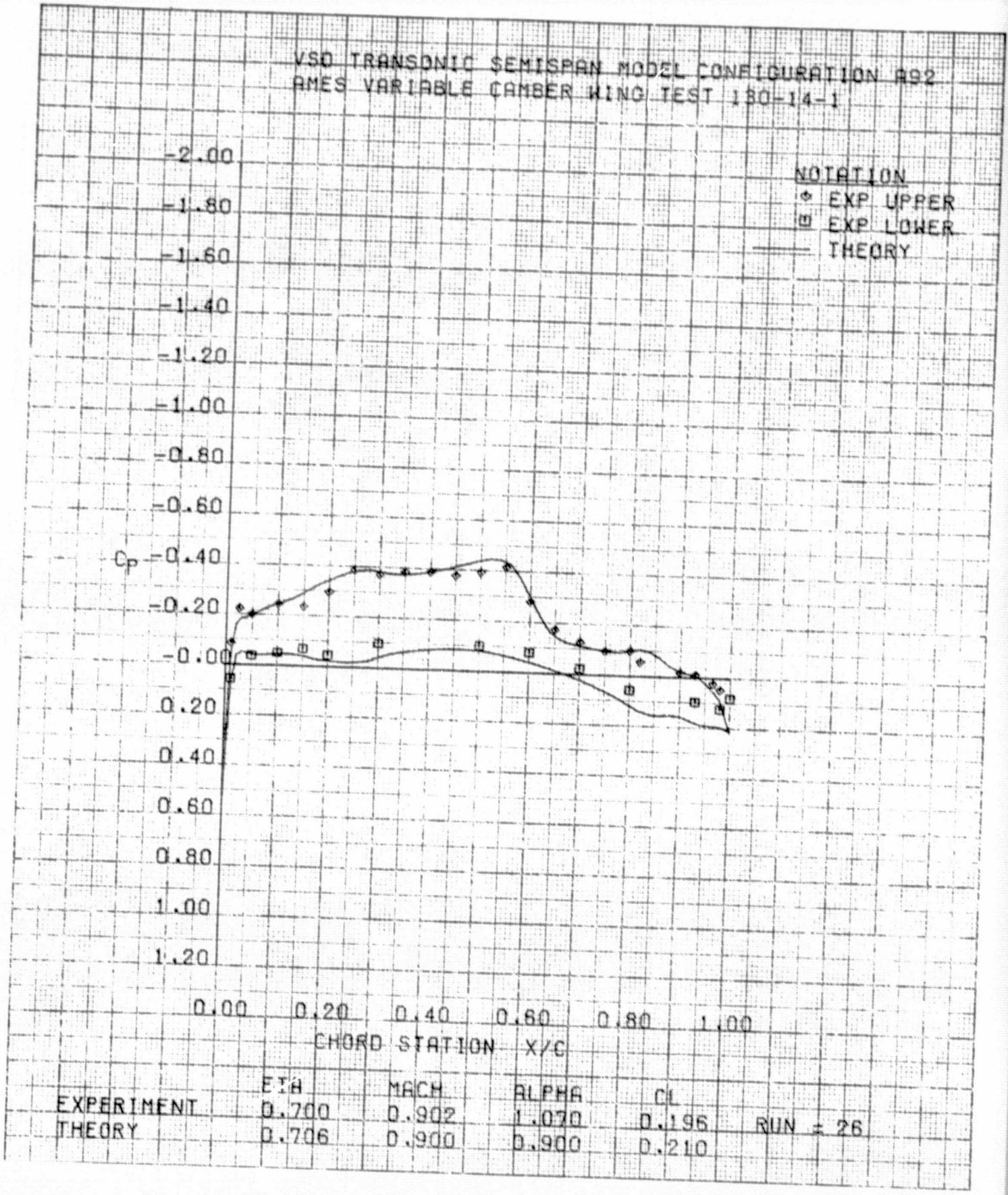

(e) η = .706

Figure 1 Continued

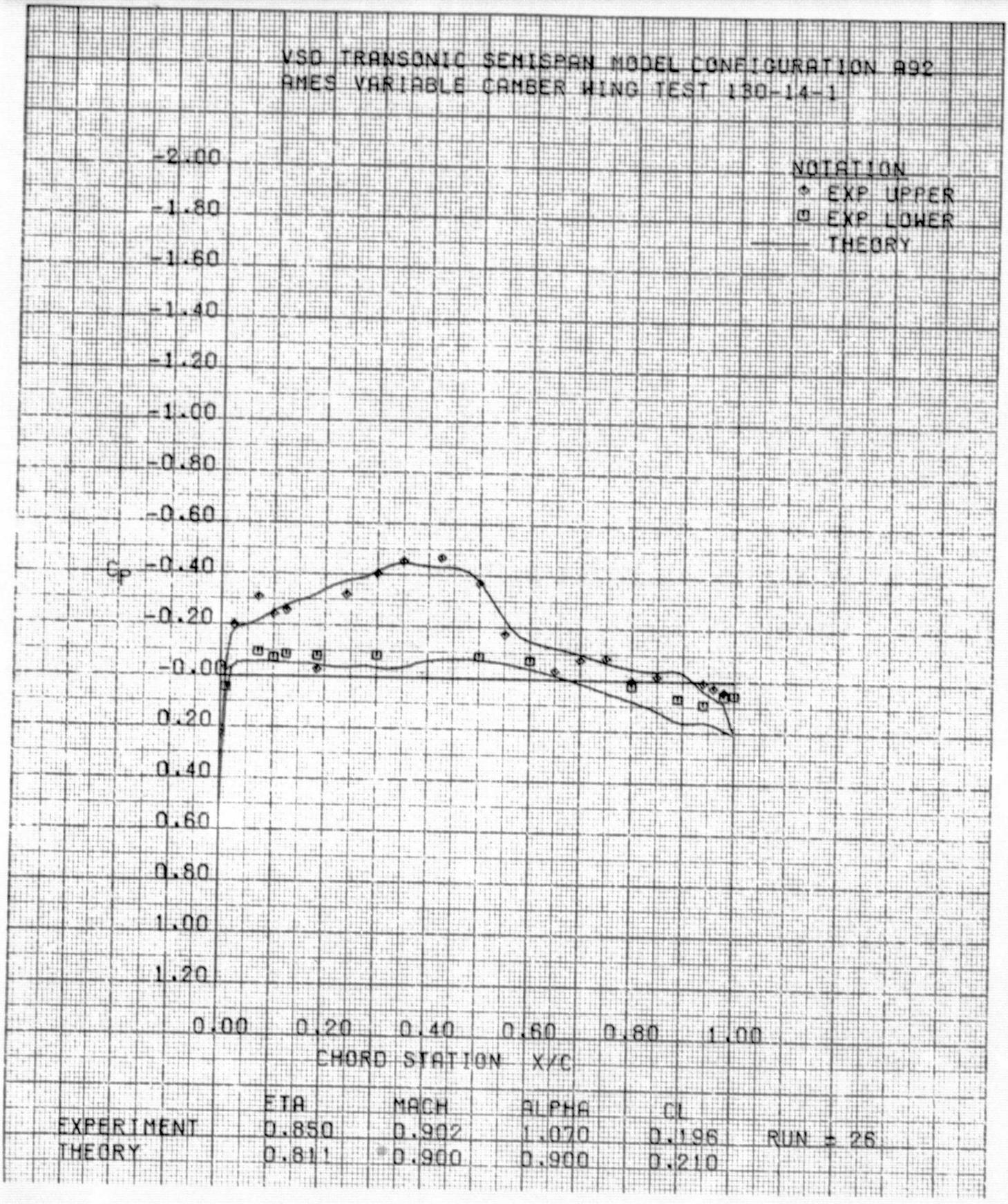

(f) η = .811

Figure 1 Continued

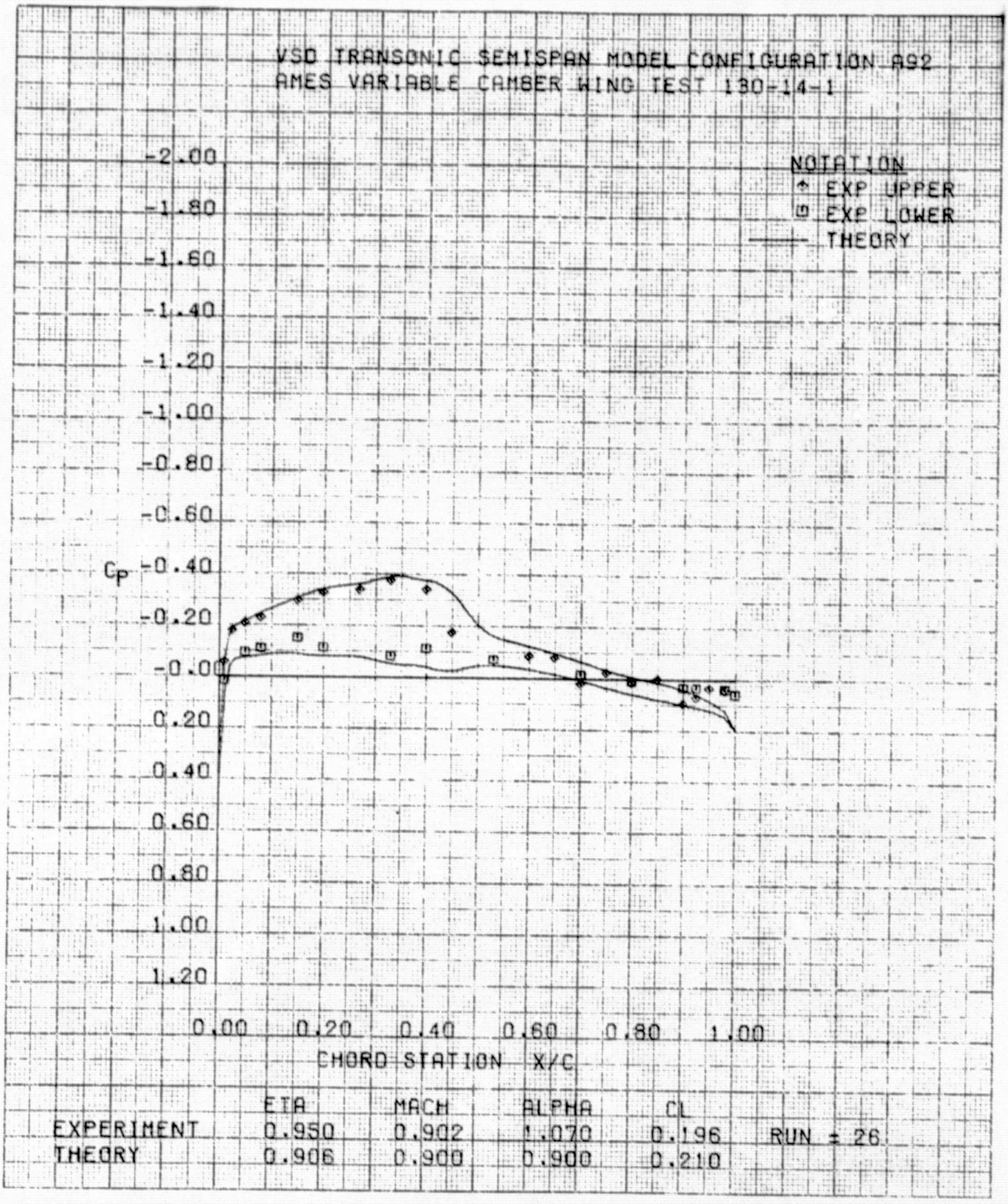

(g) η = .906

Figure 1 Concluded

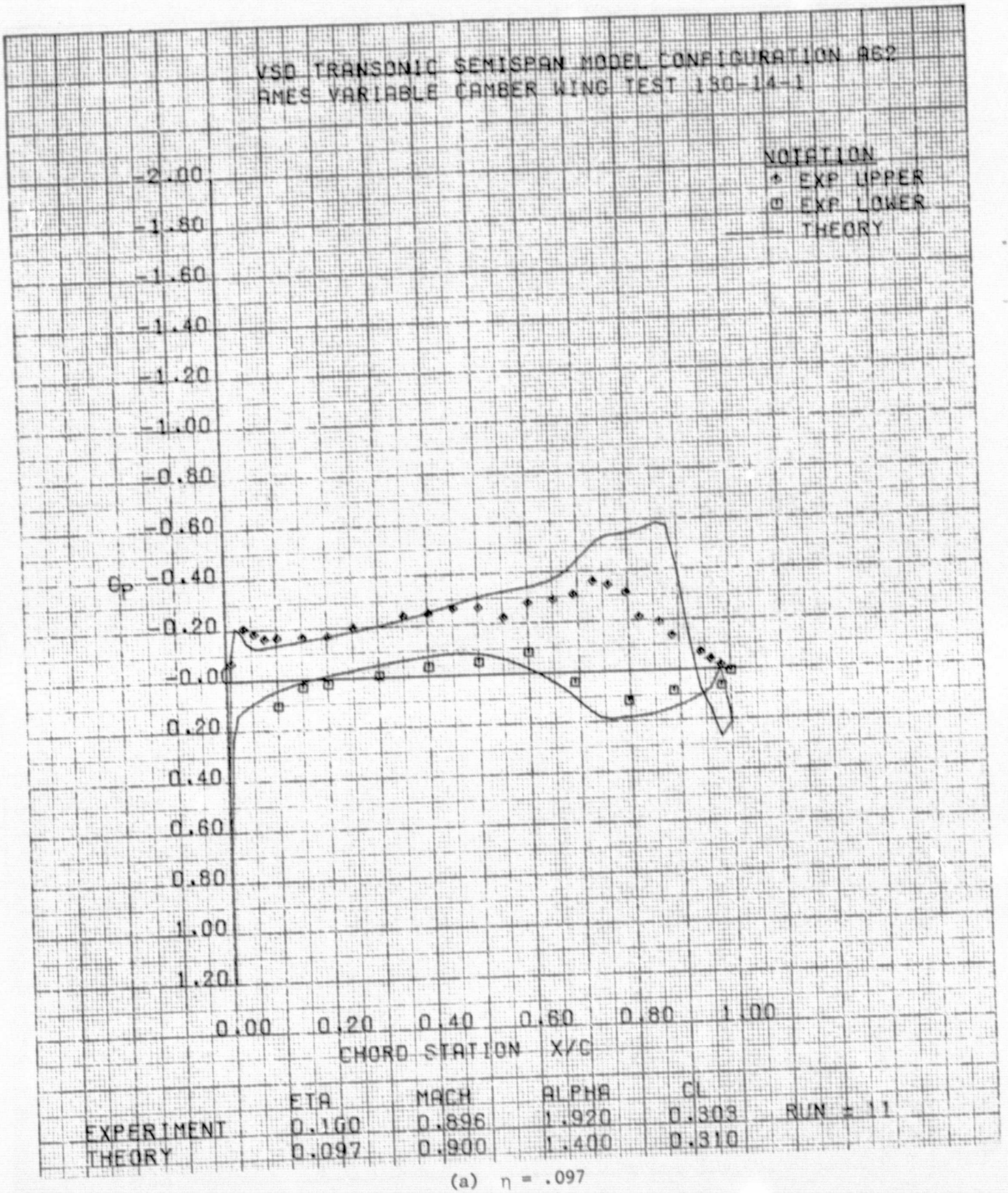

(a) η = .097

Figure 2 Comparison of Theoretical and Experimental Wing Pressures for Variable Camber Configuration A62 at C_L = .3

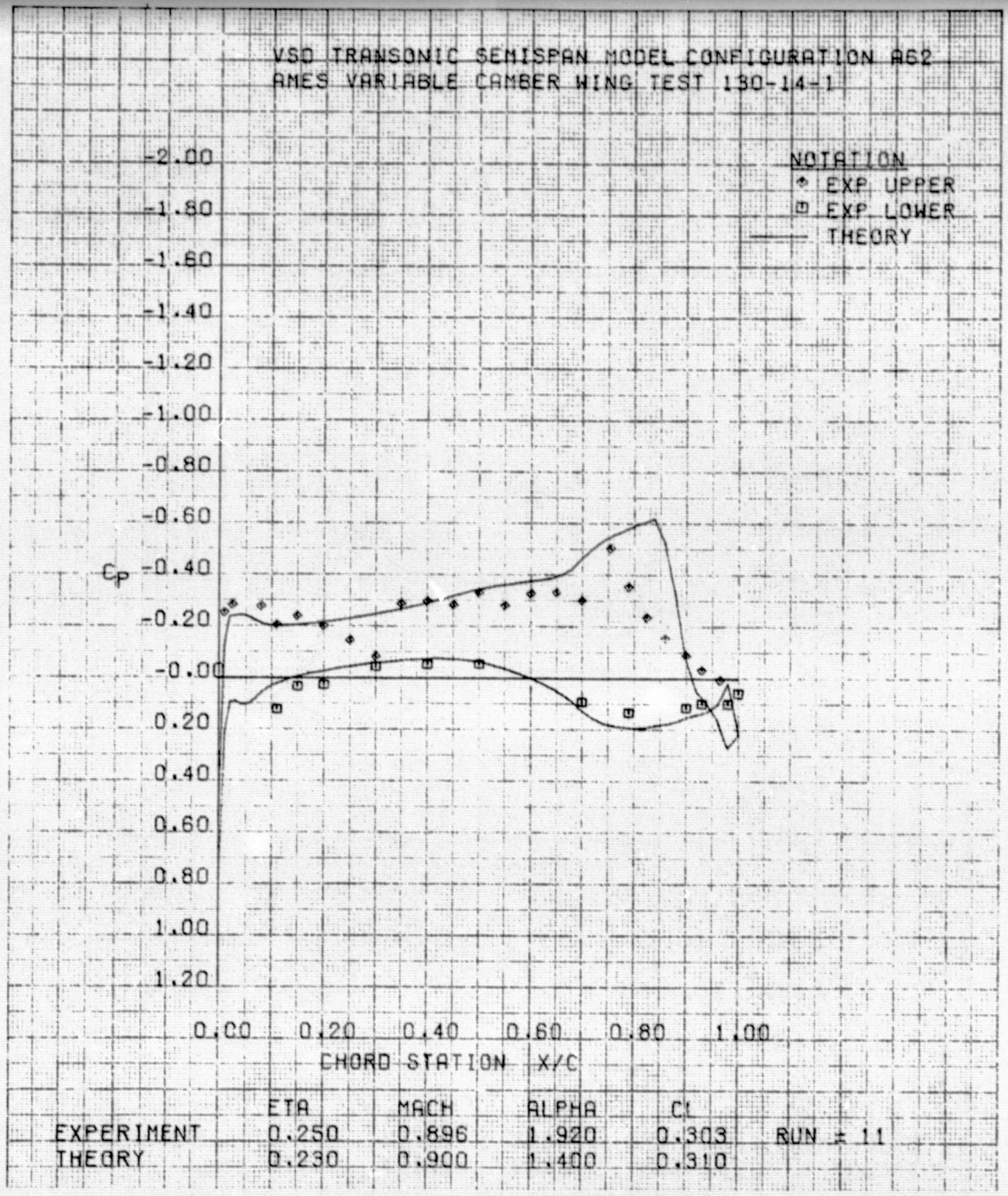

(b) η = .230

Figure 2 Continued

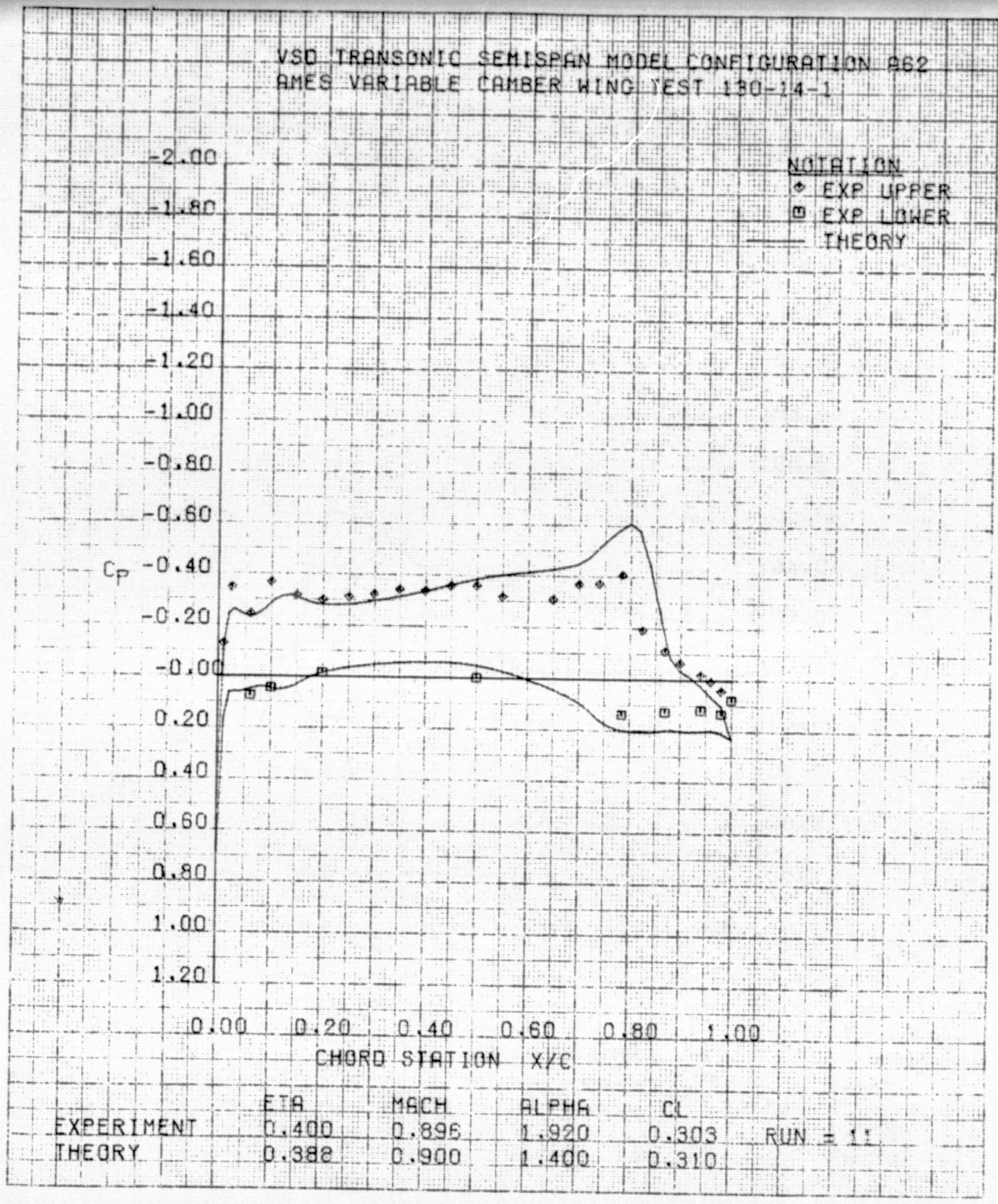

(c) η = .388

Figure 2 Continued

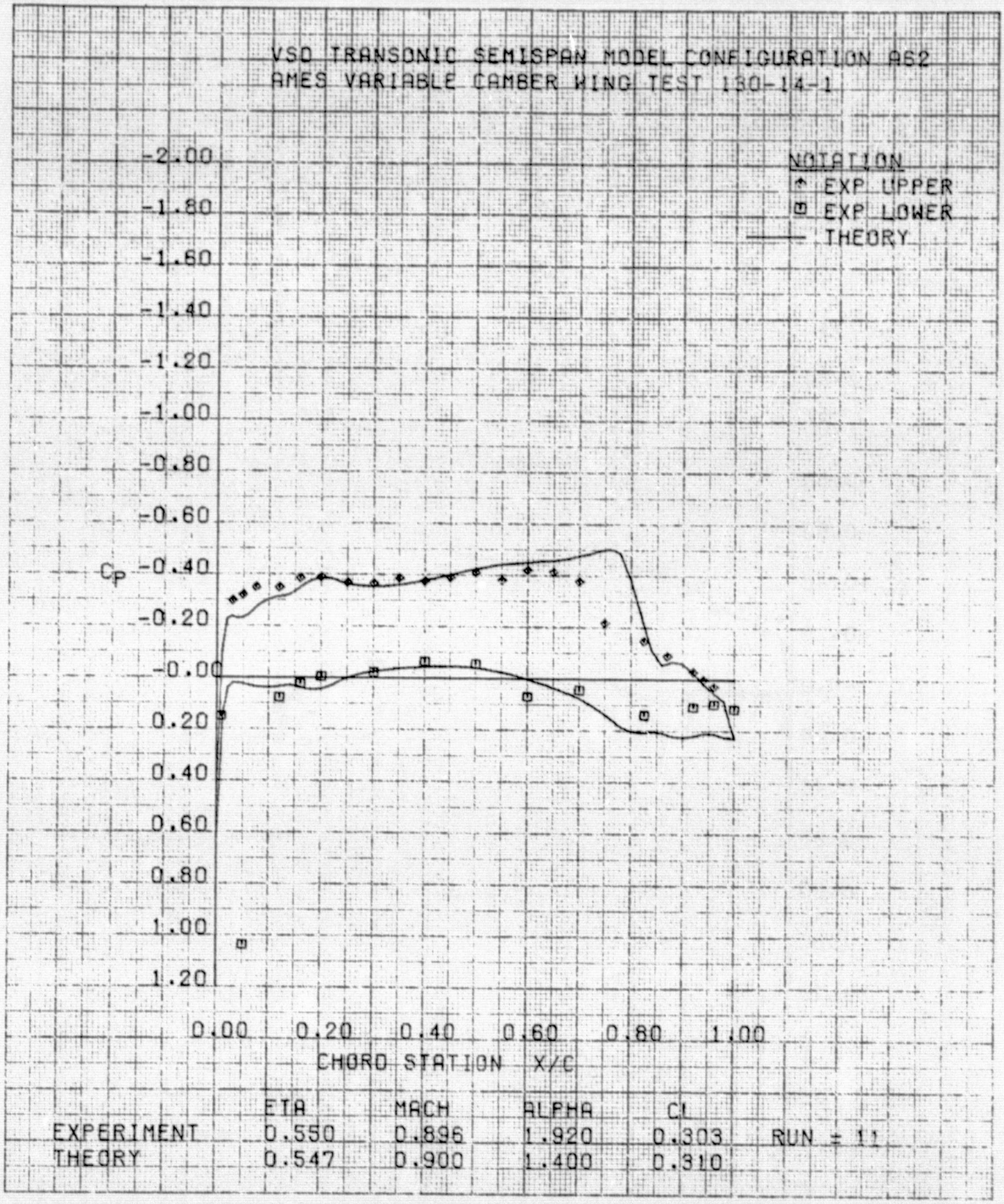

(d) η = .547

Figure 2 Continued

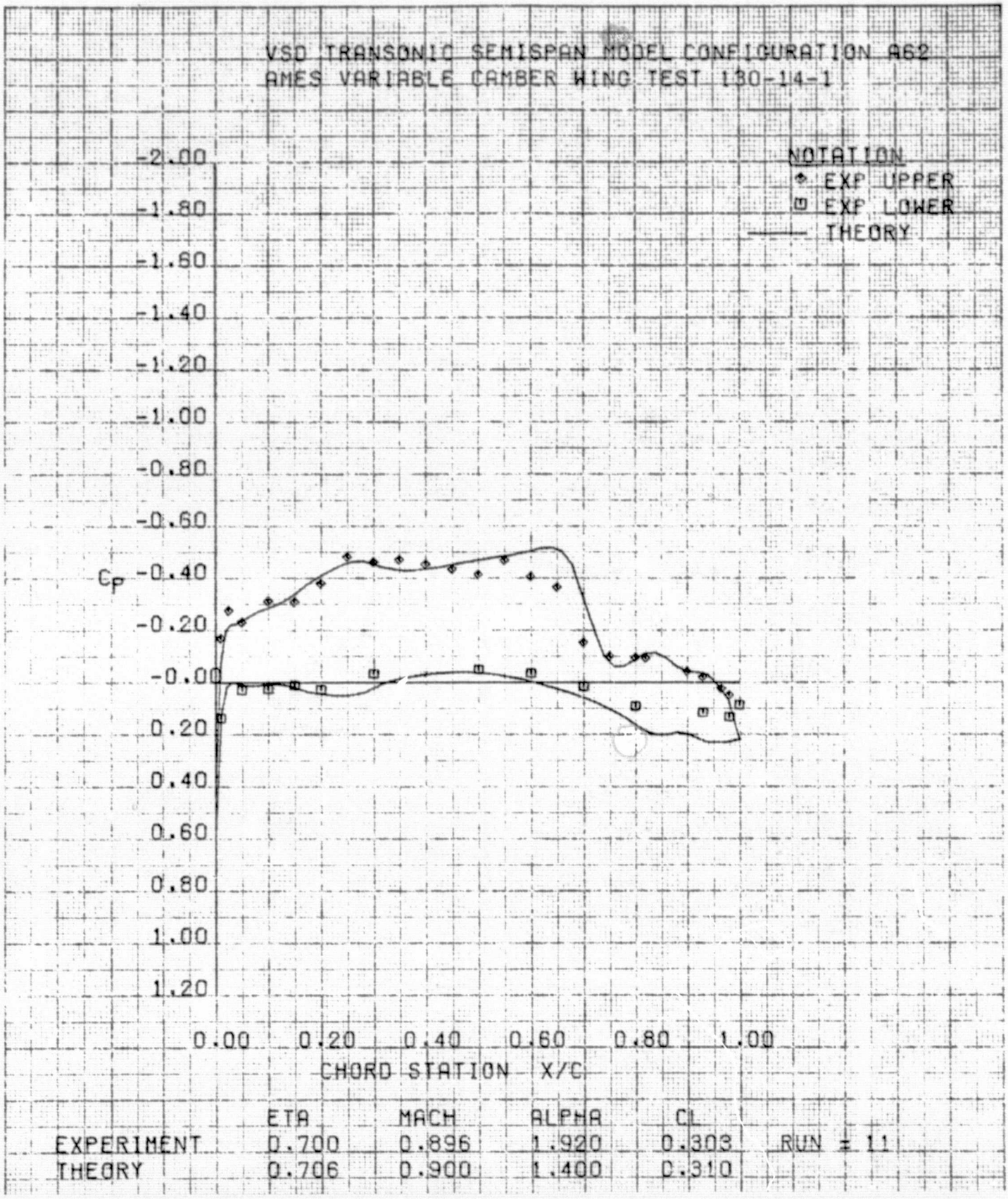

(e) η = .706

Figure 2 Continued

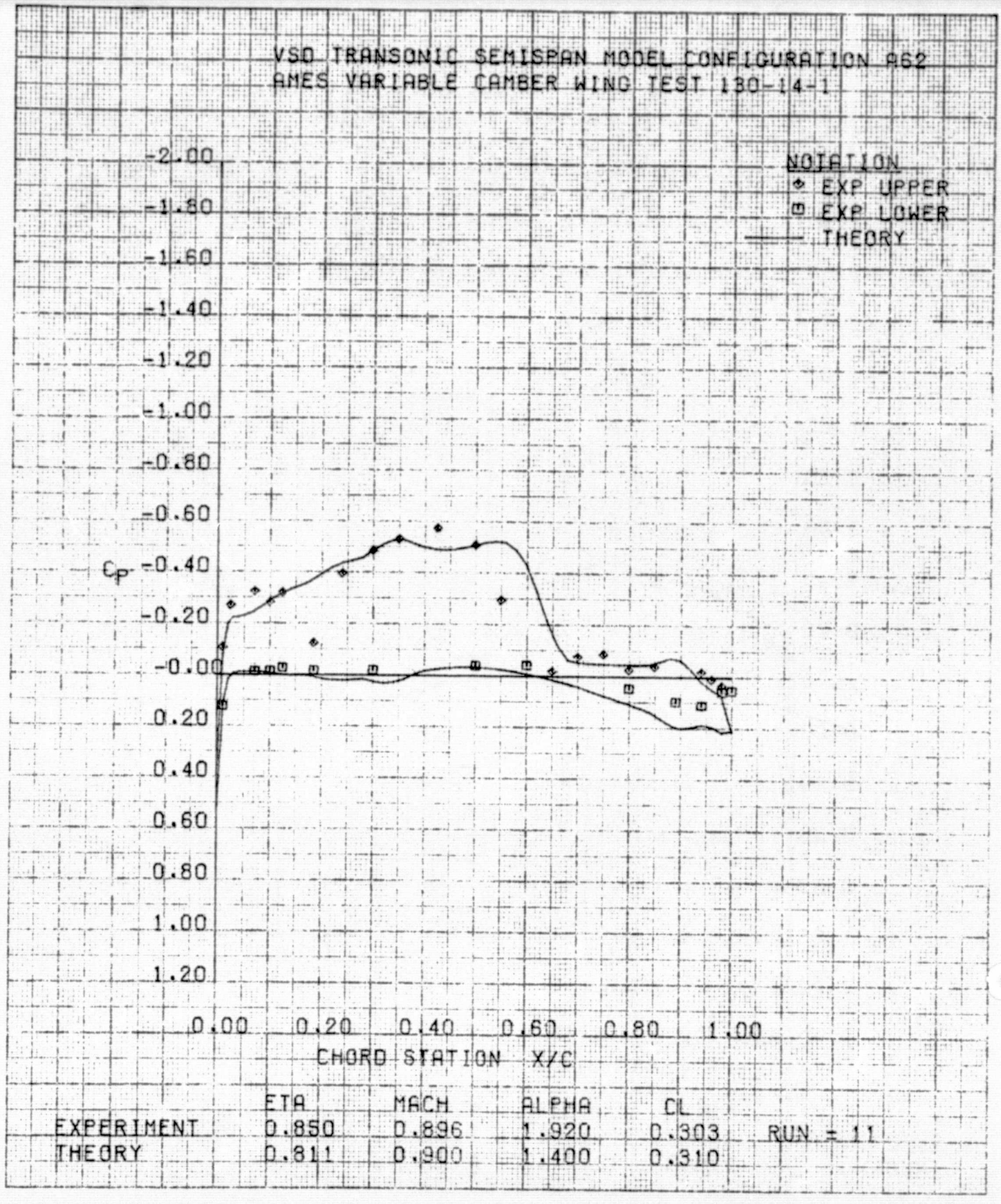

(f) η = .811

Figure 2 Continued

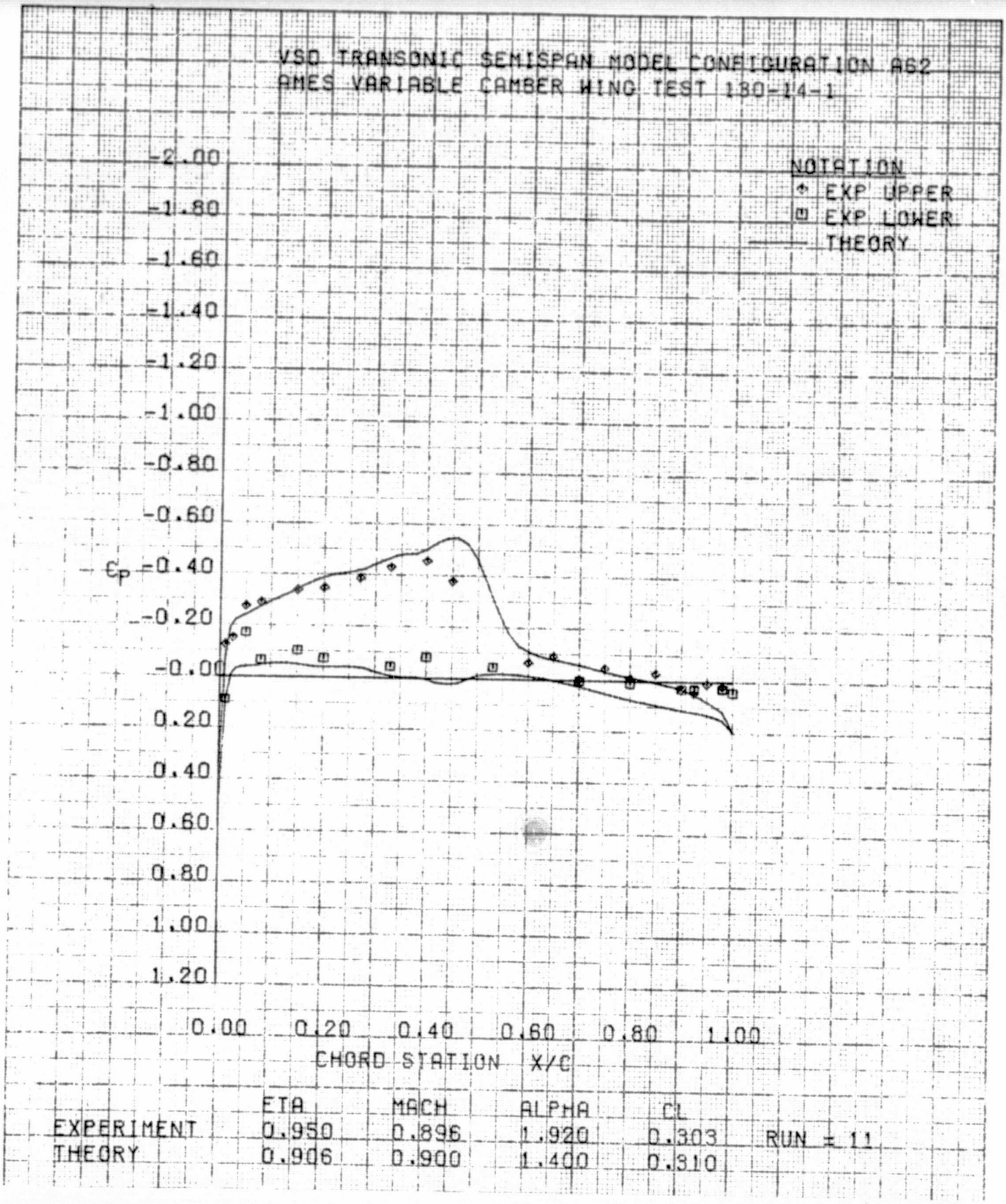

(g) η = .906

Figure 2 Concluded

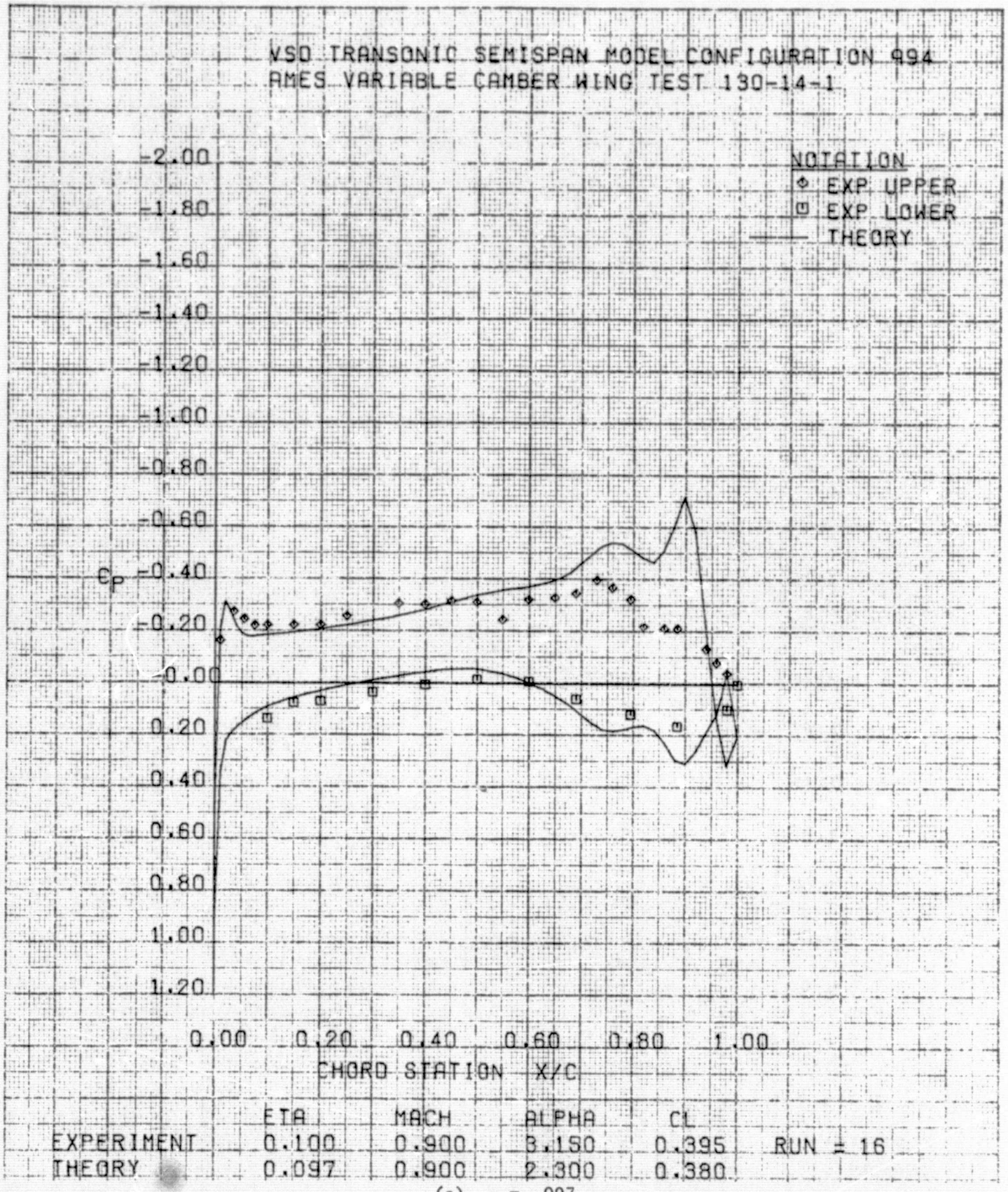

(a) η = .097

Figure 3 Comparison of Theoretical and Experimental Wing Pressures for Variable Camber Configuration A94 at C_L = .4

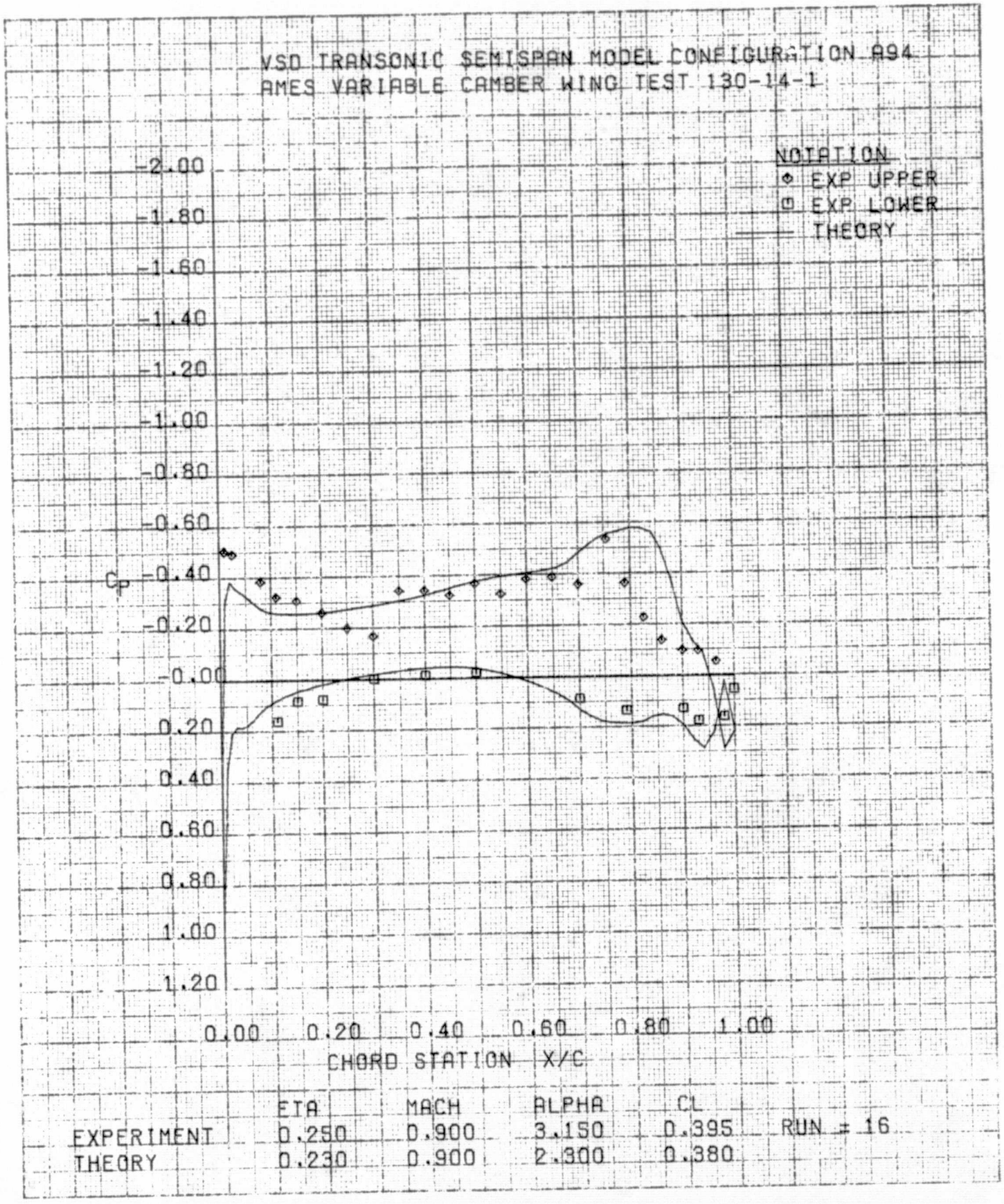

(b) η = .230

Figure 3 Continued

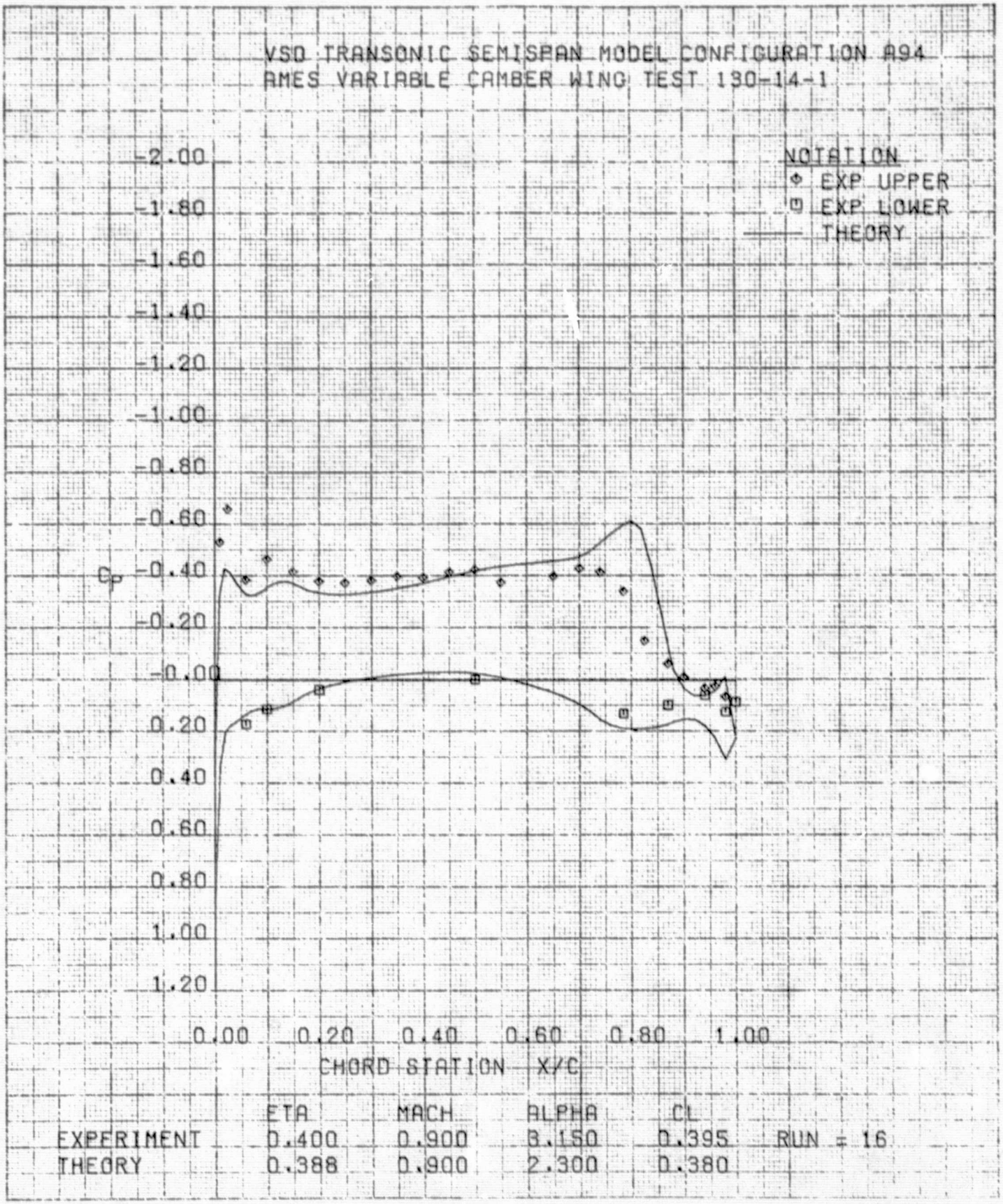

(c) η = .388

Figure 3 Continued

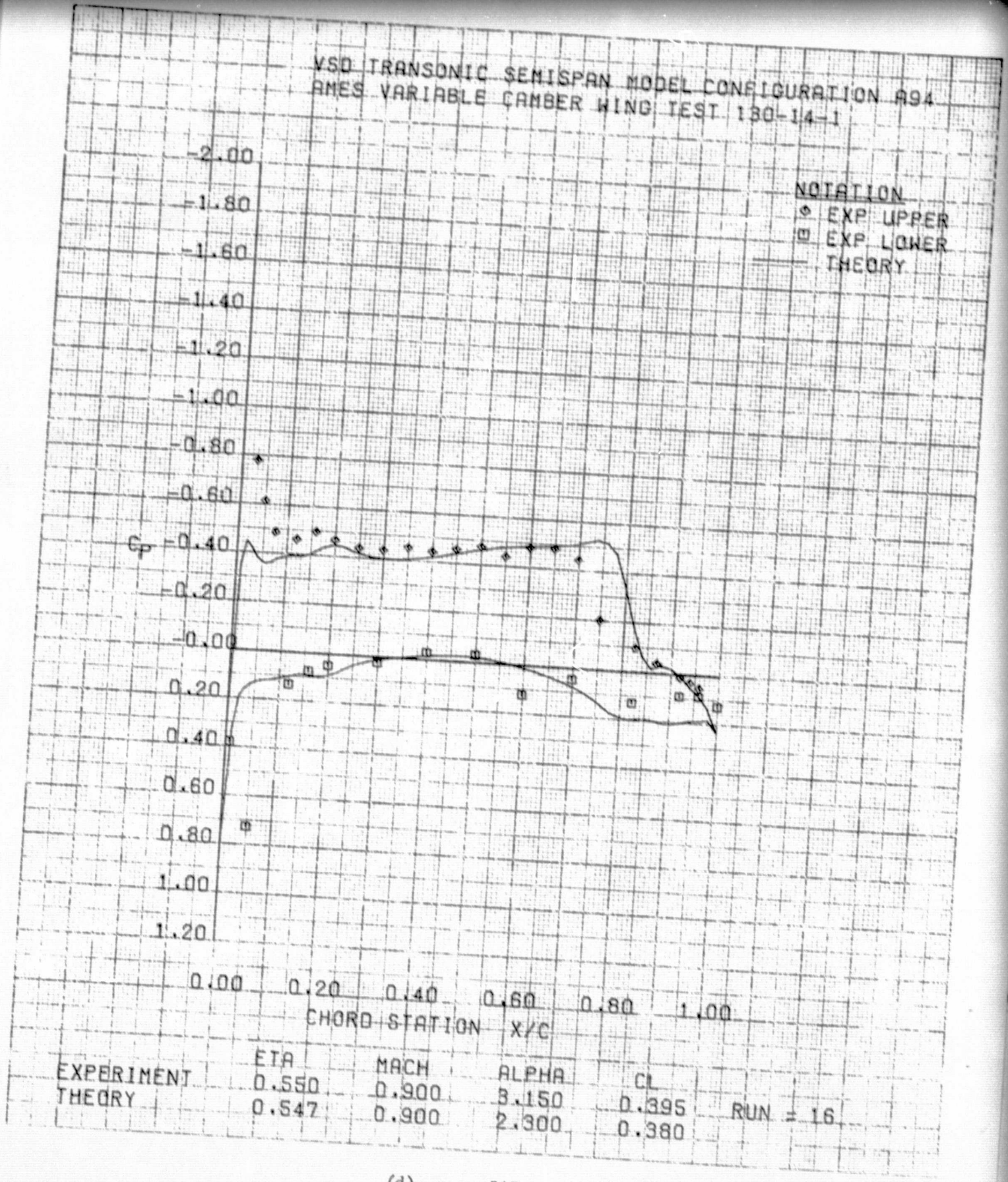

(d) $\eta = .547$

Figure 3 Continued

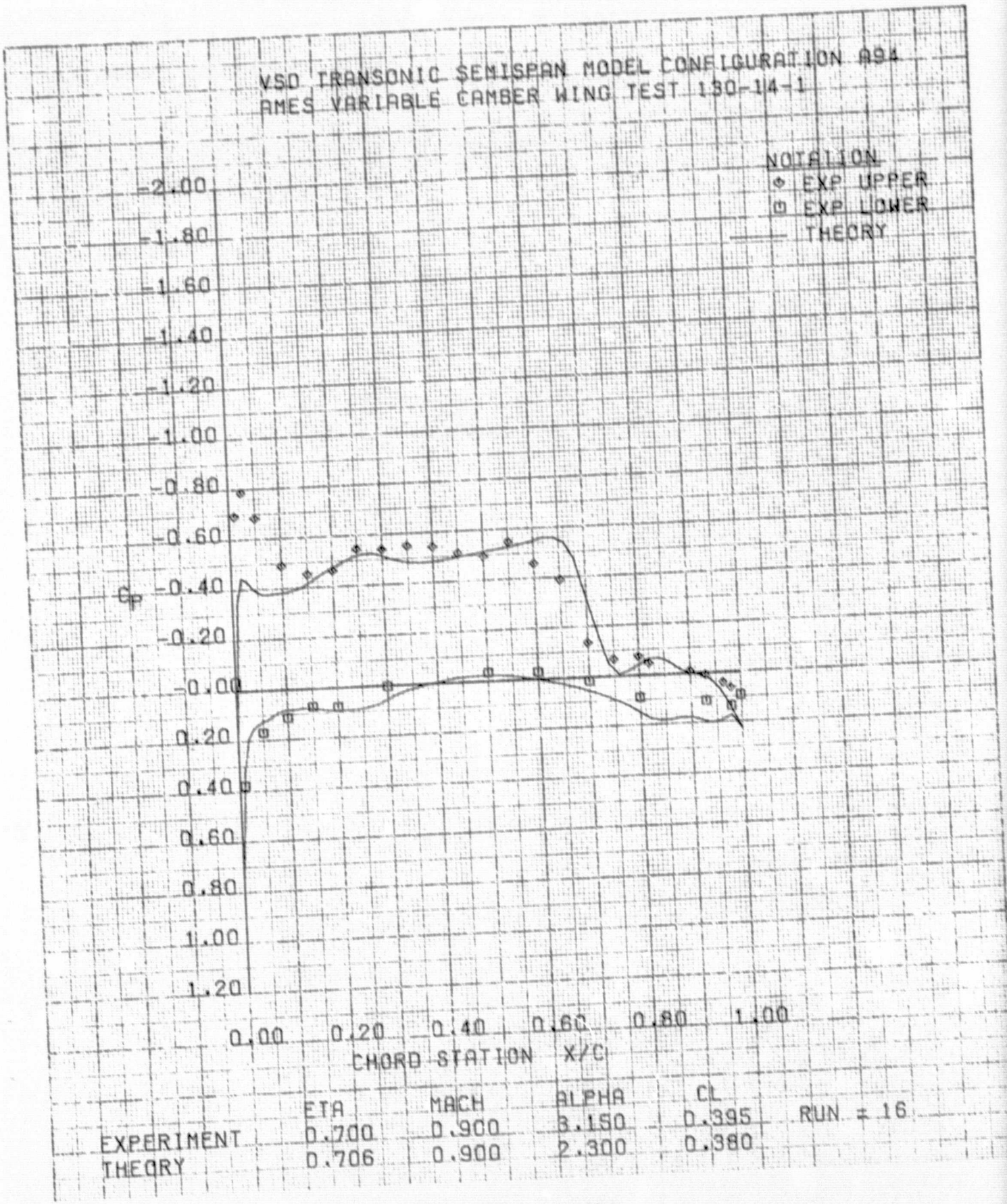

(e) $\eta = .706$

Figure 3 Continued

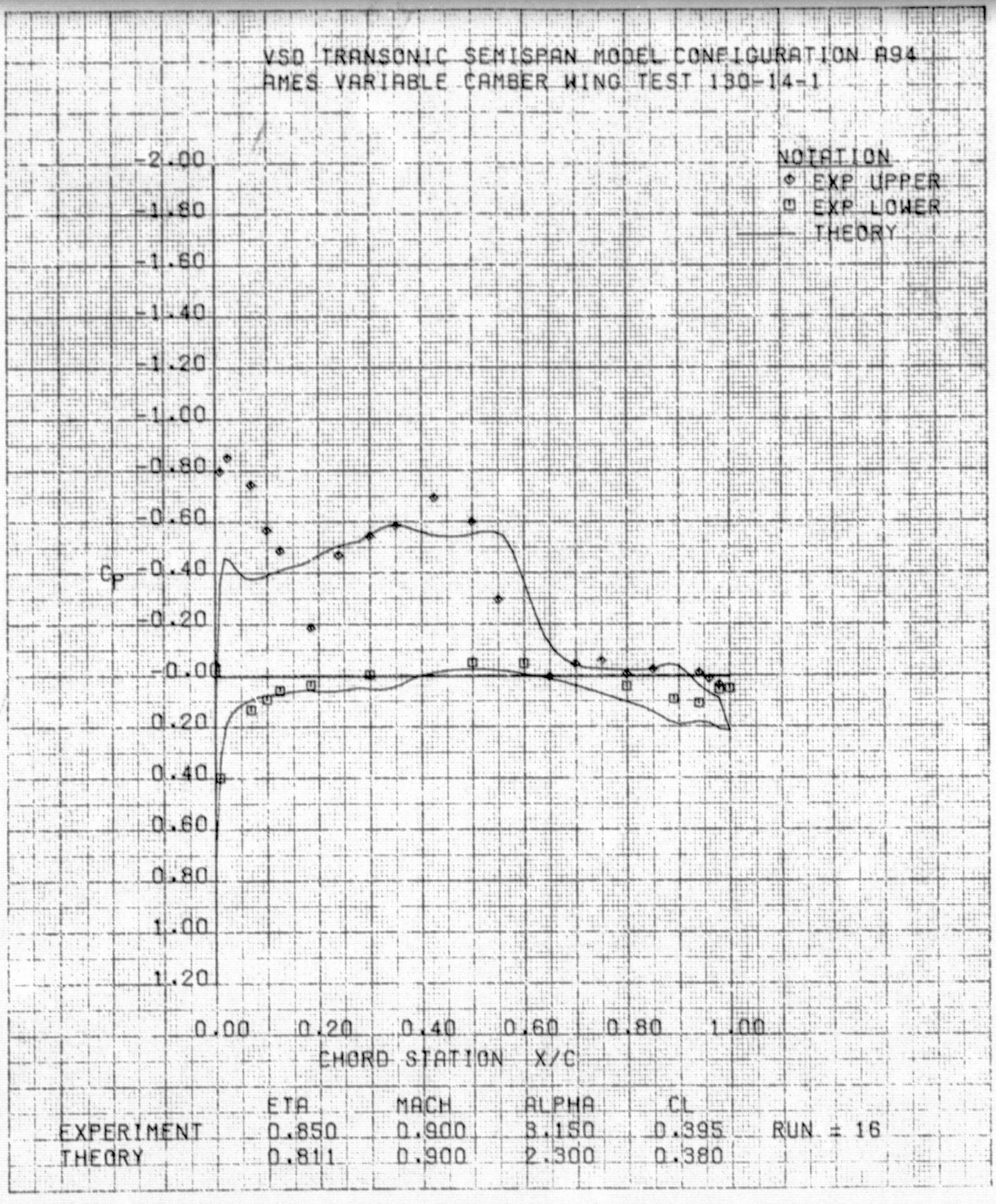

(f) η = .811

Figure 3 Continued

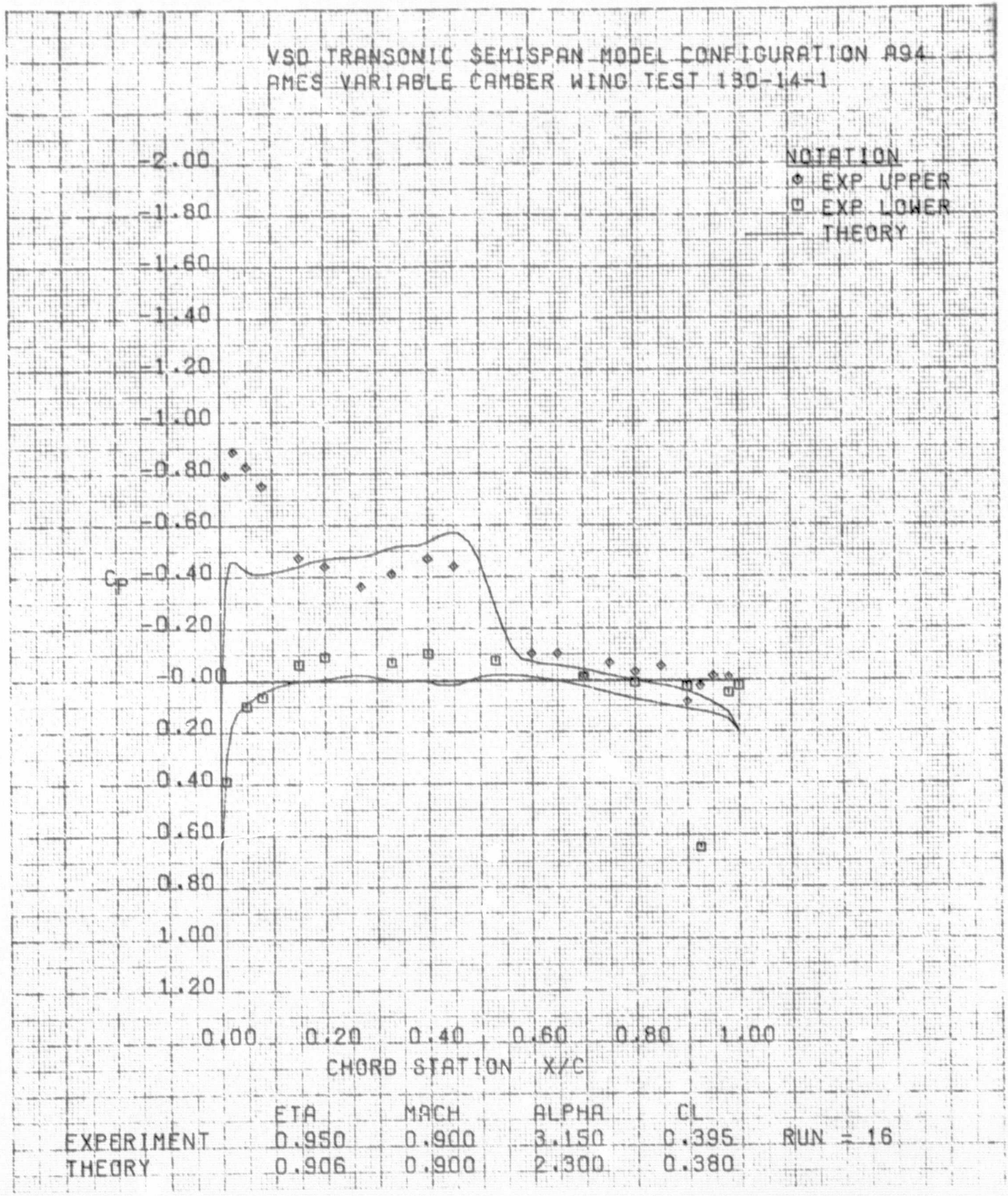

(g) η = .906

Figure 3 Concluded

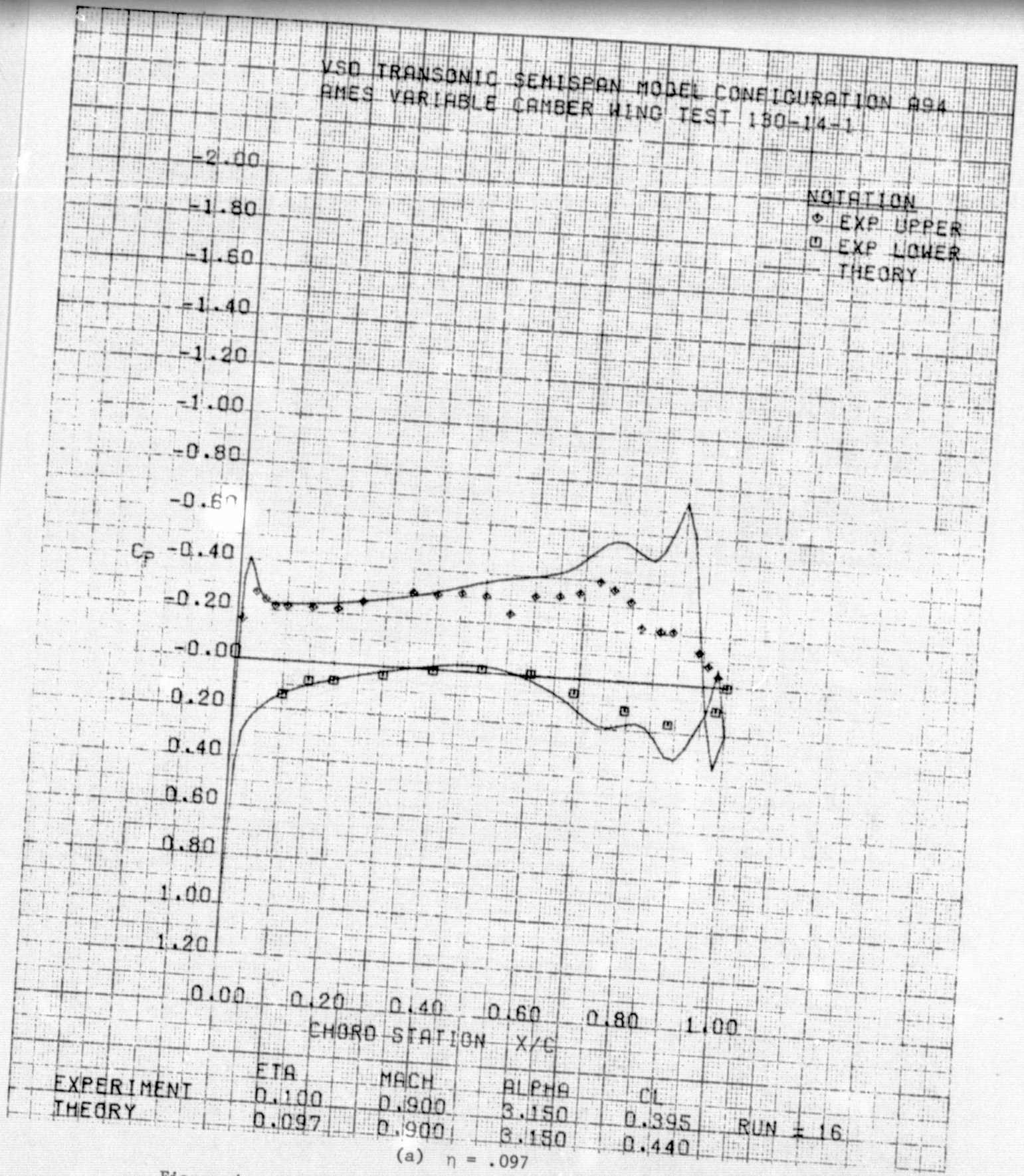

(a) η = .097

Figure 4 Comparison of Theoretical and Experimental Wing Pressures for Variable Camber Configuration A94 at $\alpha = 3.15^{o}$

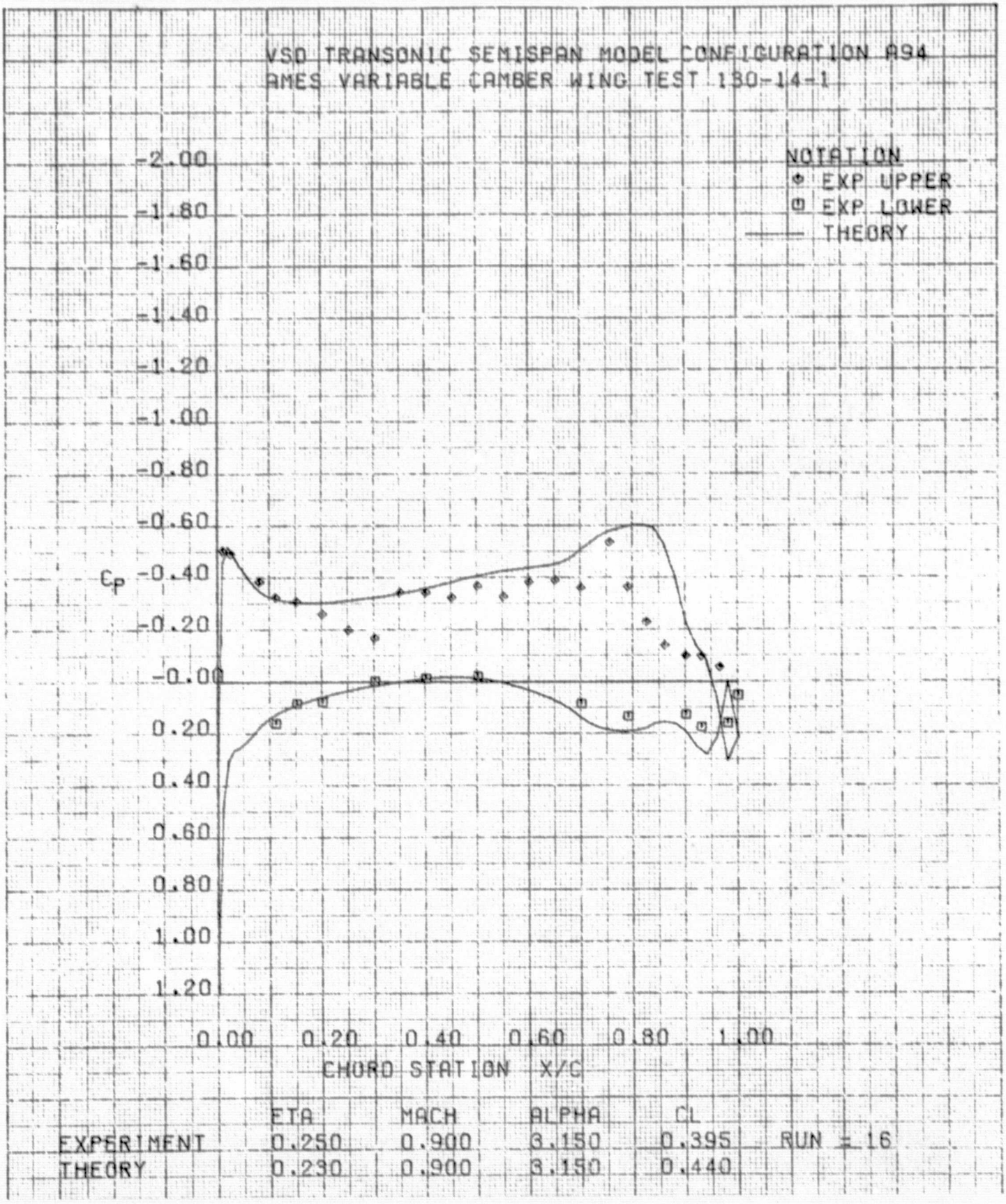

(b) η = .230

Figure 4 Continued

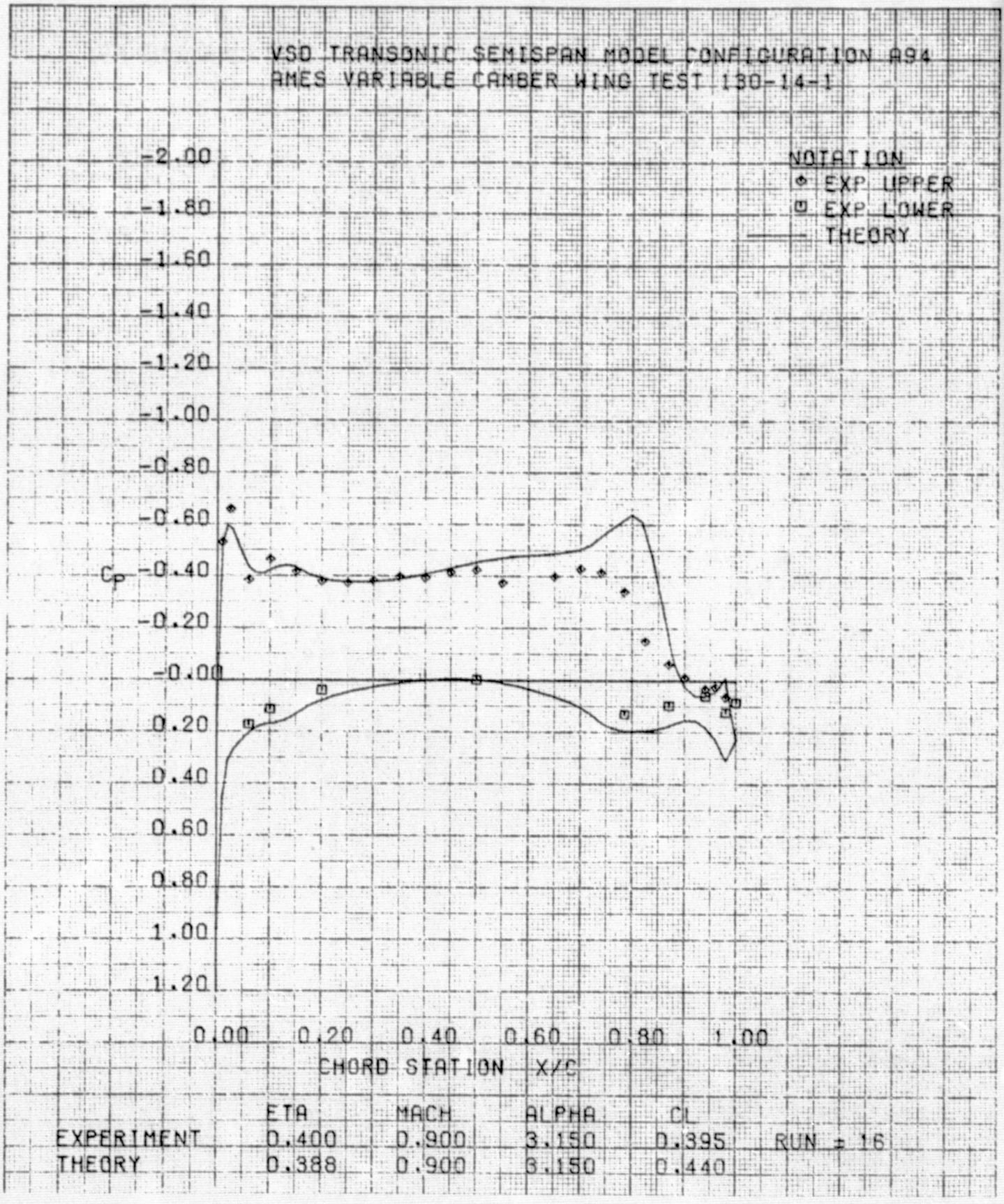

(c) η = .388

Figure 4 Continued

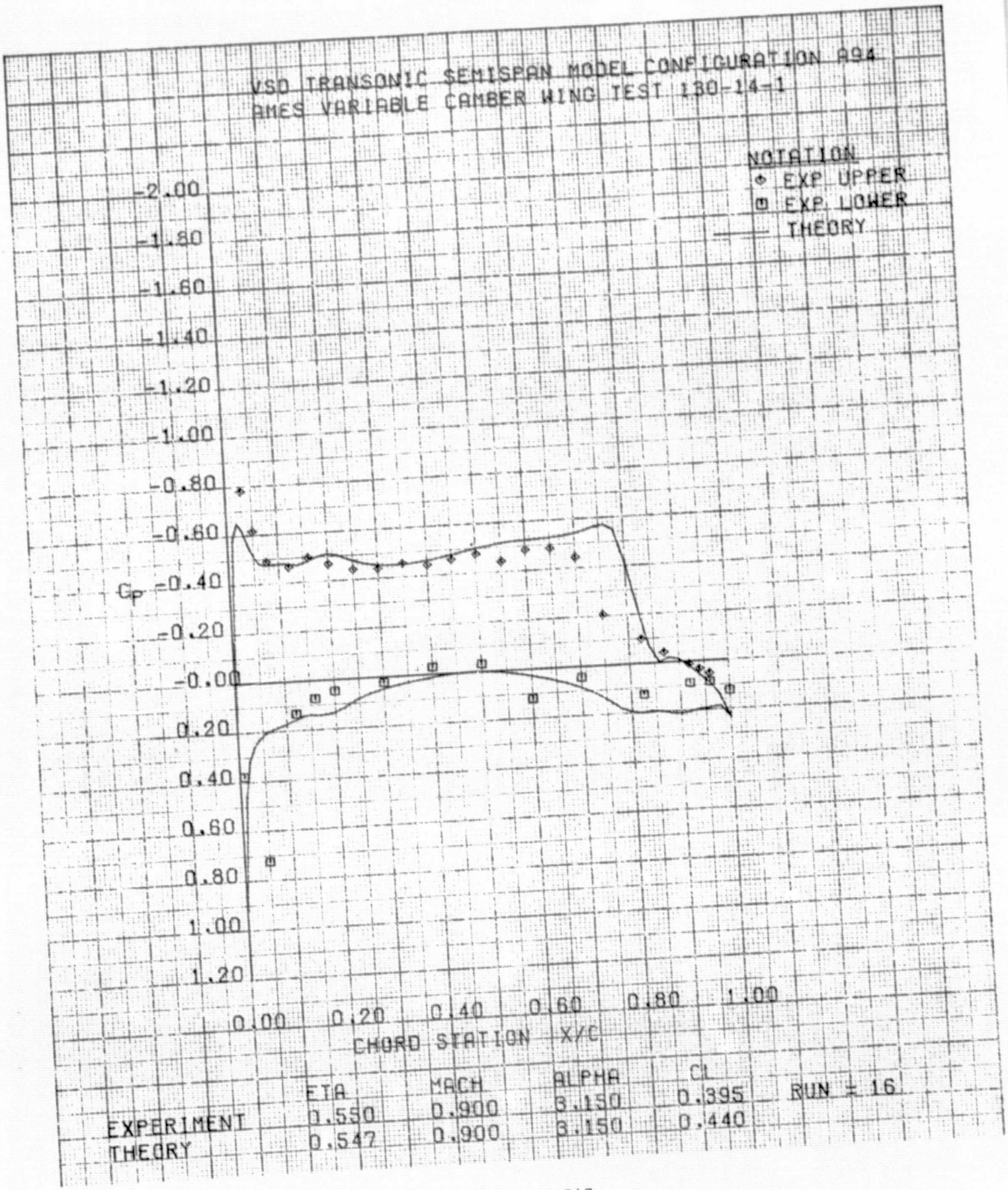

(d) η = .547

Figure 4 Continued

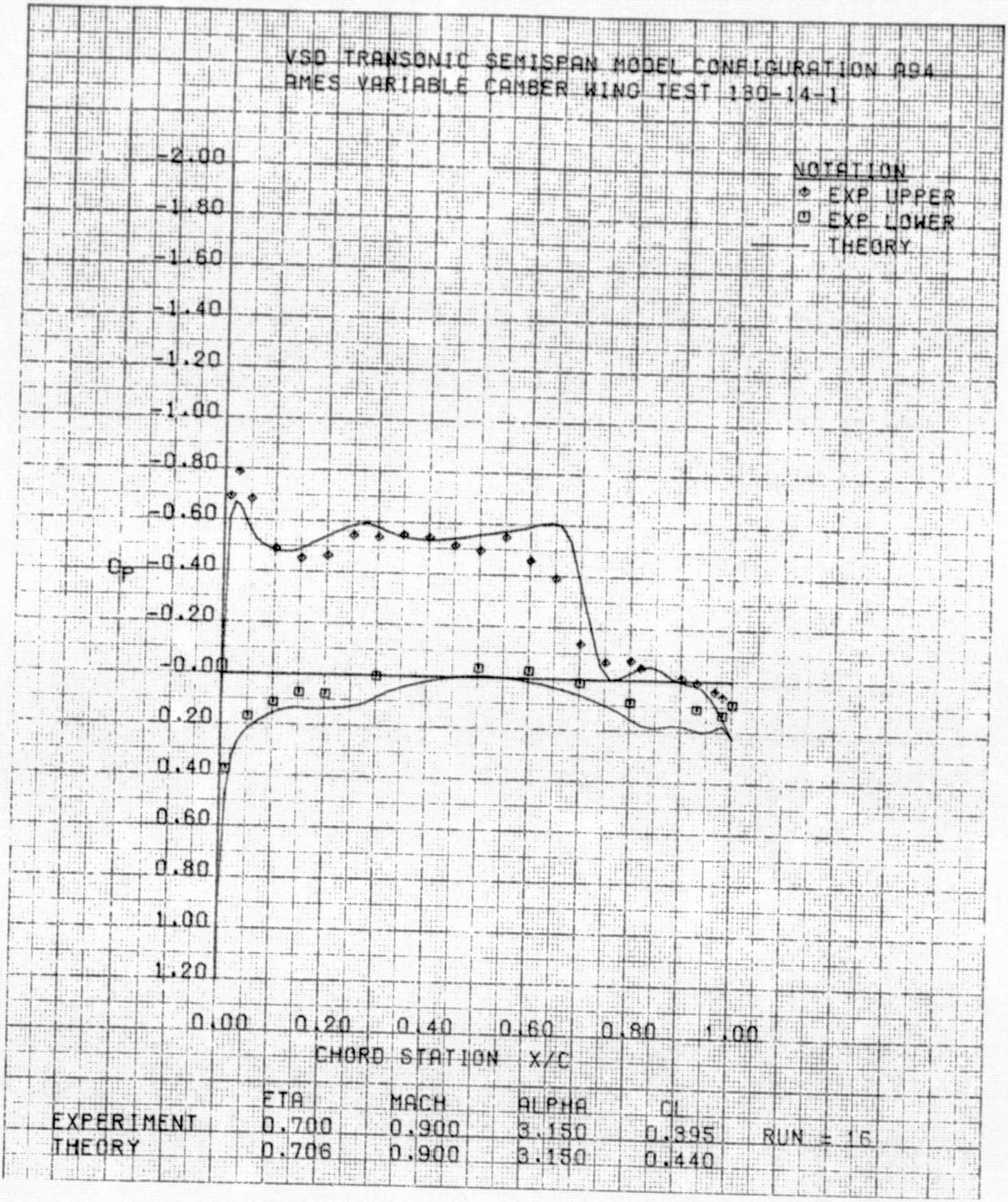

(e) η = .706

Figure 4 Continued

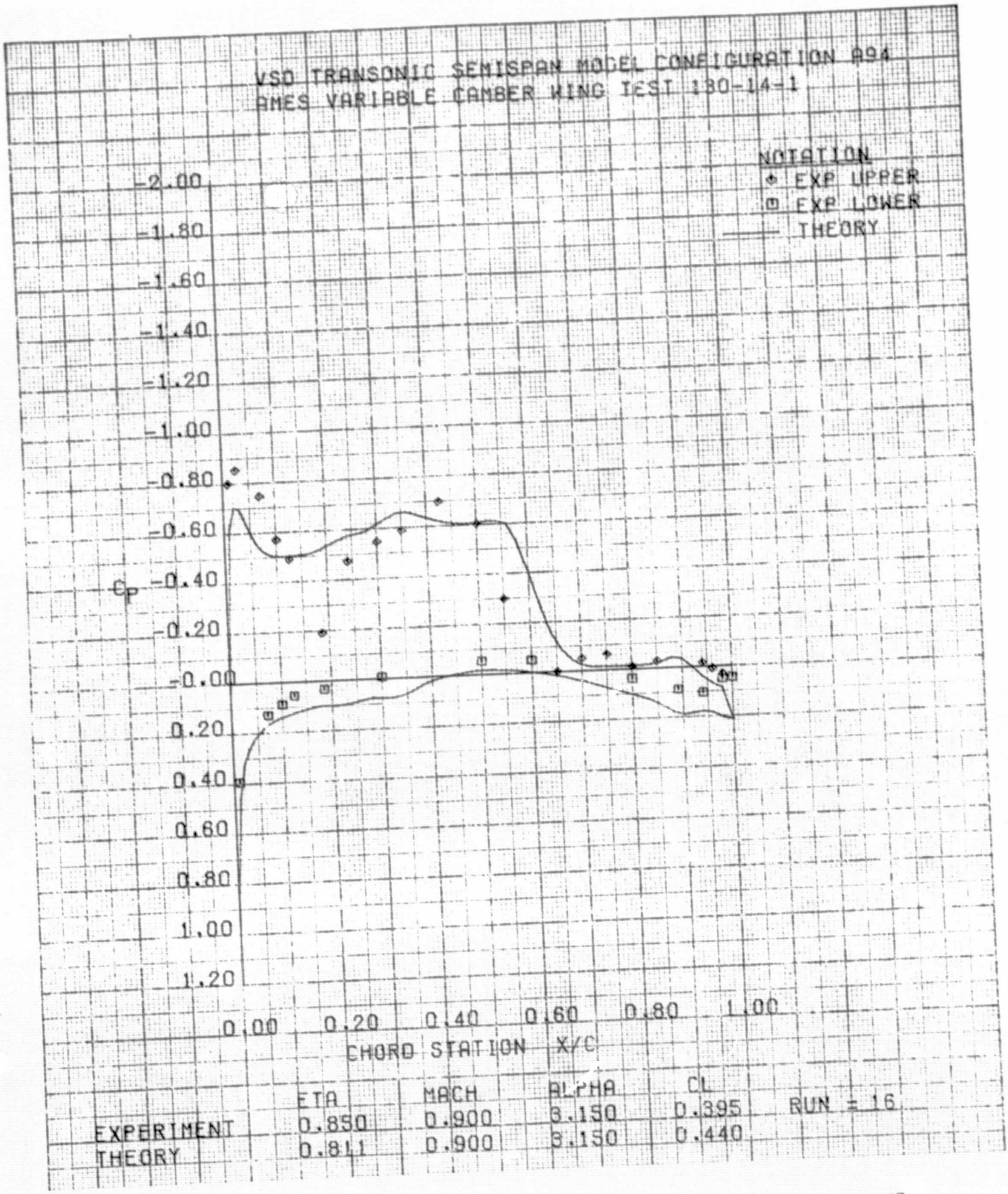

(f) η = .811

Figure 4 Continued

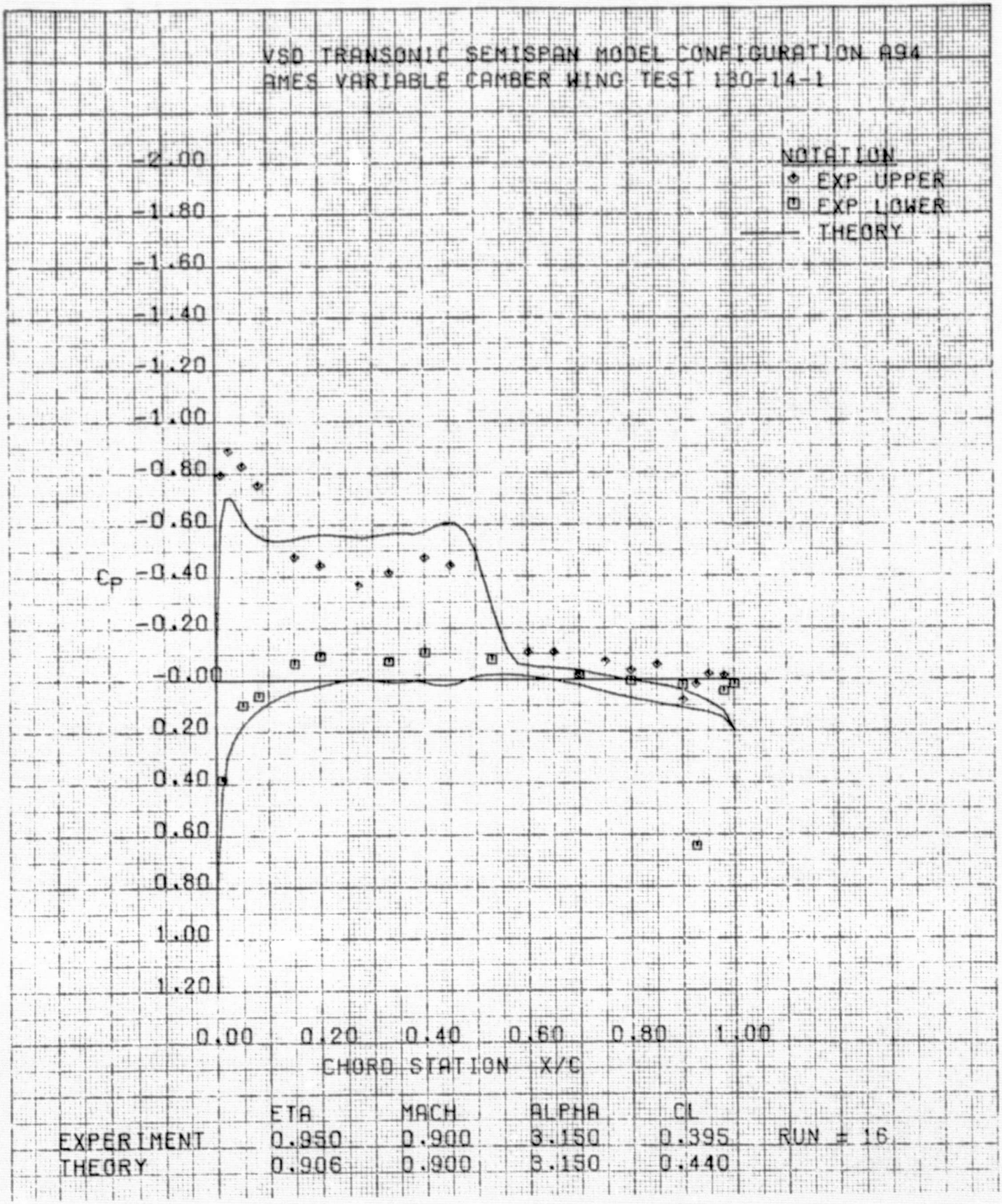

(g) η = .906

Figure 4 Concluded

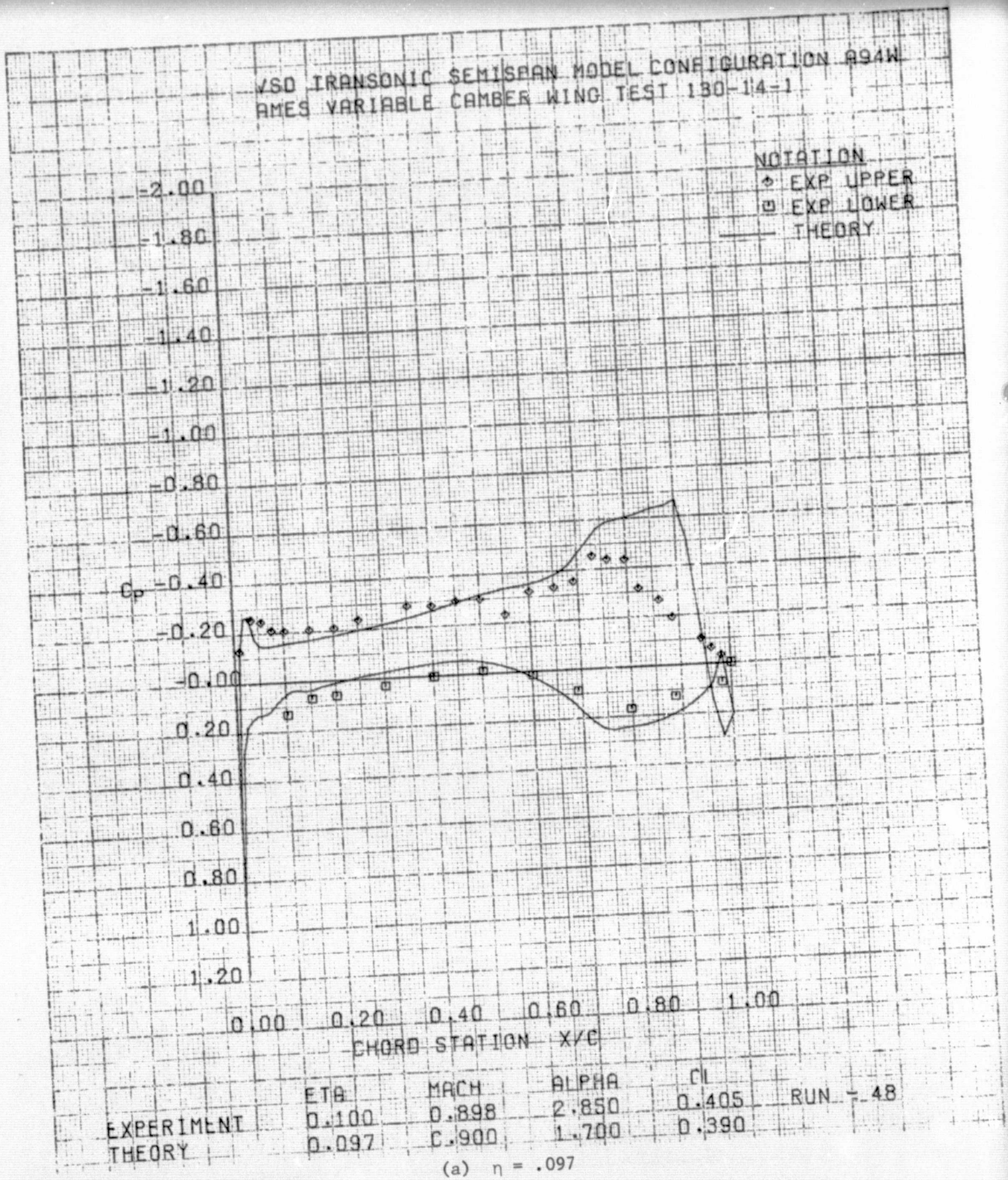

(a) η = .097

Figure 5 Comparison of Theoretical and Experimental Wing Pressures for Variable Camber Configuration A94W at C_L = .4

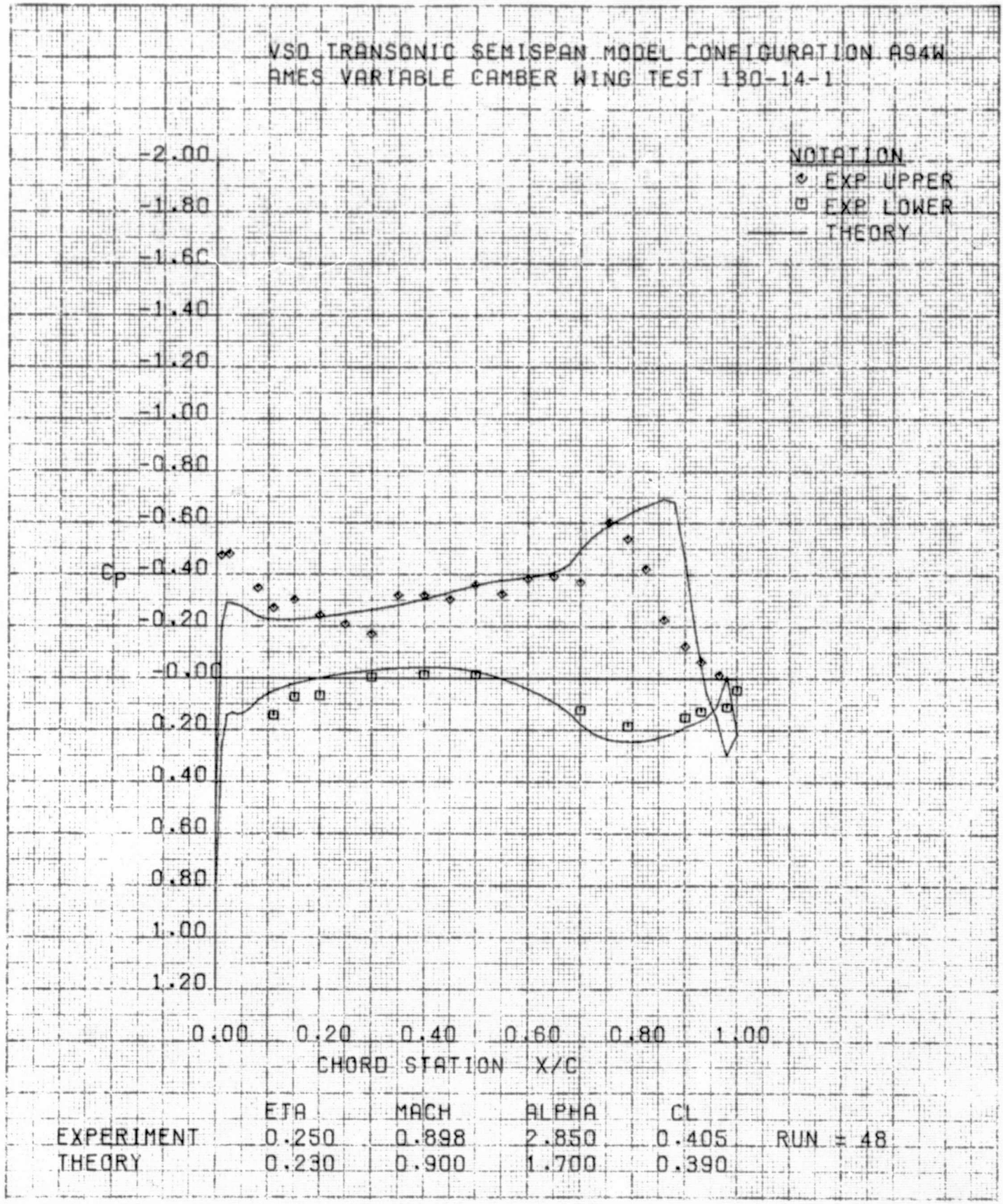

(b) η = .230

Figure 5 Continued

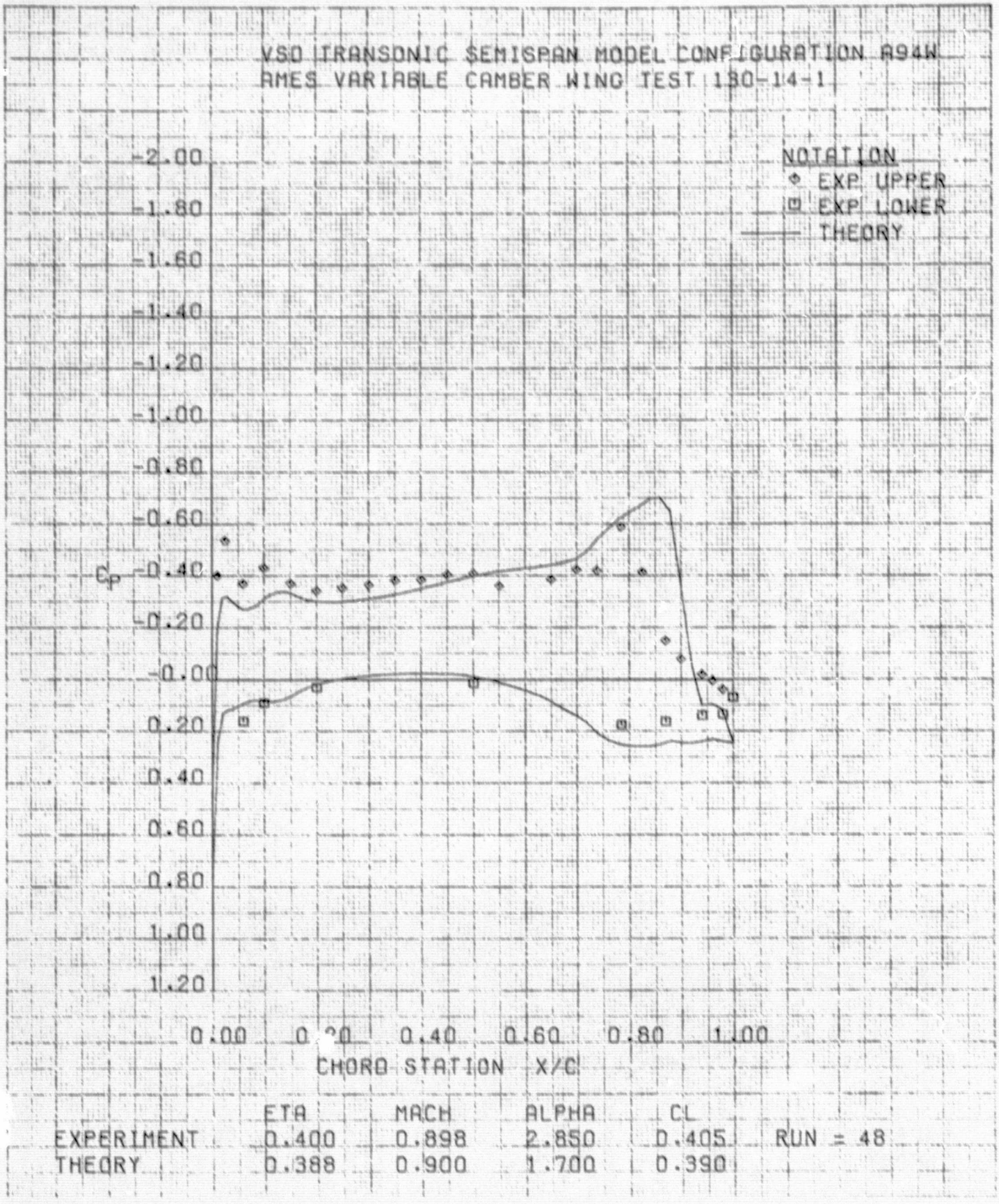

(c) η = .388

Figure 5 Continued

ORIGINAL PAGE IS
OF POOR QUALITY

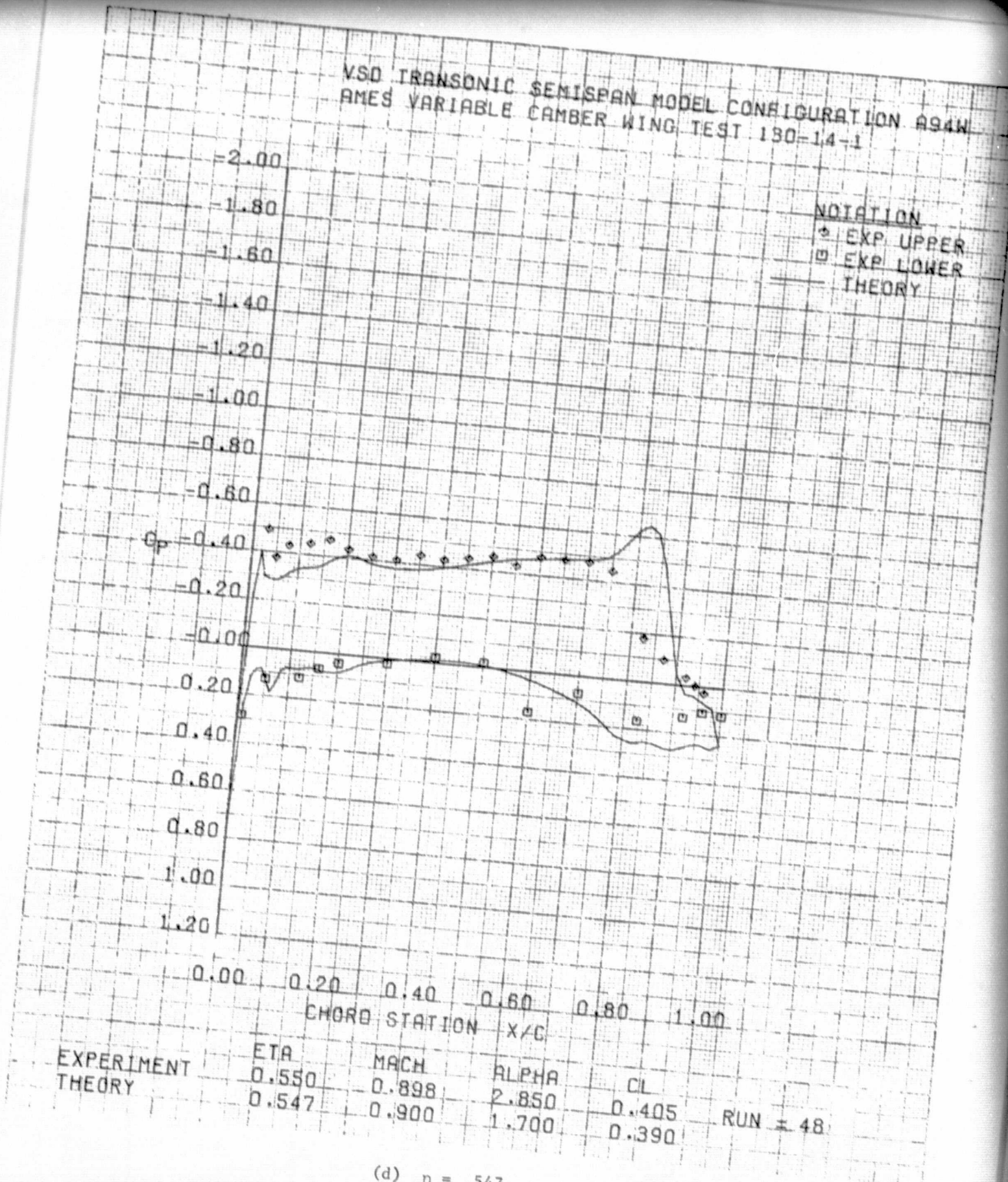

(d) η = .547

Figure 5 Continued

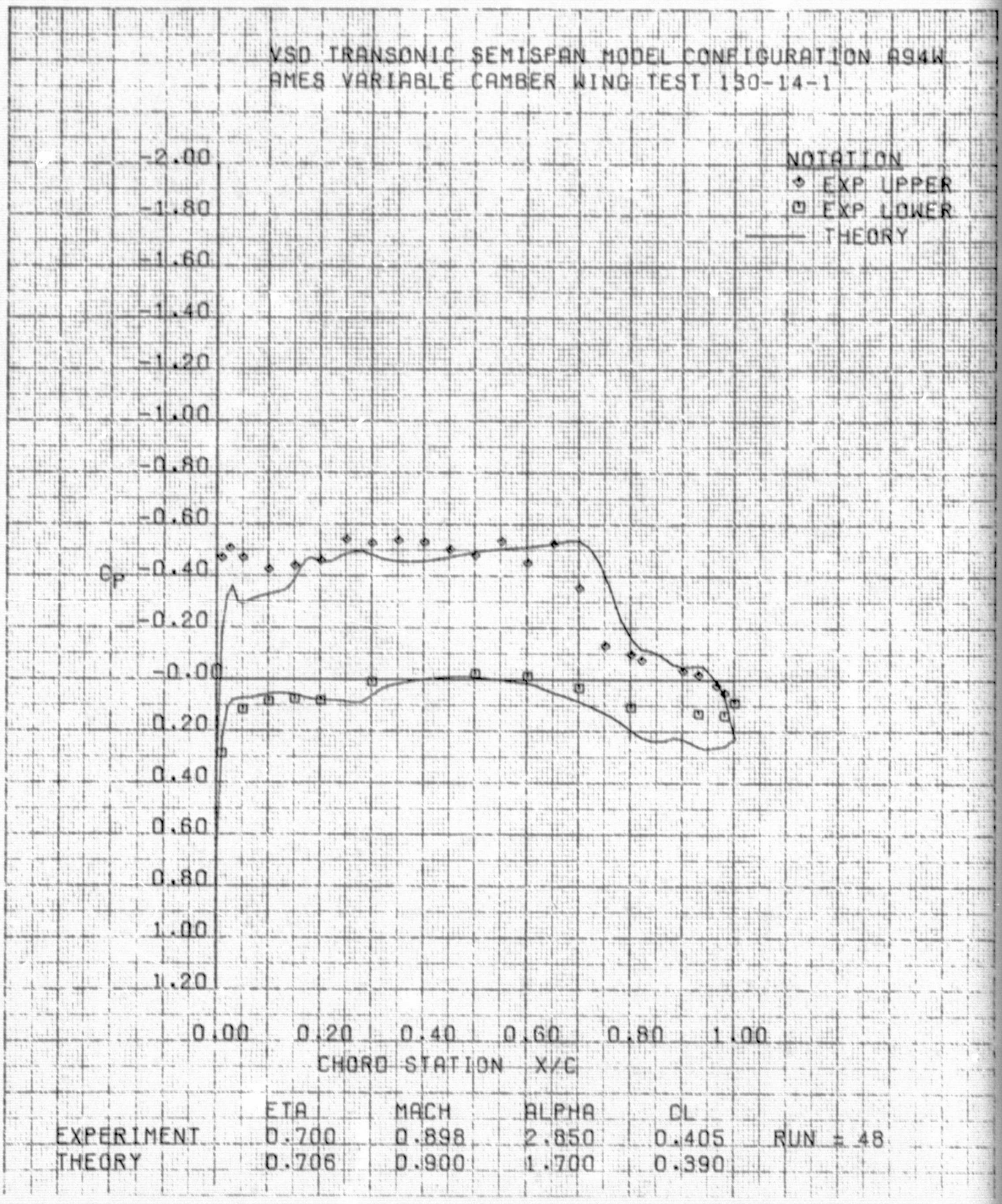

(e) η = .706

Figure 5 Continued

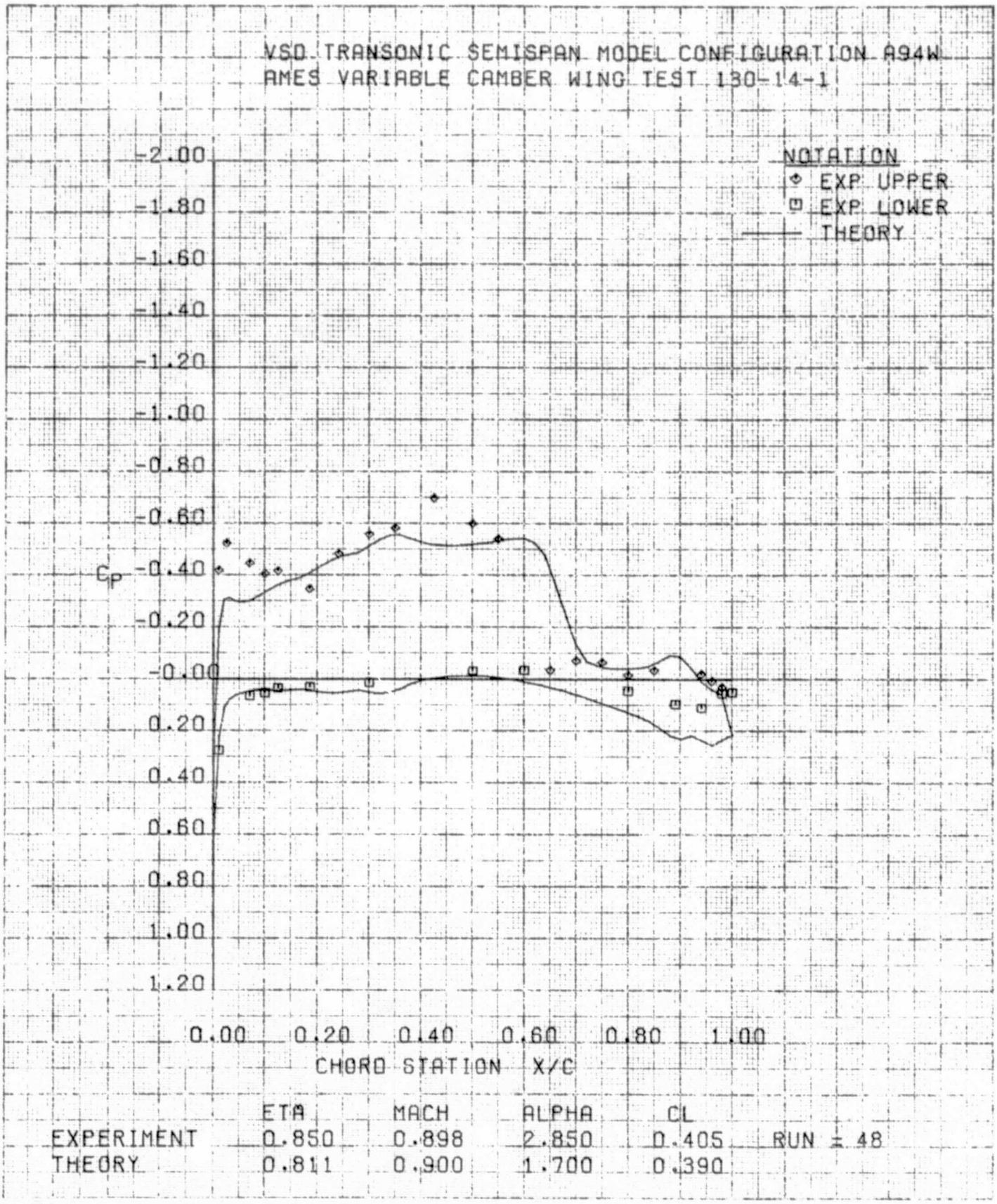

(f) η = .811

Figure 5 Continued

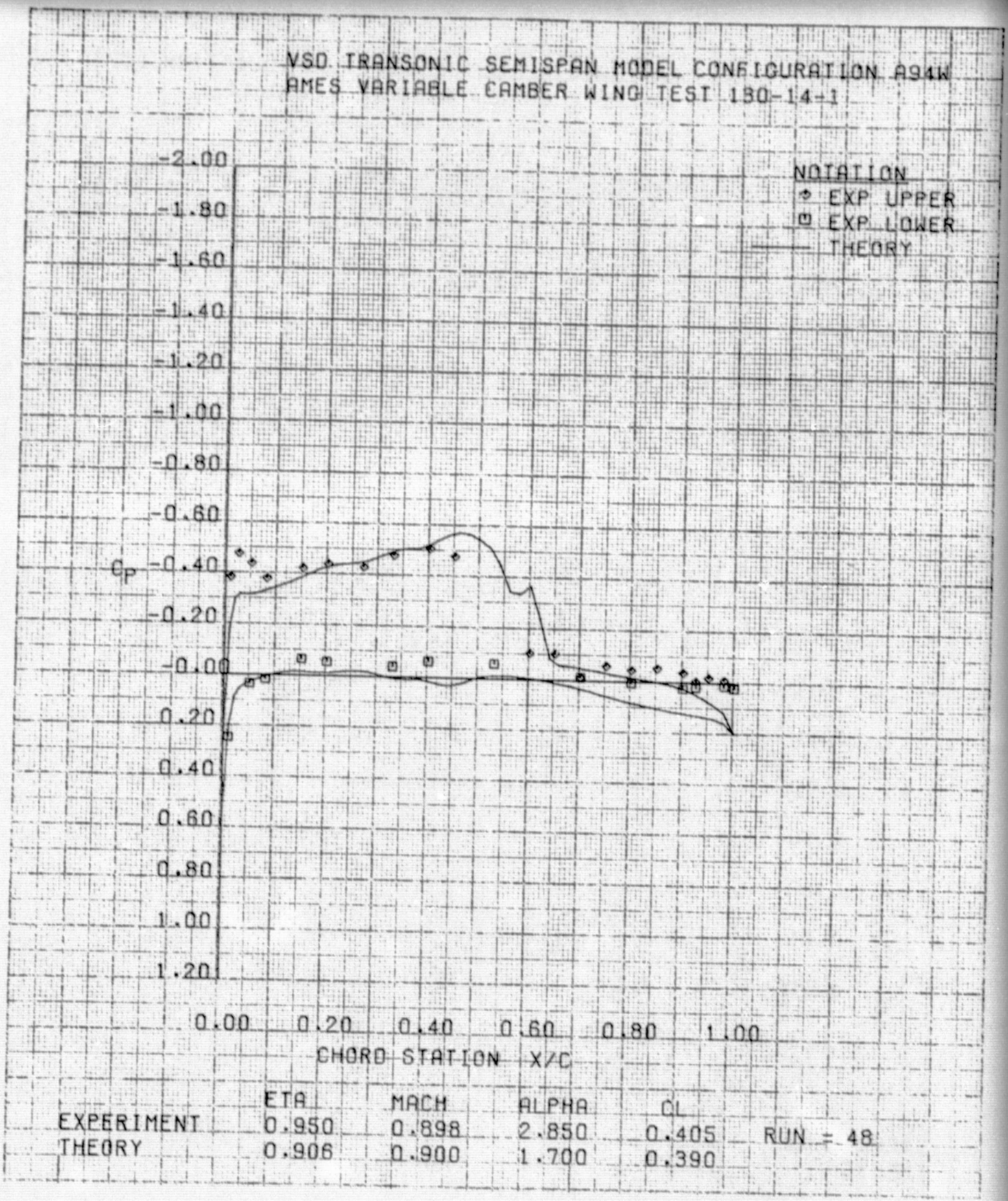

(g) η = .906

Figure 5 Concluded

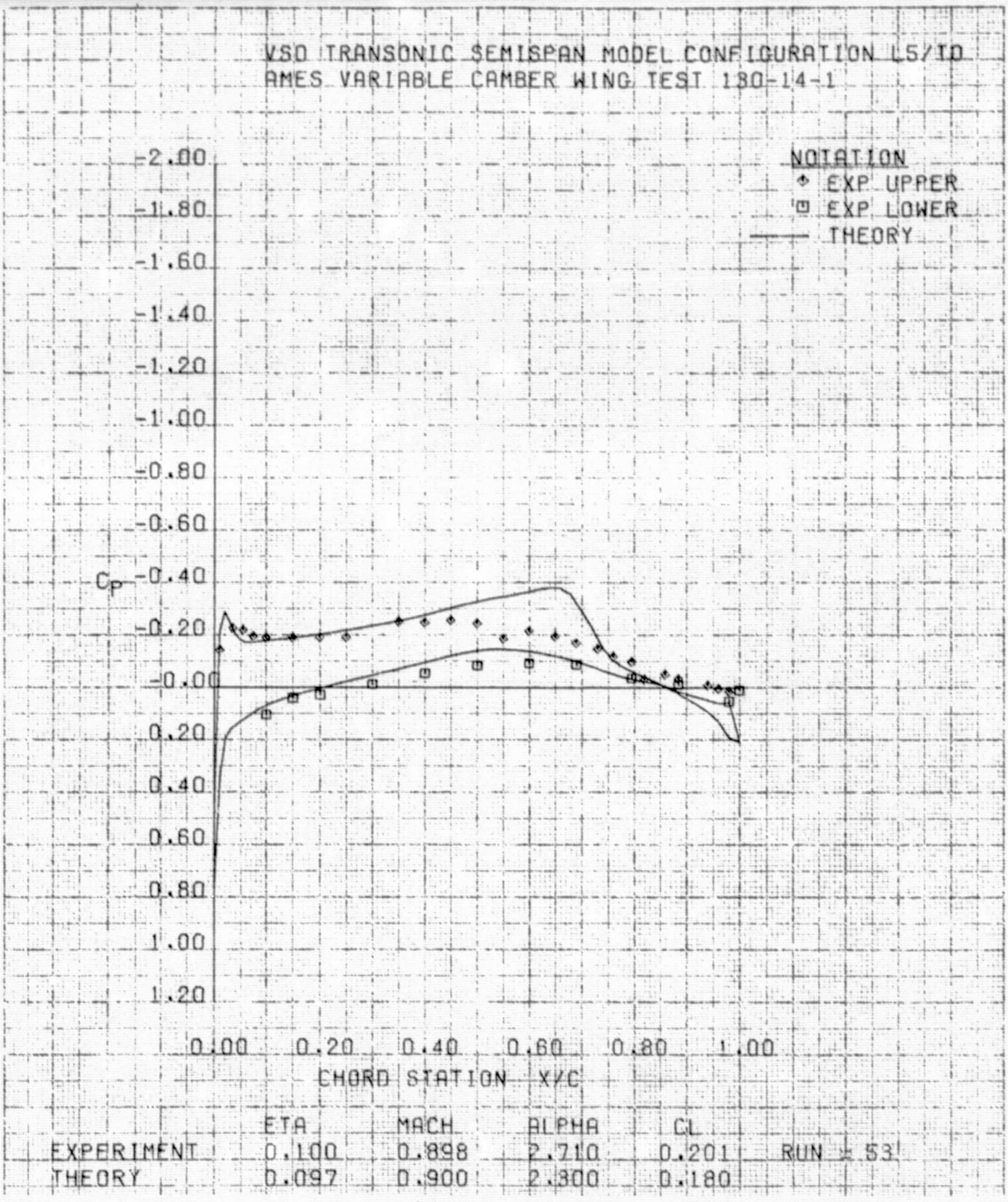

(a) η = .097

Figure 6 Comparison of Theoretical and Experimental Wing Pressures for Variable Camber Configuration L5/TO at C_L = .2

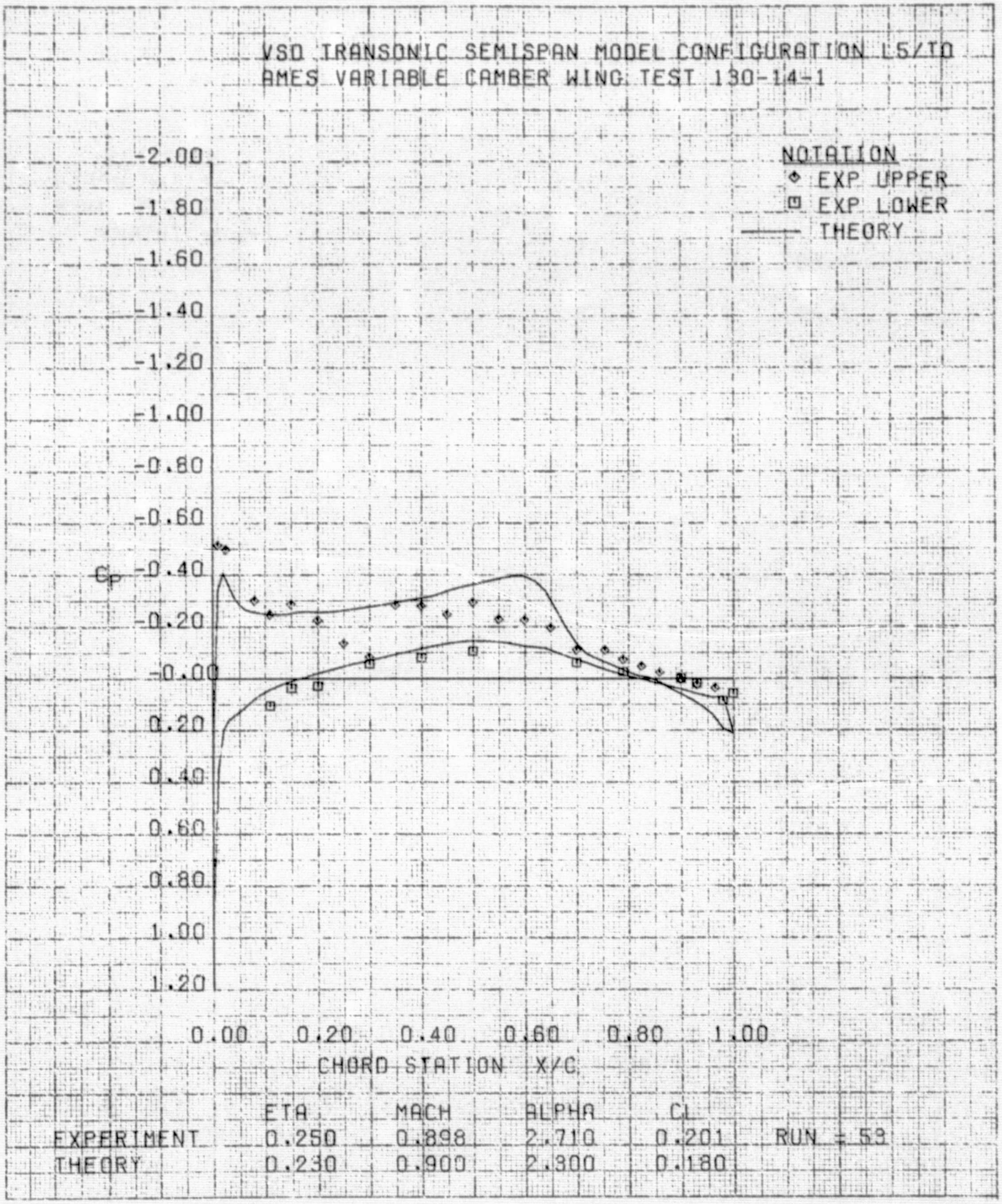

(b) η = .230

Figure 6 Continued

ORIGINAL PAGE IS
OF POOR QUALITY

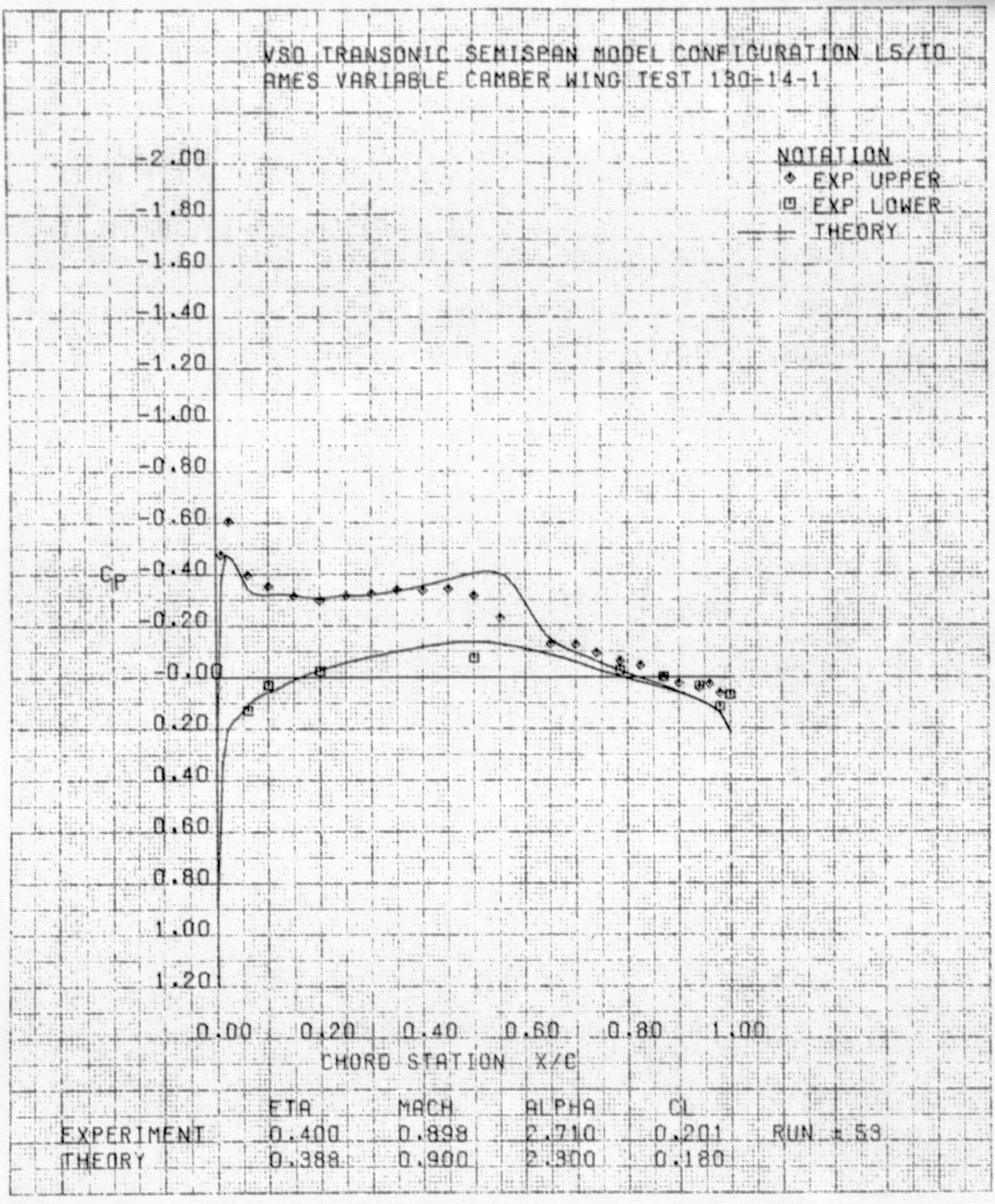

(c) $\eta = .388$

Figure 6 Continued

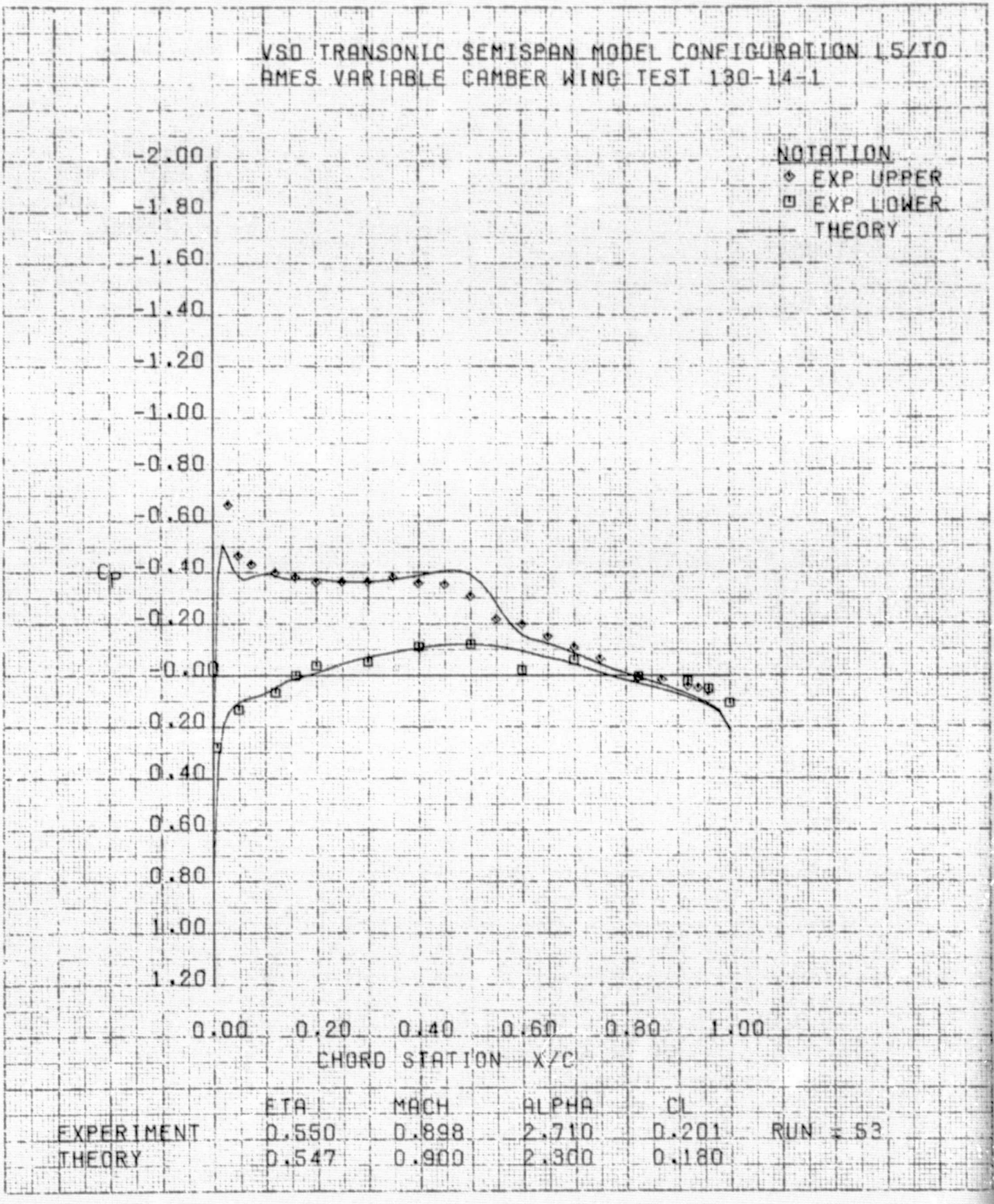

(d) η = .547

Figure 6 Continued

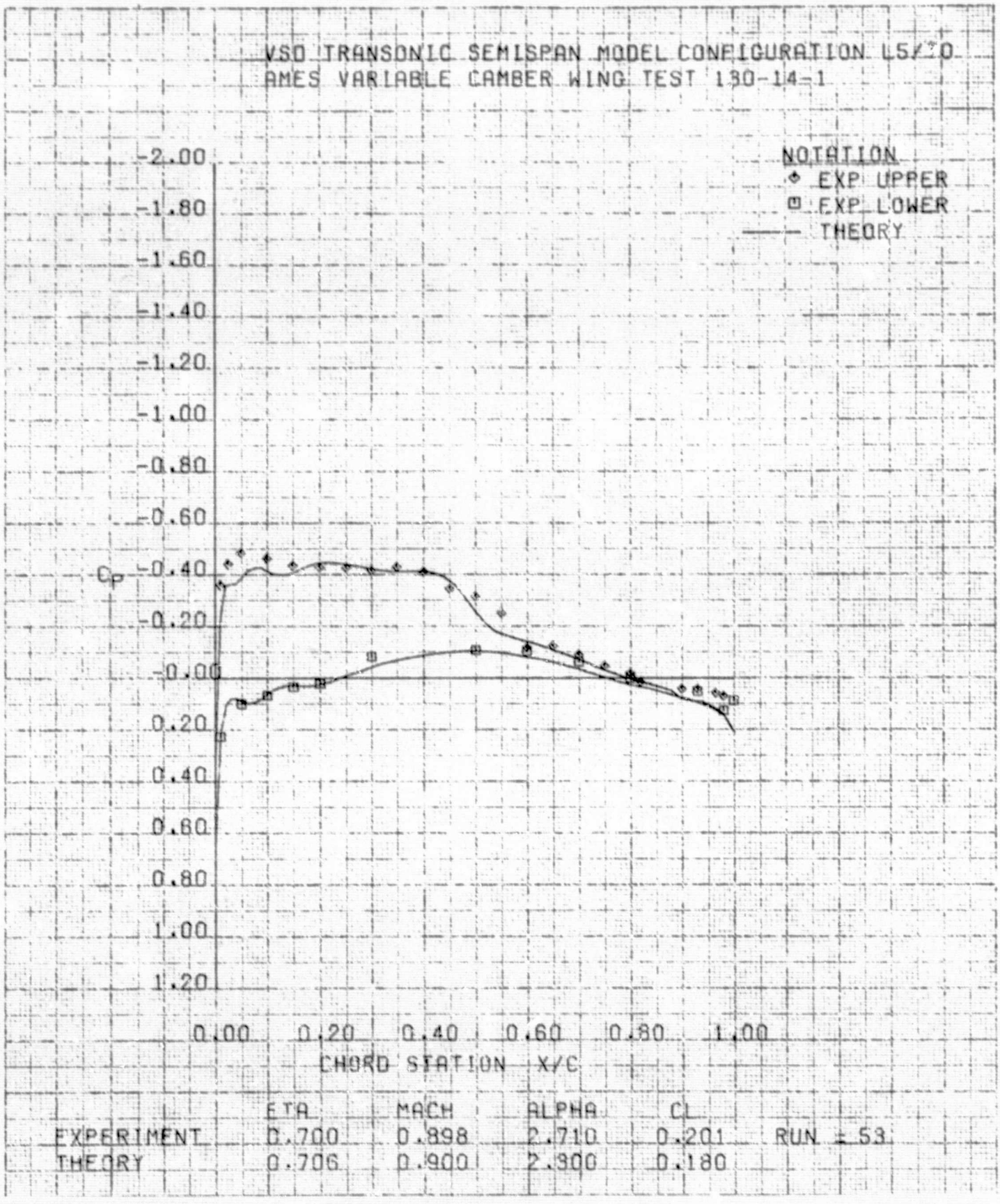

(e) η = .706

Figure 6 Continued

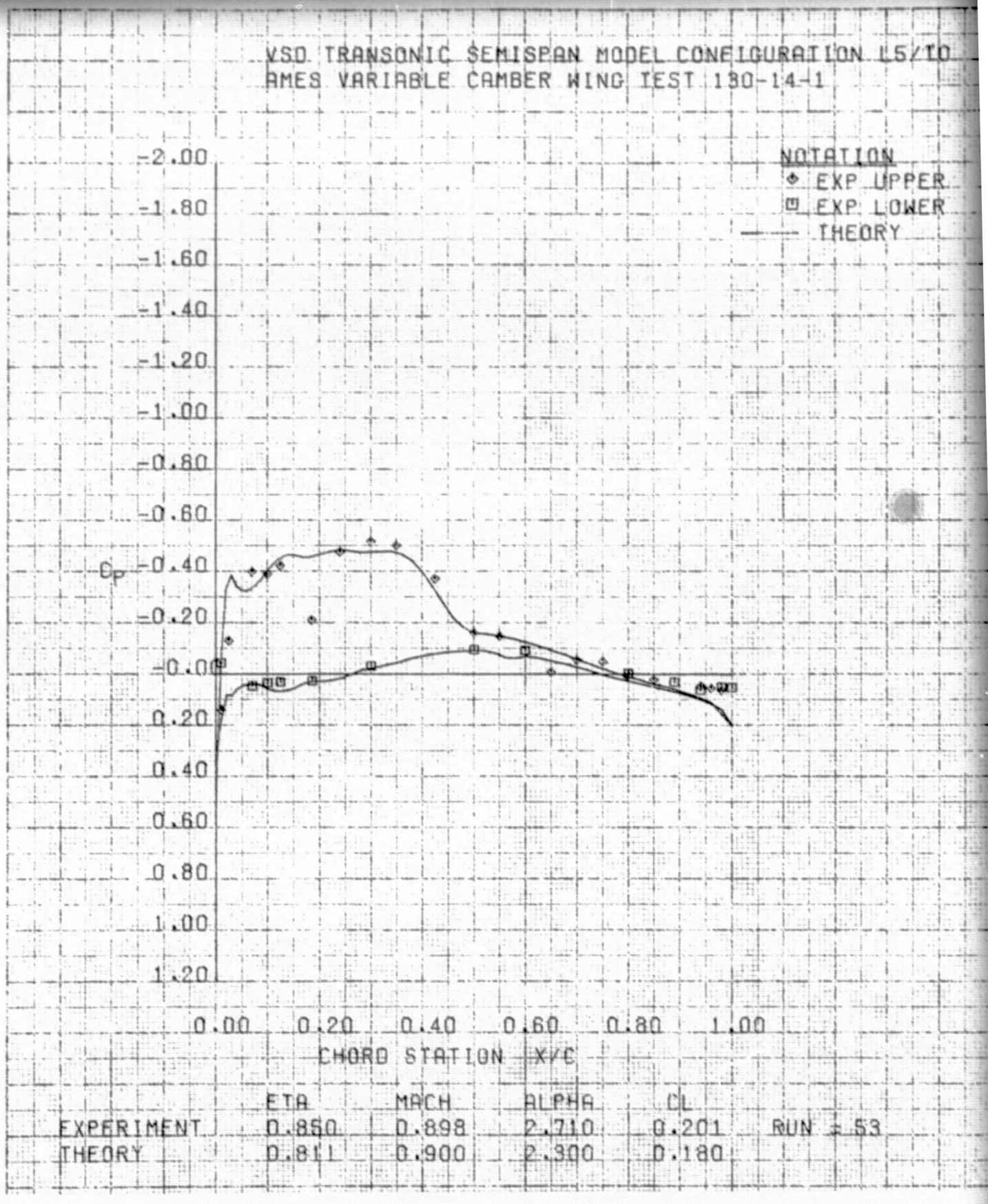

(f) η = .811

Figure 6 Continued

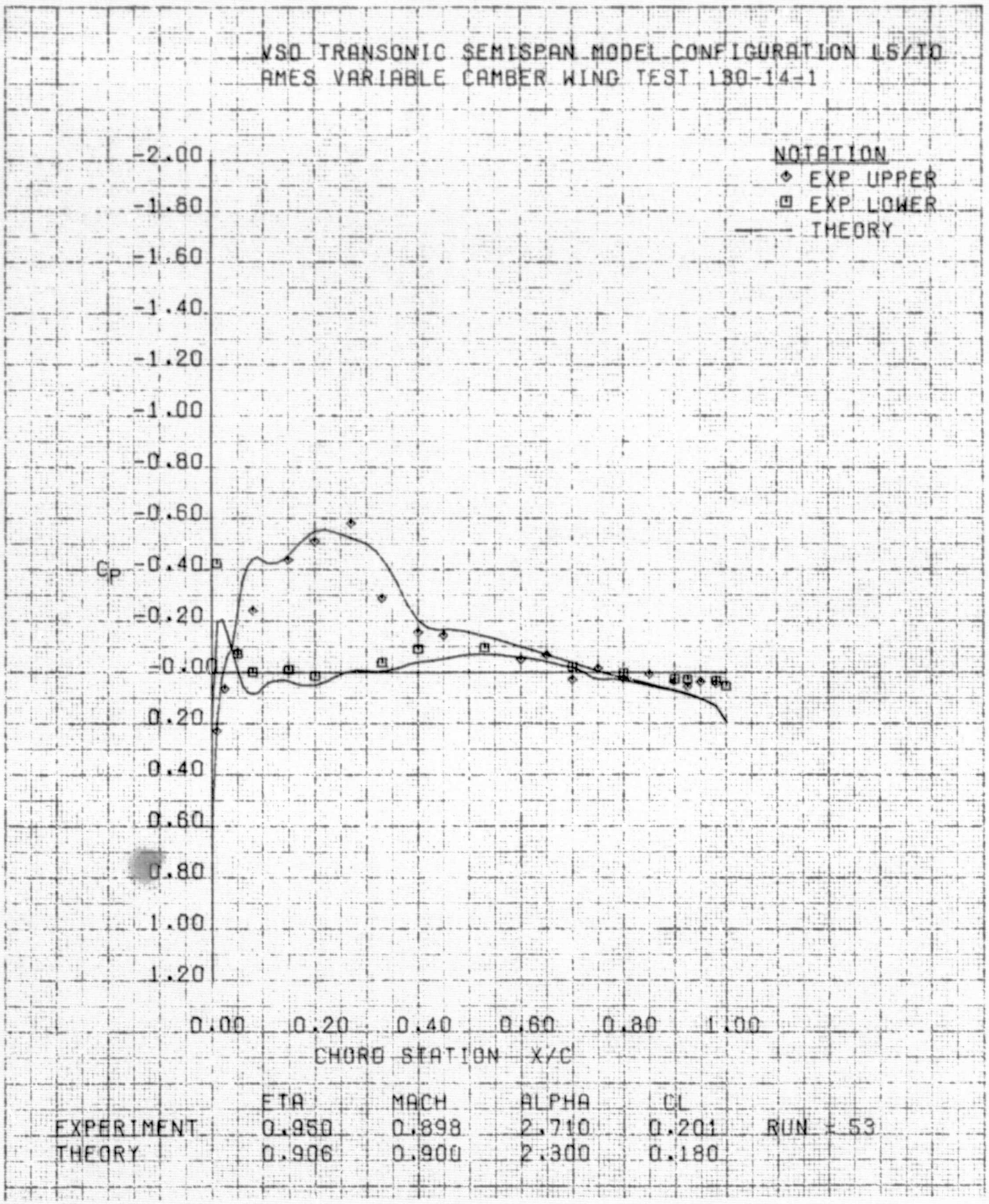

(g) η = .906

Figure 6 Concluded

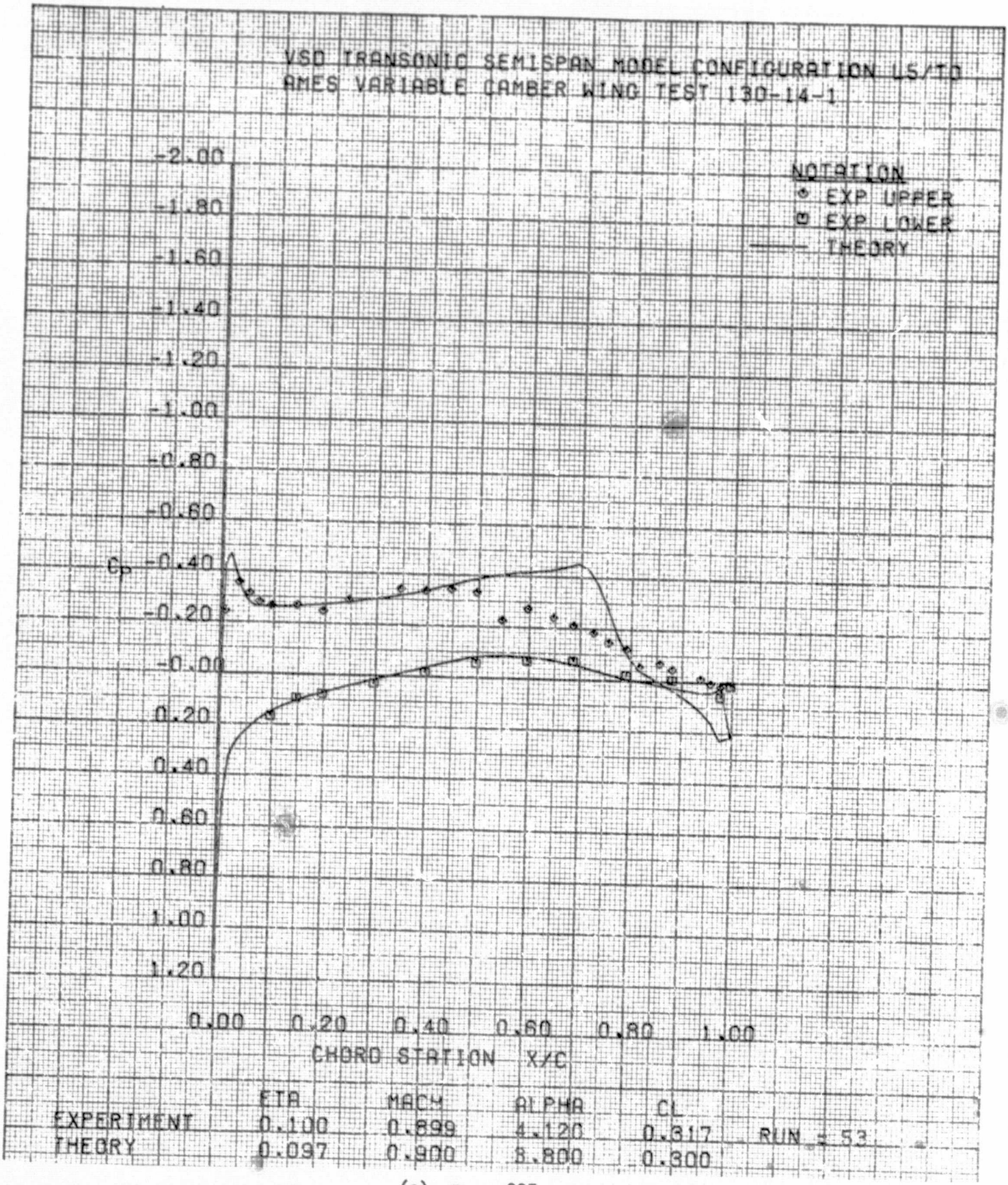

(a) η = .097

Figure 7 Comparison of Theoretical and Experimental Wing Pressures for Variable Camber Configuration L5/T0 at C_L = .3

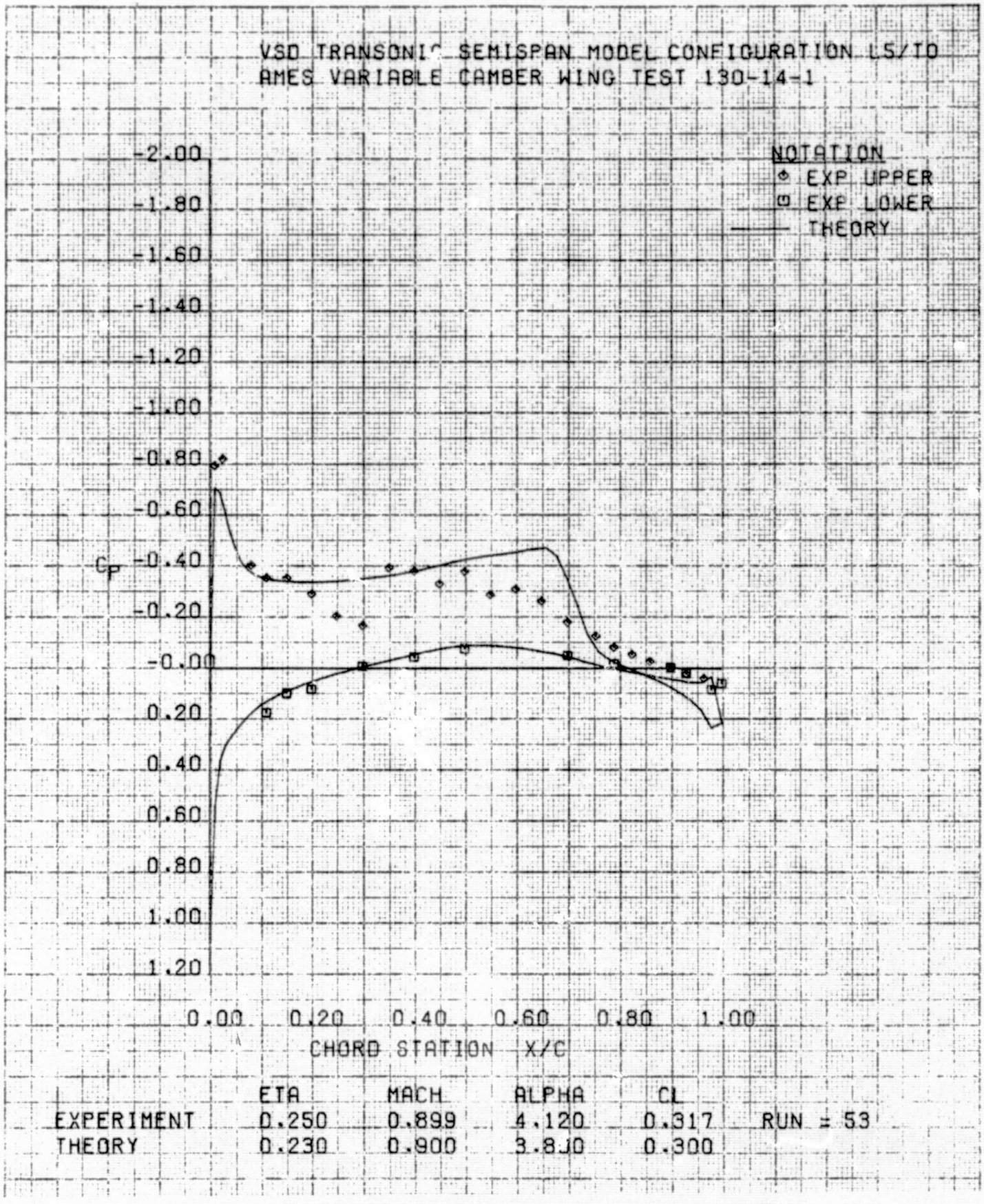

(b) η = .230

Figure 7 Continued

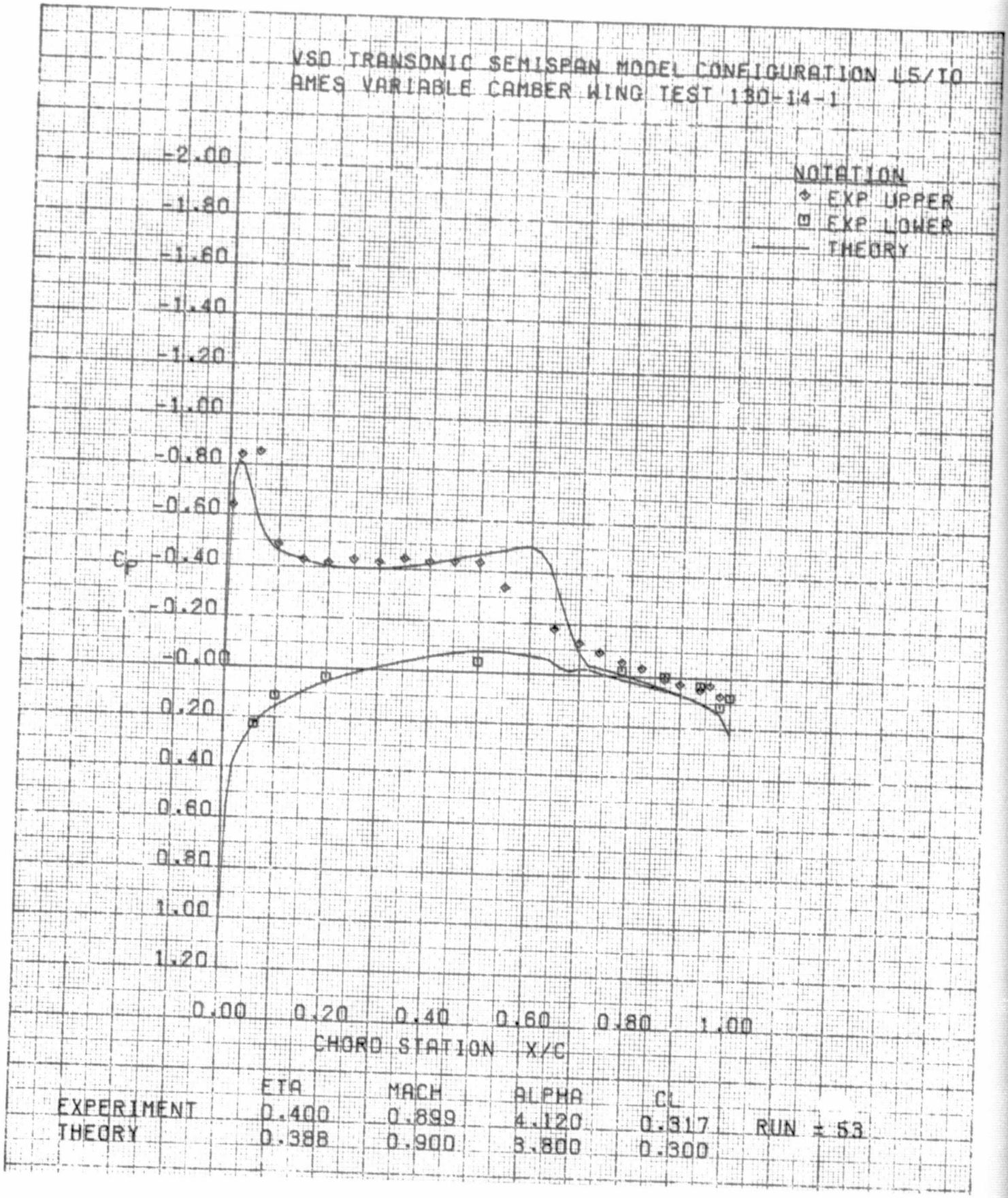

(c) η = .388

Figure 7 Continued

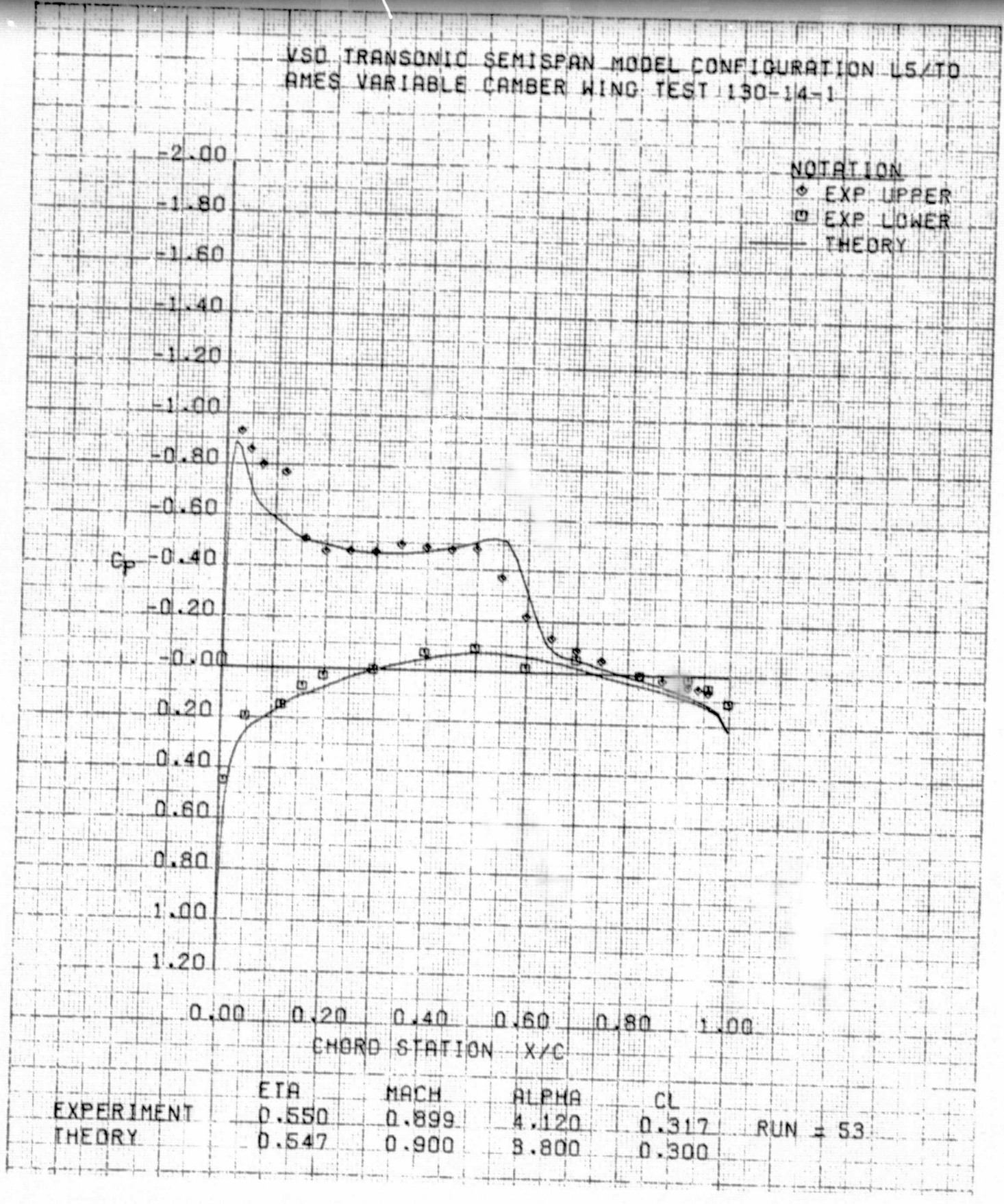

(d) $\eta = .547$

Figure 7 Continued

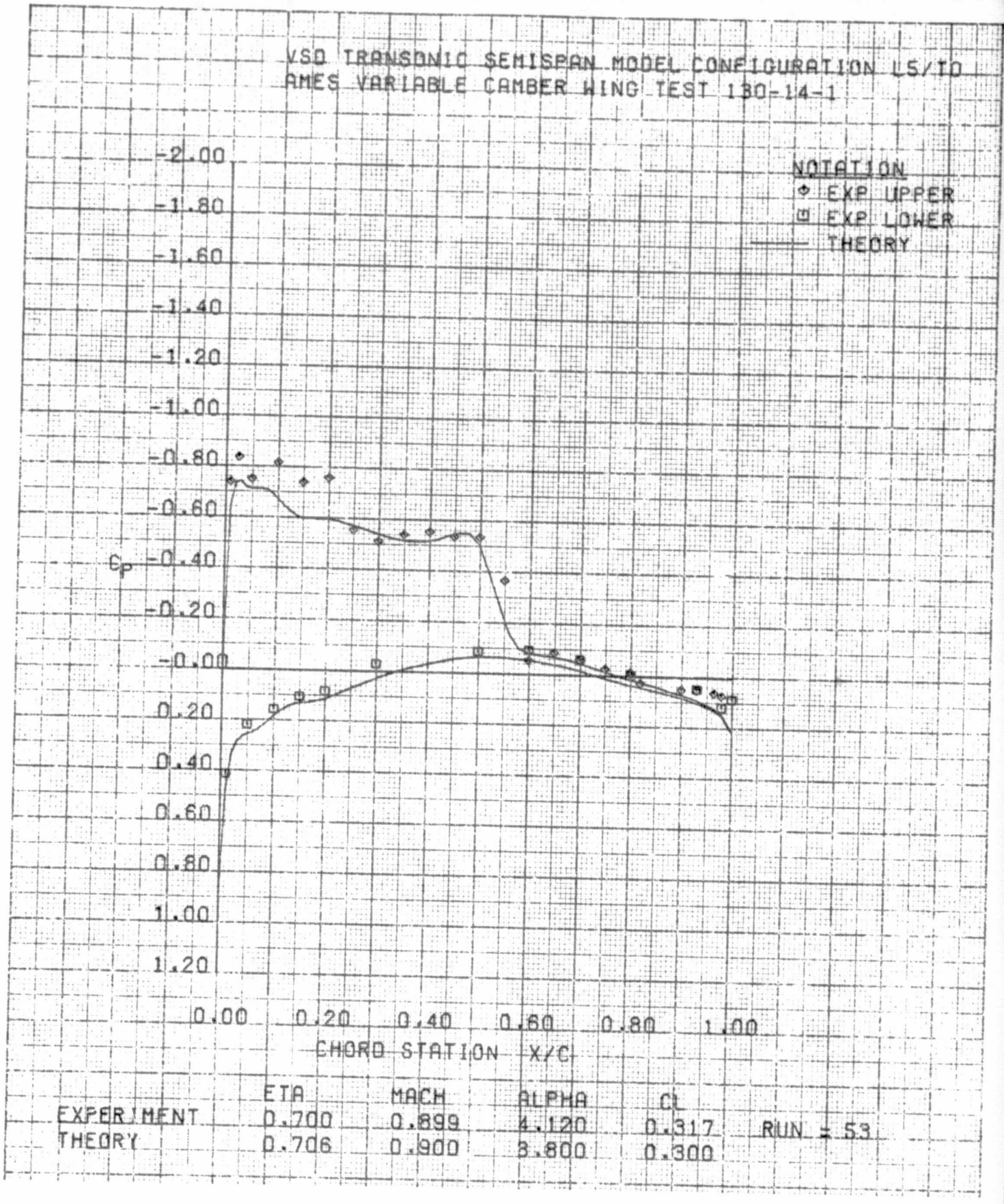

(e) η = .706

Figure 7 Continued

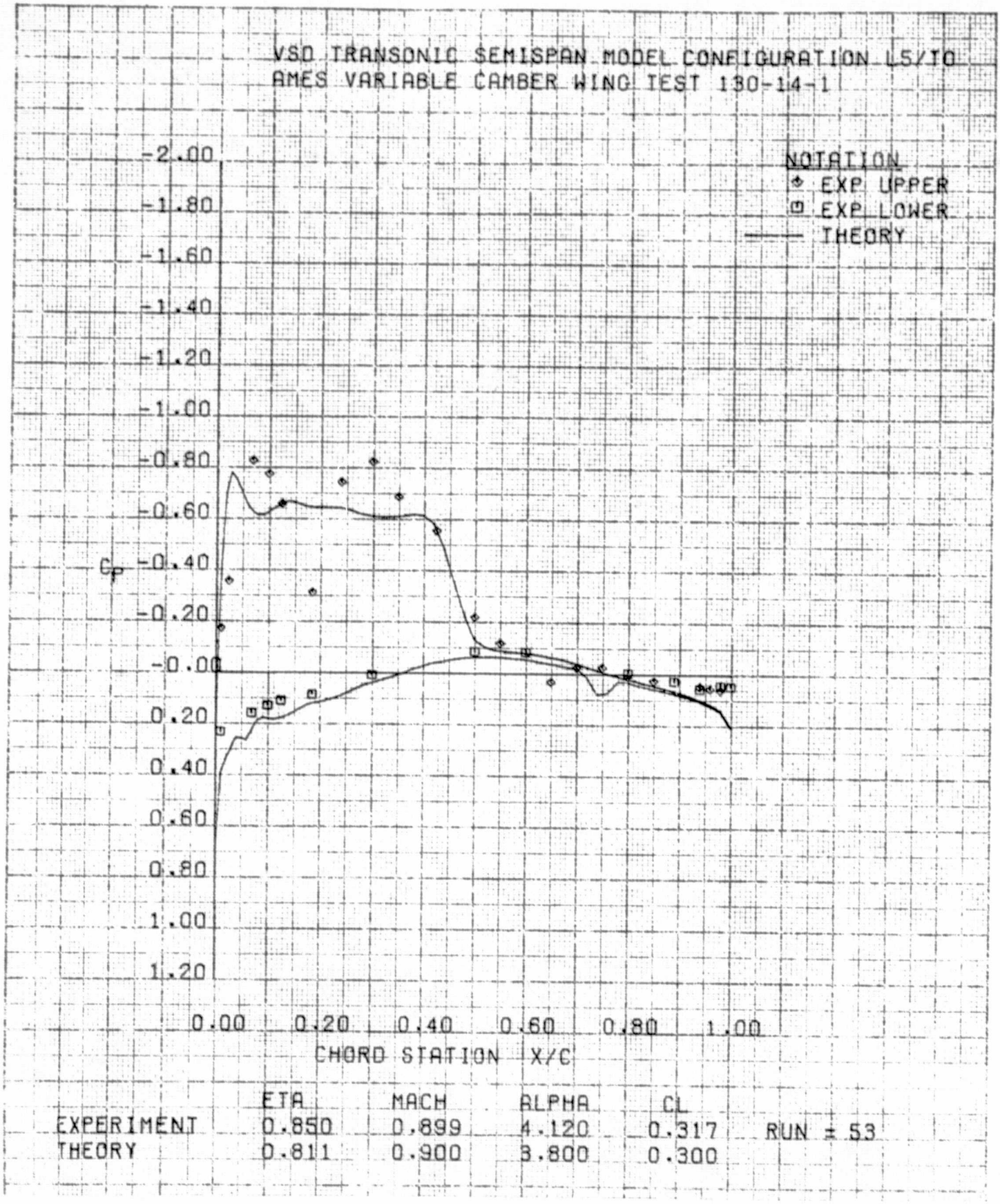

(f) η = .811

Figure 7 Continued

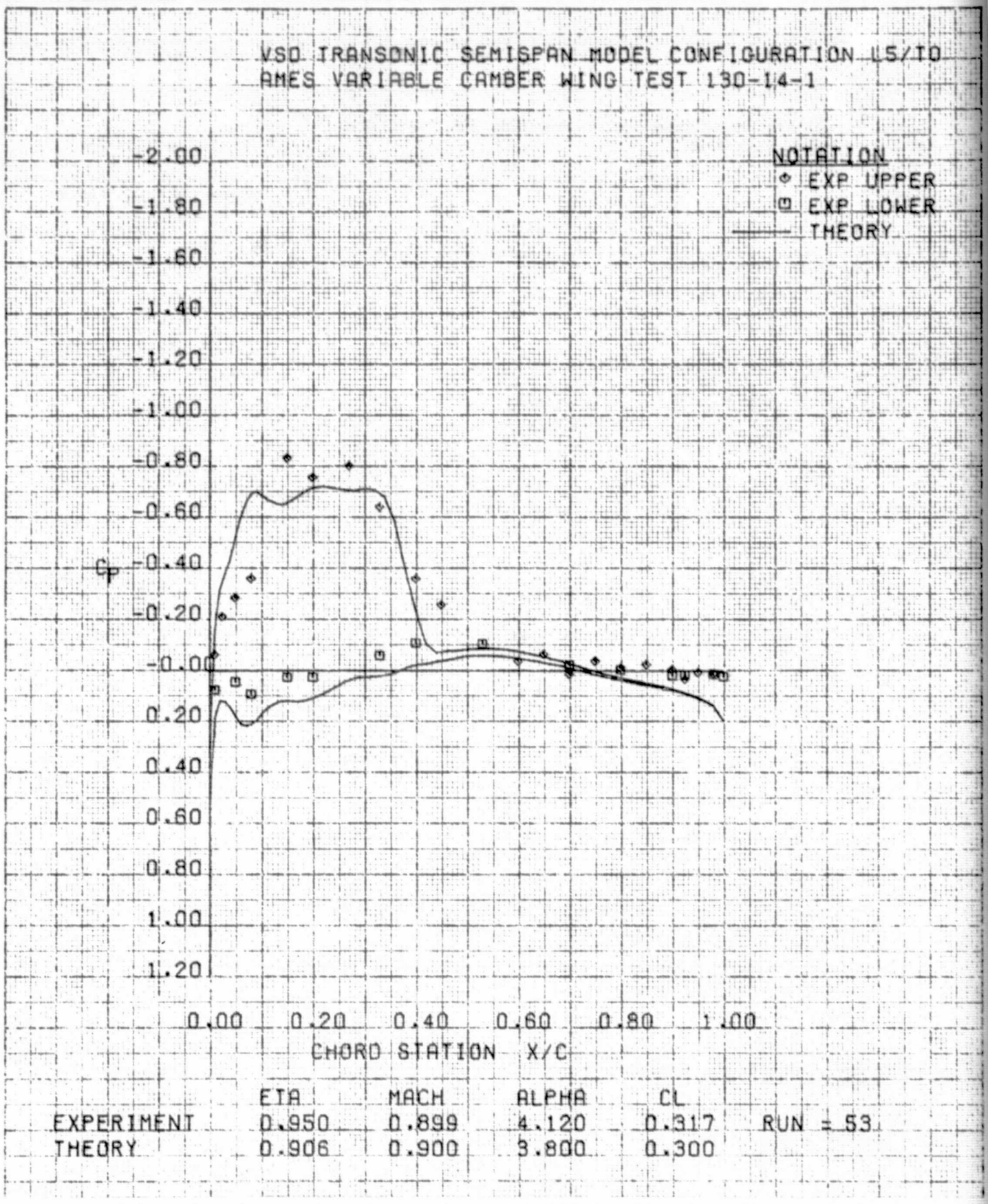

(g) η = .906

Figure 7 (continued

1. Report No. NASA TM-78480 AVRADCOM Tech. Rep. 78-33(AM)	2. Government Accession No.	3. Recipient's Catalog No.

4. Title and Subtitle	5. Report Date
COMPUTATIONAL WING OPTIMIZATION AND COMPARISONS WITH EXPERIMENT FOR A SEMI-SPAN WING MODEL	6. Performing Organization Code

7. Author(s)	8. Performing Organization Report No. A-7395
E. G. Waggoner,* H. P. Haney,* and W. F. Ballhaus	10. Work Unit No. 505-06-11
9. Performing Organization Name and Address Ames Research Center, NASA and AVRADCOM Research and Technology Laboratories Moffett Field, Calif. 94035	11. Contract or Grant No.
12. Sponsoring Agency Name and Address National Aeronautics and Space Administration Washington, D.C. 20546 and U.S. Army Aviation Research and Development Command St. Louis, MO 63166	13. Type of Report and Period Covered Technical Memorandum 14. Sponsoring Agency Code

15. Supplementary Notes

*Vought Corporation, Dallas, Texas.

16. Abstract

A computational wing optimization procedure has been developed and verified by an experimental investigation of a semi-span variable camber wing model in the NASA Ames Research Center 14-foot transonic wind tunnel. The Bailey-Ballhaus transonic potential flow analysis and Woodward-Carmichael linear theory codes were linked to Vanderplaats constrained minimization routine to optimize model configurations at several subsonic and transonic design points. The 35° swept wing is characterized by multi-segmented leading and trailing edge flaps whose hinge lines are swept relative to the leading and trailing edges of the wing. By varying deflection angles of the flap segments, camber and twist distribution can be optimized for different design conditions.

The tested configurations had been optimized at lift coefficients of 0.2, 0.4, and 0.6 for Mach numbers of 0.6 and 0.9. Several configurations which had proven to be the most efficient designs from an earlier parametric study were also tested. This offered a baseline for comparison of the computationally optimized configurations.

Following the test an improved version of the Bailey-Ballhaus code was used to analyze test configurations. Computationally predicted wing pressure distributions were compared with experimental data at selected conditions.

Study results indicate that numerical optimization can be both an effective and efficient design tool. The optimized configurations had as good or better lift-to-drag ratios at the design points as the best designs previously tested during an extensive parametric study. In addition, the predicted pressure distributions agreed well with the experiment when the improved Bailey-Ballhaus code was used.

17. Key Words (Suggested by Author(s))	18. Distribution Statement
Transonic flow Wing design Computational method	Unlimited STAR Category - 02

19. Security Classif. (of this report)	20. Security Classif. (of this page)	21. No. of Pages	22. Price*
Unclassified	Unclassified	91	$5.00

*For sale by the National Technical Information Service, Springfield, Virginia 22161